The dynamics of CO2-driven granular flows in gullies on Mars

Lonneke Roelofs[1], Susan J Conway[2], Bas van Dam[3], Arjan van Eijk[3,3], Jonathan peter Merrison[4], J. J. Iversen[5], Matthew E. Sylvest[6], Manish R Patel[6], Henk Markies[3], Marcel van Maarseveen[3], Jim McElwaine[7], Maarten G. Kleinhans[3], and Tjalling de Haas[3]

[1]Utrecht University
[2]University of Nantes
[3]Universiteit Utrecht
[4]Aarhus University
[5]University of Aarhus
[6]The Open University
[7]Durham University

April 16, 2024

Abstract

Martian gullies are landforms consisting of an erosional alcove, a channel, and a depositional apron. A significant proportion of Martian gullies at the mid-latitudes is active today. The seasonal sublimation of CO2 ice has been suggested as a driver behind present-day gully activity. However, due to a lack of in-situ observations, the actual processes causing the observed changes remain unresolved. Here, we present results from flume experiments in environmental chambers in which we created CO2-driven granular flows under Martian atmospheric conditions. Our experiments show that under Martian atmospheric pressure, large amounts of granular material can be fluidized by the sublimation of small quantities of CO2 ice in the granular mixture (only 0.5% of the volume fraction of the flow) under slope angles as low as 10°. Dimensionless scaling of the CO2-driven granular flows shows that they are dynamically similar to terrestrial two-phase granular flows, i.e. debris flows and pyroclastic flows. The similarity in flow dynamics explains the similarity in deposit morphology with levees and lobes, supporting the hypothesis that CO2-driven granular flows on Mars are not merely modifying older landforms, but they are actively forming them. This has far-reaching implications for the processes thought to have formed these gullies over time. For other planetary bodies in our solar system, our experimental results suggest that the existence of gully-like landforms is not necessarily evidence for flowing liquids but that they could also be formed or modified by sublimation-driven flow processes.

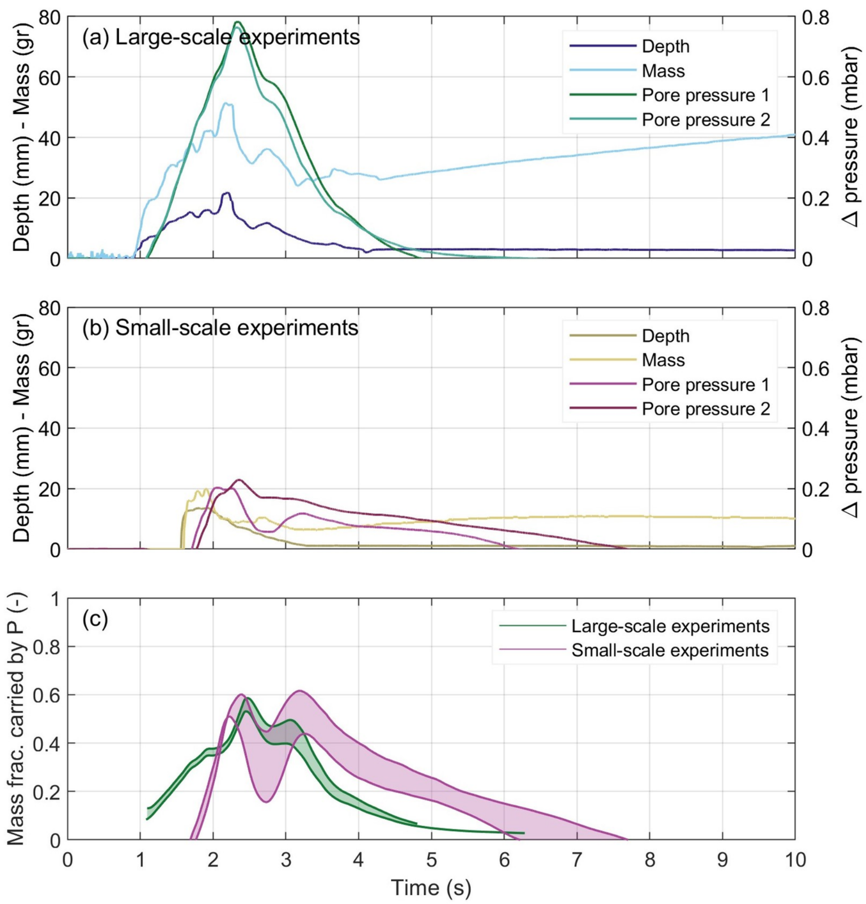

(a) Large-scale experiments
Depth
Mass
Pore pressure 1
Pore pressure 2
Depth (mm) - Mass (gr)
Δ pressure (mbar)
(b) Small-scale experiments
Depth
Mass
Pore pressure 1
Pore pressure 2
Depth (mm) - Mass (gr)
Δ pressure (mbar)
(c)
Large-scale experiments
Small-scale experiments
Mass frac. carried by P (-)
Time (s)

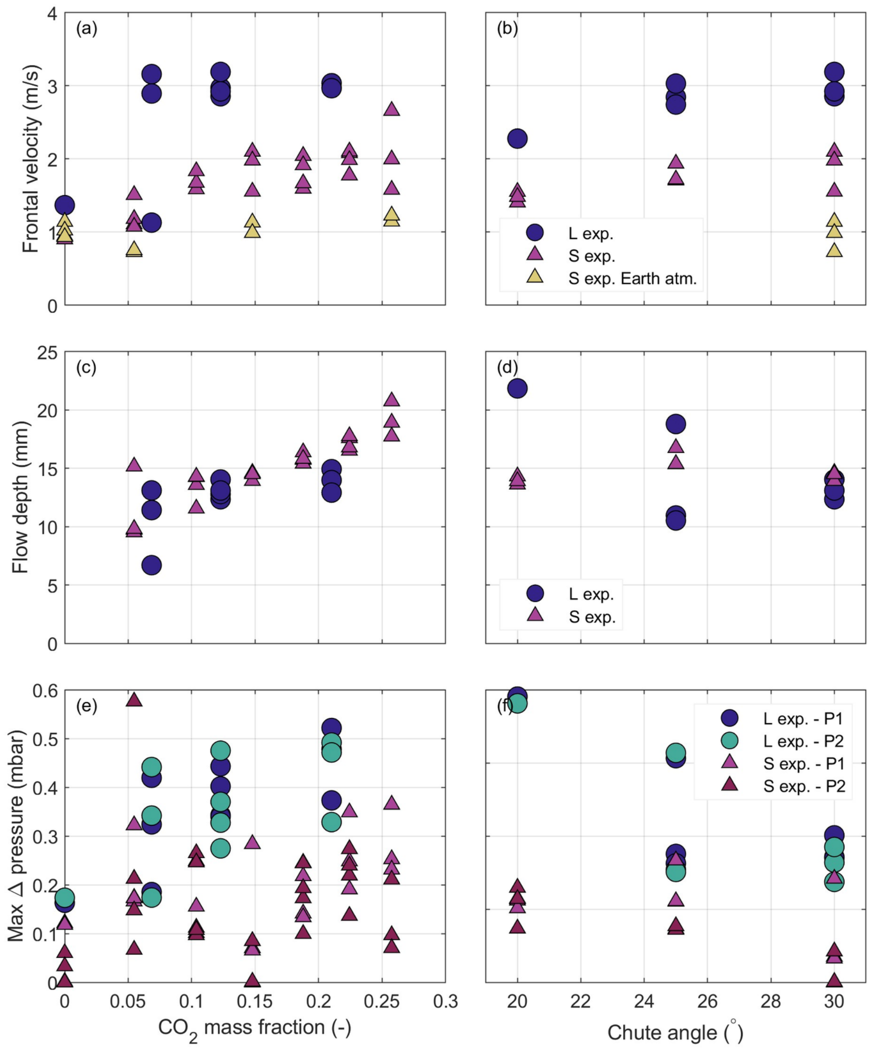

(a)
(b)
(c)
(d)
(e)
(f)
Frontal velocity (m/s)
Flow depth (mm)
Max Δ pressure (mbar)
CO_2 mass fraction (-)
Chute angle (°)
L exp.
S exp.
S exp. Earth atm.
L exp. - P1
L exp. - P2
S exp. - P1
S exp. - P2

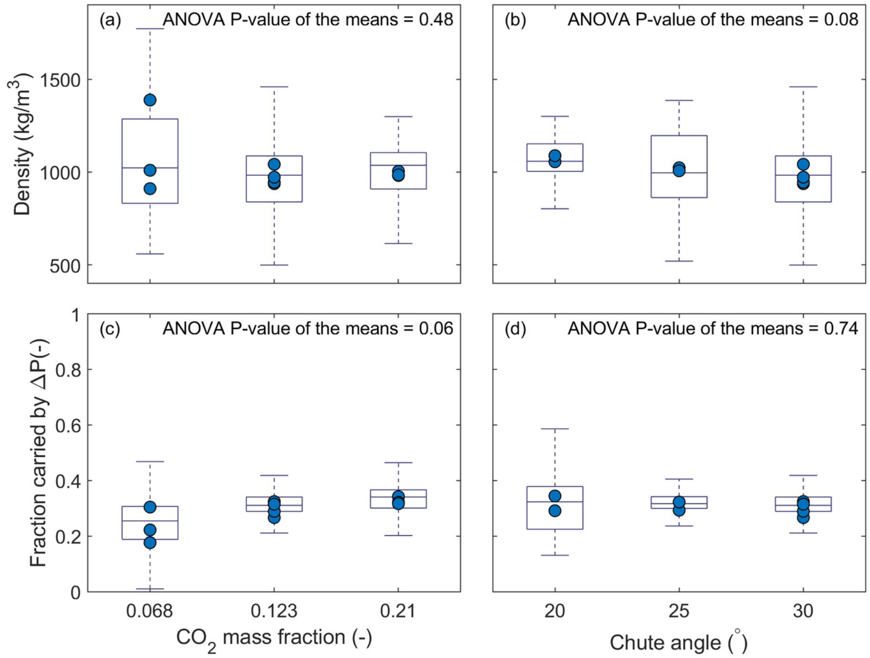

(a) ANOVA P-value of the means = 0.48
(b) ANOVA P-value of the means = 0.08
(c) ANOVA P-value of the means = 0.06
(d) ANOVA P-value of the means = 0.74
Density (kg/m3)
Fraction carried by ΔP(-)
CO2 mass fraction (-)
Chute angle (°)
0.068
0.123
0.21
20
25
30

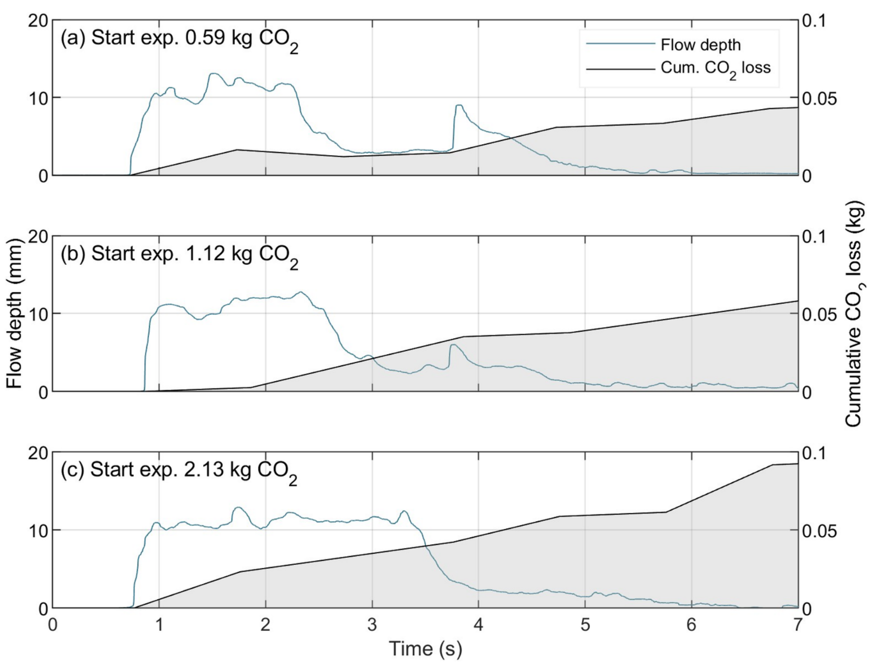

(a) Start exp. 0.59 kg CO2
(b) Start exp. 1.12 kg CO2
(c) Start exp. 2.13 kg CO2
Flow depth
Cum. CO2 loss
Flow depth (mm)
Cumulative CO2 loss (kg)
Time (s)

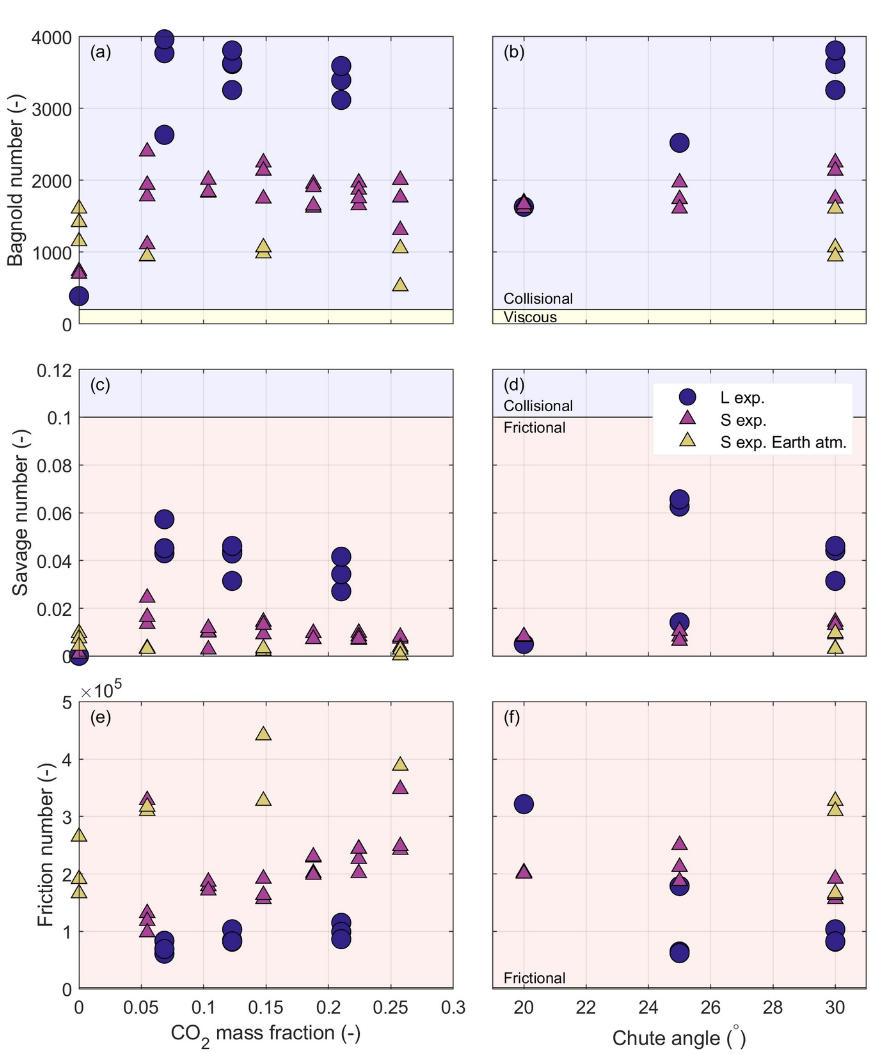

(a)
(b)
(c)
(d)
(e)
(f)
Bagnold number (-)
Savage number (-)
Friction number (-)
Collisional
Viscous
Frictional
L exp.
S exp.
S exp. Earth atm.
$\times 10^5$
CO$_2$ mass fraction (-)
Chute angle (°)

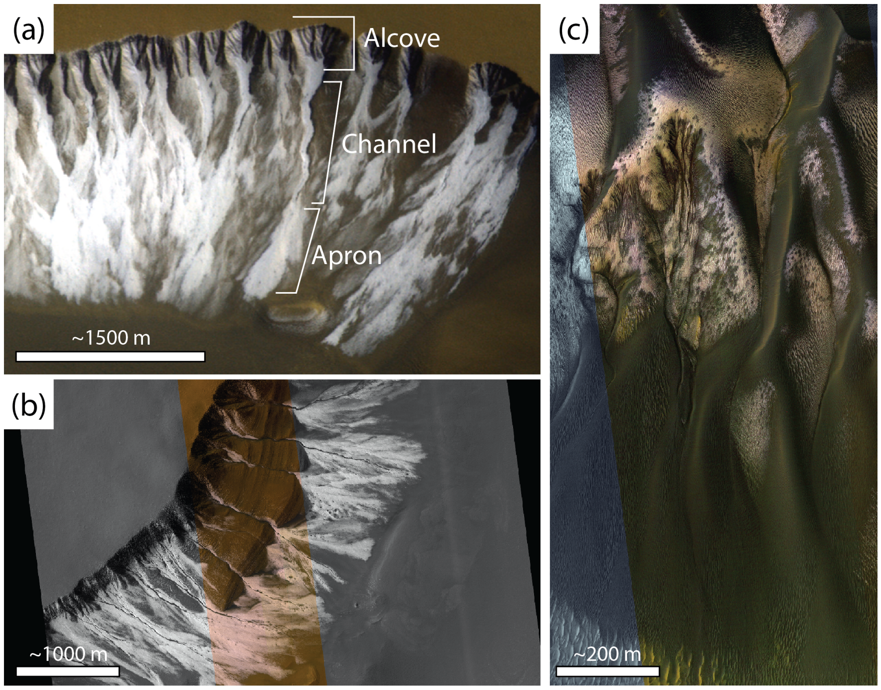
(a)
Alcove
Channel
Apron
~1500 m
(b)
~1000 m
(c)
~200 m

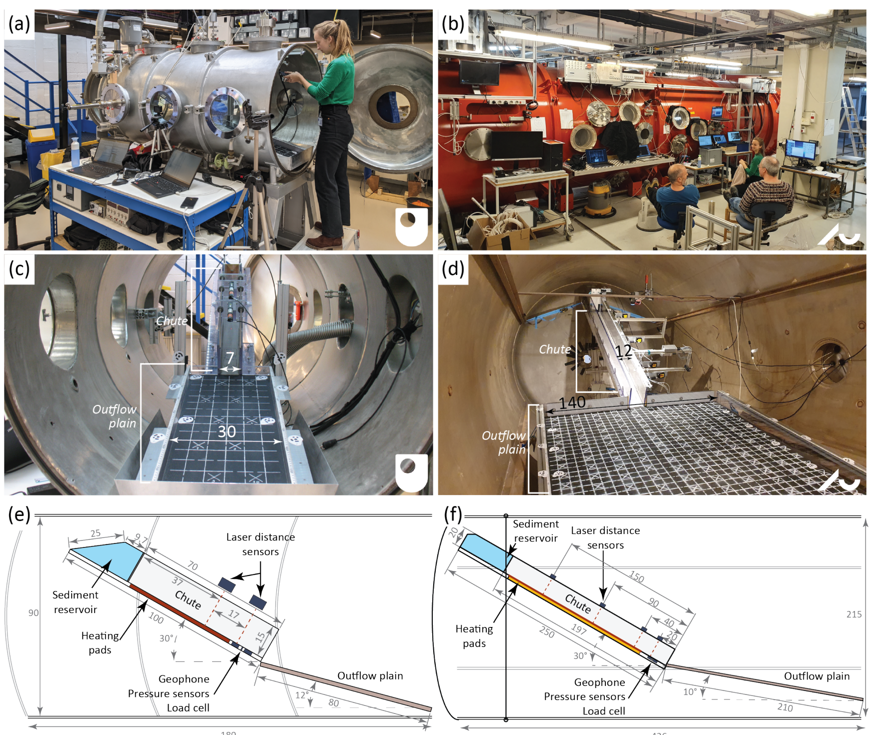
(a)
(b)
(c)
Chute
7
Outflow plain
30
(d)
Chute
12
140
Outflow plain
(e)
25
9.2
Laser distance sensors
70
37
Chute
17
15
Sediment reservoir
90
Heating pads
100
30°
Geophone
Pressure sensors
Load cell
Outflow plain
12°
80
180
(f)
20
Sediment reservoir
Laser distance sensors
150
90
Chute
40
197
250
Heating pads
30°
215
Geophone
Pressure sensors
Load cell
Outflow plain
10°
210
426

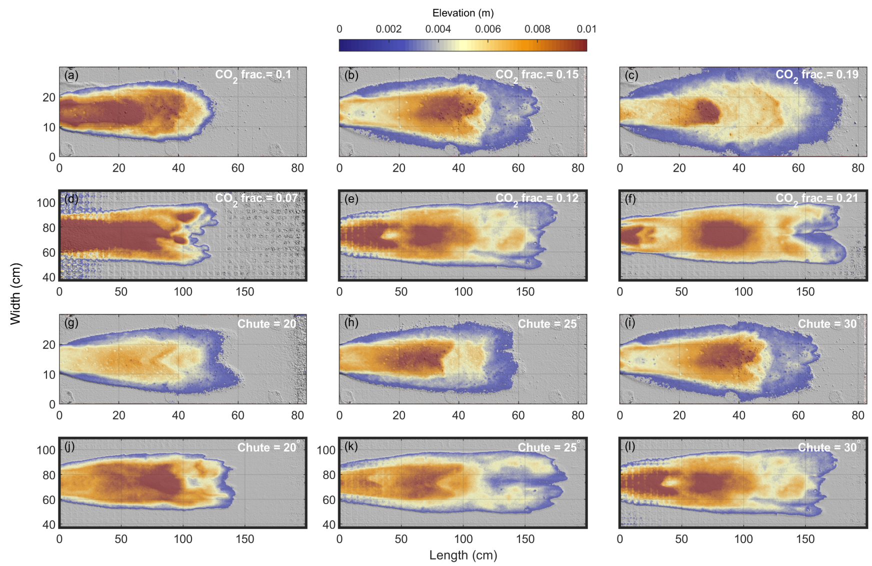

Elevation (m)
0
0.002
0.004
0.006
0.008
0.01
(a) CO2 frac.= 0.1
(b) CO2 frac.= 0.15
(c) CO2 frac.= 0.19
(d) CO2 frac.= 0.07
(e) CO2 frac.= 0.12
(f) CO2 frac.= 0.21
(g) Chute = 20
(h) Chute = 25
(i) Chute = 30
(j) Chute = 20
(k) Chute = 25
(l) Chute = 30
Width (cm)
Length (cm)

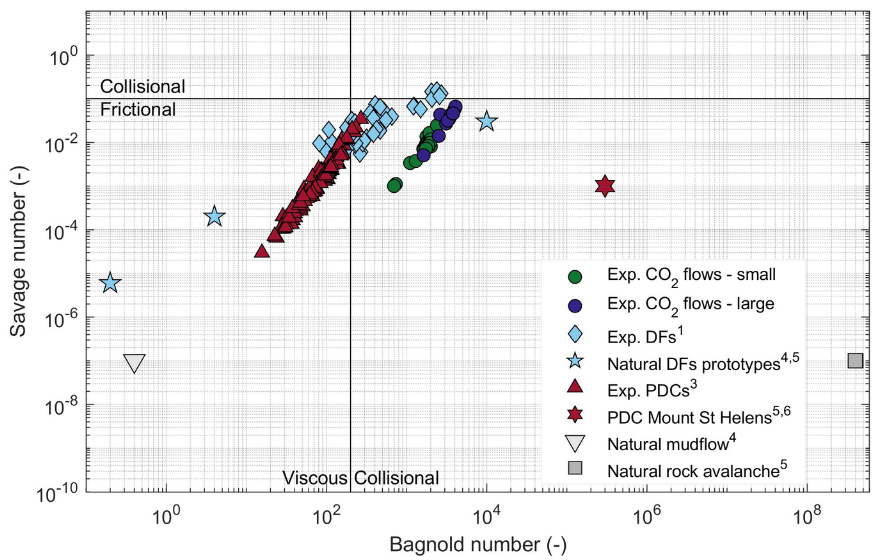

Collisional
Frictional
Viscous
Collisional
Savage number (-)
Bagnold number (-)
Exp. CO2 flows - small
Exp. CO2 flows - large
Exp. DFs1
Natural DFs prototypes4,5
Exp. PDCs3
PDC Mount St Helens5,6
Natural mudflow4
Natural rock avalanche5

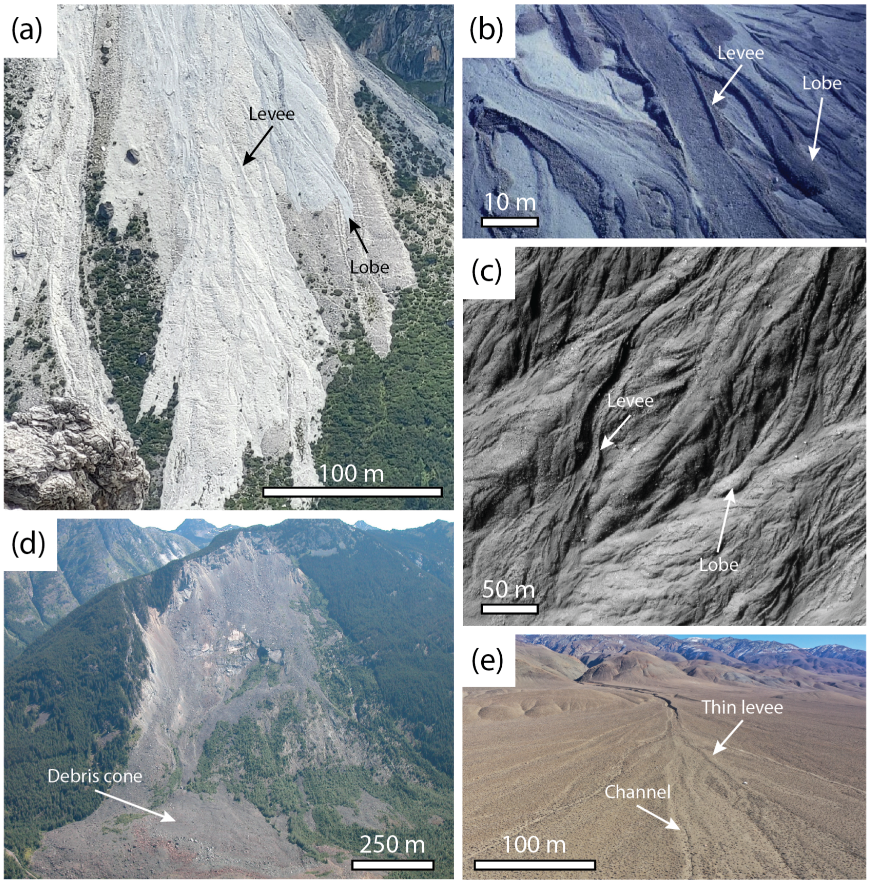
(a)
Levee
Lobe
100 m
(b)
Levee
Lobe
10 m
(c)
Levee
Lobe
50 m
(d)
Debris cone
250 m
(e)
Thin levee
Channel
100 m

The dynamics of CO_2-driven granular flows in gullies on Mars

Lonneke Roelofs [1], Susan J. Conway [2], Bas van Dam [1], Arjan van Eijk [1], Jonathan P. Merrison [3], Jens Jacob Iversen [3], Matthew Sylvest [4], Manish R. Patel [4], Henk Markies [1], Marcel van Maarseveen [1], Jim McElwaine [5], Maarten G. Kleinhans [1], Tjalling de Haas[1]

[1]Department of Physical Geography, Faculty of Geosciences, Utrecht University, Princetonlaan 8a, 3584 CB Utrecht,Netherlands
[2]Nantes Université, Univ Angers, Le Mans Université, CNRS, Laboratoire de Planétologie et Géosciences, LPG UMR 6112, 44000 Nantes, France
[3]Mars Simulation Laboratory, Aarhus University, Ny Munkegade, Bygning 520, 8000 Århus C, Denmark
[4]School of Physical Sciences, The Open University, Milton Keynes, United Kingdom
[5]Department of Earth Sciences, Durham University, Durham, United Kingdom

Key Points:

- The sublimation of small amounts of CO_2 ice can fluidize granular material on low slopes under Martian atmospheric pressure.
- The flow dynamics of CO_2-driven flows are similar to that of terrestrial fluidized two-phase flows, e.g. debris flows and dense pyroclastic flows.
- Experimental CO_2-driven granular flows create deposit morphologies similar to those observed in Martian gullies.

Corresponding author: Lonneke Roelofs, `l.roelofs@uu.nl`

Abstract

Martian gullies are landforms consisting of an erosional alcove, a channel, and a depositional apron. A significant proportion of Martian gullies at the mid-latitudes is active today. The seasonal sublimation of CO_2 ice has been suggested as a driver behind present-day gully activity. However, due to a lack of in-situ observations, the actual processes causing the observed changes remain unresolved. Here, we present results from flume experiments in environmental chambers in which we created CO_2-driven granular flows under Martian atmospheric conditions. Our experiments show that under Martian atmospheric pressure, large amounts of granular material can be fluidized by the sublimation of small quantities of CO_2 ice in the granular mixture (only 0.5% of the volume fraction of the flow) under slope angles as low as 10°. Dimensionless scaling of the CO_2-driven granular flows shows that they are dynamically similar to terrestrial two-phase granular flows, i.e. debris flows and pyroclastic flows. The similarity in flow dynamics explains the similarity in deposit morphology with levees and lobes, supporting the hypothesis that CO_2-driven granular flows on Mars are not merely modifying older landforms, but they are actively forming them. This has far-reaching implications for the processes thought to have formed these gullies over time. For other planetary bodies in our solar system, our experimental results suggest that the existence of gully-like landforms is not necessarily evidence for flowing liquids but that they could also be formed or modified by sublimation-driven flow processes.

Plain Language Summary

Martian gullies are landforms that look like landforms carved by aqueous debris flows on Earth. At the top, the gullies have an erosional alcove where material is eroded and at the bottom of the gully, a fan exists where the eroded material is deposited. For a long time, it was believed that these gullies were formed by liquid water, just like on Earth. However, the Martian gullies are active today, which cannot be reconciled with the low atmospheric pressure and resulting lack of liquid water on the surface of Mars. Data from satellites has shown that the activity in Martian gullies is correlated to a seasonal cycle of CO_2 ice deposition and sublimation. However, these observations are indirect, and therefore, we do not know whether and how CO_2 sublimation produces the observed changes in gullies. Here we show the results of flume experiments in environmental chambers in which we created CO_2-driven flows under Martian atmospheric conditions. The experiments show that granular material can be fluidized by sublimation of CO_2 ice. Furthermore, the experimental flow dynamics and morphology of the deposits are similar to debris flows and pyroclastic flows on Earth. This explains the similarity between the Martian gullies and the water-shaped gullies on Earth without the presence of liquid water on the surface of Mars today. These results also suggest that gully landforms on other planets can be formed by both sublimation-driven flows and fluid-driven flows.

1 Introduction

Despite the lack of stable liquid water on Mars today (Hecht, 2002; Richardson & Mischna, 2005), Mars is a geomorphologically active planet. Numerous studies in the last decades have documented a range of geomorphic activities (for an overview see (Diniega et al., 2021)). Among the most active landforms on Mars are Martian gullies (Figure 1). These landforms consist of an erosional alcove, a channel, and a depositional apron and resemble debris flow systems on Earth (Malin & Edgett, 2000; Costard et al., 2002; Conway et al., 2011; Johnsson et al., 2014; T. de Haas et al., 2015c). Since their discovery, Martian gullies have been a topic of scientific debate because of the possible link between their formation and liquid water (Malin & Edgett, 2000; Costard et al., 2002; T. de Haas et al., 2015c; Dickson et al., 2023), and thus planetary habitability (Hoffman, 2002; Cottin et al., 2017).

Present-day activity in gullies is observed in subsequent images as new depositional lobes on aprons, the carving of new channels, and the movement of meter-scale boulders (Dundas et al., 2010; Diniega et al., 2010; Dundas et al., 2015; Raack et al., 2020; Sinha & Ray, 2023). As this activity is observed on slopes as low as 10° (Dundas et al., 2019), the material needs to have been fluidized to a certain degree (T. de Haas et al., 2019) and thus dry granular processes cannot have been the cause of the change. In the last decade, the leading hypothesis behind the recent activity in these gullies has shifted from water-driven flows (with or without the involvement of brines) (e.g., Malin & Edgett, 2000; Costard et al., 2002; Knauth & Burt, 2002; Lanza et al., 2010; Levy et al., 2010; Conway et al., 2011; Johnsson et al., 2014; T. de Haas et al., 2015c) to flows driven by the sublimation of CO_2 frost (e.g., Diniega et al., 2010; Dundas et al., 2010, 2012, 2015; Raack et al., 2015, 2020; Pilorget & Forget, 2016; T. de Haas et al., 2019; Khuller et al., 2021; Dundas et al., 2022; Pasquon et al., 2023; Sinha & Ray, 2023). This shift is inspired by the lack of stable water on the Martian surface (Hecht, 2002; Richardson & Mischna, 2005) and a suite of remote sensing studies, showcasing the correlation between the spatial and temporal distribution of gully activity with that of CO_2 frost on the surface of Mars (Diniega et al., 2010; Dundas et al., 2010, 2012, 2015; Raack et al., 2015; Pasquon et al., 2019; Raack et al., 2020; Khuller et al., 2021; Dundas et al., 2022; Pasquon et al., 2023; Sinha & Ray, 2023) (for examples see Figure 1). The CO_2-driven granular flow hypothesis is supported by modelling studies advocating for the possibility of CO_2 gas to fluidize granular material under the thin Martian atmosphere when CO_2 sublimates (Pilorget & Forget, 2016; Cedillo-Flores et al., 2011; T. de Haas et al., 2019). Furthermore, experimental studies have proven that the sublimation of CO_2 ice in the thin Martian atmosphere can destabilize granular materials on slopes (Sylvest et al., 2016, 2019) and even fluidize small volumes of granular material on low angles (Roelofs et al., n.d.). The low atmospheric pressure of the Martian atmosphere is key in this process because of the large gas flux that is created when CO_2 ice sublimates and turns into CO_2 gas (Diniega et al., 2013; Sylvest et al., 2016; T. de Haas et al., 2019; Sylvest et al., 2019; Roelofs et al., n.d.). The gas flux, induced by the sublimation, depends on the ratio between the density of CO_2 ice and gas. In the thin Martian atmosphere (∼800 Pa), the gas flux created by CO_2 sublimation is >100 larger than under Earth's atmosphere and thus likely sufficient to fluidize sediments (Cedillo-Flores et al., 2011; T. de Haas et al., 2019).

There are currently two "source-to-sink" hypotheses that attempt to explain how and why CO_2 ice sublimates near granular material on Mars, how this process mobilizes the granular material, and how it transports it over longer distances. The first hypothesis considers a layer of translucent CO_2 ice on top of a layer of regolith (Pilorget & Forget, 2016). This hypothesis is, in essence, the 'Kieffer model' explaining the formation of high-latitude defrosting spots (Kieffer, 2007) on a slope. According to this model, the translucency of CO_2 ice allows the solar radiation at the end of winter to heat up the underlying regolith during the day. This heat causes basal sublimation of the overlaying ice layer, building up the air pressure underneath the ice. This pressure can be large enough to lift the ice layer and eventually break it, forming jets of pressurized CO_2 gas (Hoffman, 2002; Kieffer, 2007). The gas flux created can potentially destabilize large amounts of slope material, also underneath the ice (Pilorget & Forget, 2016). However, the requirement of slab ice means that the latter mechanism is only applicable to Martian gullies at latitudes > 40°S where evidence for slab ice is observed (Dundas et al., 2017, 2019), whereas half of the observed active gully sites on the southern hemisphere are present at latitudes < 40°S (Dundas et al., 2022). Furthermore, this hypothesis does not explain how the pressurized flows underneath a layer of CO_2 ice would result in the deposition of new lobate deposits and the movement of meter-scale boulders.

The second hypothesis explains the observations of fluidized granular flow via two effects within a mix of sediment and CO_2 ice tumbling down a gully (Dundas et al., 2017). The initial mass movement can be triggered by many different processes, unrelated and related to CO_2 ice sublimation, for example, dry raveling, rock fall, marsquakes, meteor impacts or CO_2 sublimation-induced slumping (Sylvest et al., 2016, 2019). In the event that a mixture of CO_2 ice and granular material starts to move, the potential energy of the fall is converted to kinetic energy that must be dissipated as heat or latent heat loss in the form of sublimating CO_2 (Dundas et al., 2017; T. de Haas et al., 2019; Roelofs et al., n.d.). Furthermore, eroded and entrained sediment from the shallow subsurface or unfrosted areas could add additional heat to the mixture, enhancing sublimation (Hoffman, 2002; Dundas et al., 2017). The sublimation of the ice in the sediment-ice mixture is hypothesized to create a gas flux large enough to decrease intergranular friction and fluidize the mixture in such a way that it explains recent flows (T. de Haas et al., 2019; Roelofs et al., n.d.).

Details aside, all current theories on the CO_2-driven fluidization of granular material on Mars agree on two crucial points; (1) heat is needed to sublimate the CO_2, and (2) increased pore pressure, from the CO_2 gas, in the granular material is crucial to decrease intergranular friction and cause fluidisation. However, major research questions remain unanswered. First, it remains speculative whether and exactly how the sublimation of CO_2 ice is able to fluidize granular material. Second, it is unknown how much CO_2 ice needs to sublimate to explain the observed changes. Third, it is unclear how CO_2-driven granular flows on Mars create landforms that are practically identical to landforms created by water-driven debris flows on Earth. Active depositional aprons on both Earth and Mars show lobate deposits with clear levees, and contain meter-scale boulders that are transported through the gully system (T. de Haas et al., 2019; Raack et al., 2020; Dundas et al., 2022). The similarity in key elements in these landforms suggests similarity in the flow dynamics, but this remains unproven.

In this work, we experimentally study the fluidization of granular material by CO_2 ice sublimation under Martian conditions. We aim to (1) resolve the boundary conditions needed to fluidize granular material by CO_2 ice sublimation on Mars, (2) understand the fluid dynamics of CO_2-driven granular flows, and (3) understand the similarities between the CO_2-driven granular flow deposits on Mars and debris-flow deposits on Earth.

To overcome the lack of in-situ observations of CO_2-driven granular flows, we designed two experimental granular flow set-ups that were used to conduct experiments under Martian atmospheric pressure in environmental pressure chambers. In these experiments, granular flows driven by the sublimation of CO_2 in a mixture of sediment and CO_2 ice were created under different boundary conditions, i.e. CO_2 content and slope, and on two different scales to understand potential scale effects. The results of these experiments provide new insights into the flow dynamics of CO_2-driven granular flows on Mars and the resulting deposit morphologies. It is important to note that with our research we specifically aim at studying the transport and deposition processes of CO_2-driven granular flows, rather than the initiation mechanisms behind these flows.

2 Materials and Methods

To study if and how a mixture of CO_2-ice and granular material is fluidized under Martian atmospheric conditions we designed two experimental set-ups at two different scales based on terrestrial debris flow flumes (Iverson et al., 2010; T. de Haas et al., 2015b; Roelofs et al., 2022). The flumes were placed in two environmental chambers of different sizes to enable us to conduct experiments under Martian atmospheric conditions (Figure 2.a–b). Similar to terrestrial debris flow flumes, our flumes consisted of a steep and narrow chute ending on a larger outflow plain with a lower angle (Figure 2.c–f). The steep and narrow chute is used to study flow characteristics, e.g. flow depth, velocity, and pore pressures. Whereas the larger plain is used to study deposit morphology. The angle of the chute was varied during our experiments, whereas the angle of the outflow plain was kept constant (Figure 2.e–f). As is common practice in debris flow experiments, we stored the material that makes up the granular flow in a reservoir at the top of the flume before controlled release. Using flumes of two different sizes enabled us to study possible scaling issues known to influence the behaviour of experimental terrestrial debris flows (Iverson, 2015). The small-scale flume has a total length of 1.80 m and has a material reservoir that can store between 1.0 and 1.6 kg of material (Figure 2.e). The large-scale flume has a total length of 4.60 m and has a material reservoir that can store between 8.0 and 11.2 kg of material (Figure 2.f). This means that, while the large flume is only a factor 2.5 longer than the small flume, the granular flow it supports is 10 times larger.

The small-scale flume was used for conducting experiments in the Mars chamber of the Hyper Velocity and Impact lab (HVI-lab) at the Open University in Milton Keynes in the United Kingdom in the autumn of 2021. The large-scale flume was used for conducting experiments in the Mars Simulation Wind Tunnel at Aarhus University in Denmark in the autumn of 2022. To compare results between the flumes, experiments were performed with similar initial and boundary conditions. In this manuscript, 46 experiments conducted in the small-scale set-up in the Mars chamber of the Open University are presented, and 15 experiments conducted in the large-scale set-up in the Mars Simulation Wind Tunnel are presented.

2.1 Chamber and flume details

The Mars chamber of the HVI-lab at the Open University is a cylindrical low-pressure chamber with a length of 2 m and an inner diameter of 0.9 m (Conway et al., 2011; Sylvest et al., 2016) (Figure 2.a). The chamber can replicate Martian atmospheric conditions and a range of different temperatures.

The Mars Simulation Wind Tunnel at Aarhus University is a cylindrical low-pressure wind tunnel, originally designed to simulate eolian transport processes on Mars (Holstein-Rathlou et al., 2014) (Figure 2.b). The chamber has a total length of 8 m and an inner diameter of 2.15 m. In both chambers, electrical and mechanical feedthroughs exist to enable the operation of the experimental set-up in the chamber from the outside. Both chambers have multiple porthole windows that allow for videography of the experiments.

Both the large-scale and the small-scale flume were mostly constructed out of Lexan, a transparent polycarbonate resin thermoplastic, that can deform considerably without cracking or breaking. The transparency of the Lexan was an important design prerequisite because it allowed us to study the granular flow from the side of the chute. The bottom of the chute was created out of aluminium, with heating pads installed underneath it that controlled the temperature of the chute bottom, which was kept at 20 °C during the experiments. On the edges of the outflow plain, markers were attached that were used for creating 3D models of the outflow morphologies using photogrammetry with Agisoft Metashape software. The outflow plains of the flumes were further covered with antislip material (3M Safety-Walk 500 series, equal to 80 grit sandpaper with 0.2 mm median sand diameter) to mimic natural roughness. To achieve the same for the chute bottom, the aluminium was sandblasted. The sediment and ice reservoirs on top of the flumes were constructed out of copper for the small set-up, and out of aluminium for the large set-up, because of their relatively low deformation under low temperatures. The reservoirs in both flumes are opened by means of mechanically operated trap doors. In the small-scale flume the entire reservoir opened at once, whereas in the large-scale flume, the opening height was set at 5 cm. This difference in design allowed a more constant and stable flow of granular material in the large-scale experiments, providing better insight into the flow dynamics.

In both flumes, the same sensors were used to study the flow dynamics. In the downstream part of the chute, four sensors were installed underneath the chute bottom plate (Figure 2.e-f); a geophone (Geospace GS-20DX), two relative gas pressure sensors (Honeywell TruStability HSCDRRD006MGAA5), and a load cell (HBM PW6D – 3 kg). The geophone and the load cell were attached to individual load plates of 5 by 5 cm. The geophone recorded seismic vibrations during the experiment, the pressure sensors recorded the gas pressure at the bottom of a flow relative to the ambient pressure, and the load cell recorded the weight of the granular material as the flow passed. Above the flume, multiple laser distance sensors (Baumer OADM 20U2480/S14C) were installed that recorded the flow depth at sub-mm accuracy. In the small-scale set-up two laser distance sensors were used, whereas in the large-scale set-up, four laser distance sensors were used. With the time difference of the arrival of the flow front at the different laser distance sensors, reconstructed from the flow depth data, flow velocity was calculated. In both set-ups, the last laser distance sensor was installed above the load cell (Figure 2e-f). This allowed us to reconstruct the density of the flow, ρ_m, according to:

$$\rho_m = \frac{M}{AH} \tag{1}$$

where M is the mass recorded by the load cell (kg), A is the area of the load cell (m^2), and H is the flow depth (m). Furthermore, by combining the load cell data and the data from the pore pressure sensors, the percentage of the material in the flows carried by the gas pressure could be quantified. The latter is a measure of the degree of fluidisation. For more detailed photos of the chambers, the flumes and the sensors see Supplementary Figure 1.

The amount of CO_2 ice sublimating during the flow in the large-scale set-up could be calculated from the data produced by a capacitance pressure sensor in the Mars Simulation Wind Tunnel. By adding the pressure drawdown caused by the pumping to the observed pressure increase during the experiment we reconstructed the amount of CO_2 released into the chamber during the flow for three individual experiments with varying amounts of CO_2 ice in the granular mixture (Figure 7).

Multiple video cameras were installed in and around both chambers. For the small-scale set-up, every experiment was recorded with a Go-Pro camera from the side and a camcorder from the front. For the large-scale set-up, every experiment was recorded with two webcams in the chamber that looked at the chute from the side, and one high-speed camera that filmed the flow at the transition from the chute to the outflow plain at a frame rate of 600 Hz.

2.2 Materials used and experimental routine

Two materials form the ingredients of the granular mixture in our experiments; sand and CO_2 ice. The sand for the experiments is a mixture of fine-grained sand (silver sand of marine origin, D_{50} of 270 μm) and coarse-grained sand (builders sand of fluvial origin, D_{50} of 490 μm), combined in a specific ratio (0.6–0.4) to create a broad grain size distribution (D_{50} of 310 μm, Supplementary Figure 2) that minimizes gas permeability relative to a mono-disperse sand, and thus slows down the gas escape rate. Experiments conducted with only silver sand or only builders sand behave similarly overall, although finer mixtures flow further onto the outflow plain. Results of these experiments are presented in the Supplementary Material (see Supplementary Figure 6). The sand was predried in the oven and cleared of any excess moisture in the environmental chambers by putting it in a vacuum prior to the experiments.

The CO_2 ice used for our experiments was ordered in pellet form from commercial parties close to the labs. The CO_2 ice pellets were then crushed to the size of the coarsest sand grains. For the small-scale experiments, this was done by hand with the use of a mortar and pestle. For the large-scale experiments, the ice was crushed with the KitchenAid 5KGM grain mill. Despite the difference in methods, the resulting CO_2 ice grains are similar in size and shape (see Supplementary Figure 3.c-d). To limit the contamination of the CO_2 ice with water, the CO_2 ice was stored in closed polystyrene foam containers in a sealed freezer (Supplementary Figure 3.a-b), and the ice was refreshed at least once a week.

For every experiment, CO_2 ice would be freshly crushed and mixed with a specific amount of sand. To control the amount of CO_2 ice at the start of an experiment, the combined weight was monitored during the mixing process. The loss of CO_2 due to sublimation was compensated by adding more crushed CO_2 ice. Once the desired weight ratio of sediment and CO_2 ice was reached, the mixture was poured into the sediment-ice reservoir in the flume. After this, the chamber was closed and depressurized to an atmospheric pressure of $\sim$8 mbar, a process that took between 12–15 min in the Mars Chamber at the Open University and between 20–25 min in the Mars Simulation Wind Tunnel at Aarhus University. At this pressure, the mixture was released into the flume, while the sensor data was logged and the videos recorded the passing of the granular flow.

2.3 Explored parameter-space

To determine the conditions under which CO_2-driven granular flows can occur on Mars, experiments were conducted under different initial and boundary conditions. For both the experiments in the small-scale and the large-scale set-up, the CO_2-sediment ratio was systematically varied, as well as the slope of the chute. The CO_2-sediment ratio was varied between 0 and 0.6 in the small-scale experiments and varied between 0 and 0.4 for the large-scale experiments (Table 1), while keeping the flume chute at a stable angle of 30°. Note that the mass ratio here is the ratio between the mass of the CO_2 and the sediment before depressurization of the chamber. During depressurization the CO_2 sublimates, which causes the mass ratio to change. We quantified this change for both the small- and large-scale setup by doing initial tests tracking the weight of the mixture inside the sediment-ice reservoir while depressurizing the chamber. The results of these tests can be found in Supplementary Figure 4. In the subsequent sections of this manuscript, we switch from using the initial CO_2-sediment mass ratios to using the mass fraction of CO_2 at the start of an experiment derived from these tests.

Table 1. Parameters explored in the experiments and the tested values. All parameters and values reported in this table are tested in the small-scale setup. The values of the parameters in bold font and teal colour are the ones also tested in the large-scale setup. For more details on the grain-size distributions see Supplementary Figure 2. For a full list of all experiments see Supplementary material.

Variable	Unit	Standard value	Tested values
CO_2-sediment ratio	(kg/kg)	0.3	**0**, 0.1, **0.2**, **0.3**, **0.4**, 0.5, 0.6
Chute angle	°	30	**20**, **25**, **30**
Sediment type		Sand mixture	**Sand mixture**, Fine, Coarse
Atmospheric pressure	mbar	8	**8**, 1000

The angle of the chute was varied between 20 and 30 degrees in both the small-scale and the large-scale experiments (Table 1), while keeping the initial CO_2-sediment mass ratio at 0.3. In the small-scale experiments, we did additional tests with different sediment types and under Earth atmospheric pressure (Table 1). To account for the effects of natural variability, each experimental setting was repeated at least twice, and when time allowed three times. A complete list of all experiments and their initial and boundary conditions can be found in the Supplementary material 8.

2.4 Flow characterization

To characterize the dynamics of the CO_2-driven granular flows and objectively compare the flows of different sizes three dimensionless numbers are used; the Bagnold, Savage, and friction numbers. These numbers are used in both debris flow (Iverson, 1997; Iverson & Denlinger, 2001; Roelofs et al., 2022, 2023) and pyroclastic literature (Smith et al., 2020) and therefore also allow for comparison between the CO_2-driven granular flows, and terrestrial debris flows and pyroclastic flows. The numbers describe the relationship between the motion-resisting forces in granular flows; collisional forces, frictional forces, and viscous forces (Iverson, 1997; Parsons et al., 2001; Iverson et al., 2010). The relative importance of these forces plays a big role in both erosional (T. d. de Haas & Woerkom, 2016; Roelofs et al., 2022) and depositional processes (T. de Haas et al., 2015b; Zhou et al., 2019) and is, therefore, an important tool in understanding how certain flows lead to certain morphological features. The Bagnold number describes the ratio between collisional and viscous forces (Iverson, 1997):

$$Nb = \frac{v_s \rho_s \delta^2 \gamma}{v_f \mu} \tag{2}$$

wherein v_s is the volumetric solids fraction, ρ_s is the density of the sediment grains, δ is the D_50 grain size of the sediment (m), v_f is the volumetric fluid fraction, μ is the dynamic viscosity of CO_2 gas under Martian atmospheric conditions, which is $9.82{*}10^{-6} Ns/m^2$ (Bardera et al., 2020), and γ is the flow shear rate ($1/s$):

$$\gamma = \frac{u}{H} \tag{3}$$

wherein u is the is the flow velocity (m/s). According to Iverson (1997), collisional forces dominate at $N_b > 200$.

The Savage number quantifies the ratio between collisional and frictional forces:

$$N_s = \frac{\rho_s \delta^2 \gamma^2}{(\rho_s - \rho_f) g H \tan\phi} \tag{4}$$

wherein g is the gravitational acceleration (m/s^2), ρ_f is the density of the fluid, in our case this is the density of the CO_2 gas at 8 mbar, and ϕ is the internal angle of friction, assumed to be 42° (Parsons et al., 2001; T. de Haas et al., 2015b). The density of the CO_2 gas at a certain pressure can be calculated from the ideal gas law:

$$\rho_f = \frac{P M_m}{RT} \tag{5}$$

wherein P is the atmospheric pressure (Pa), M_m is the molar mass of CO_2, R is the universal gas constant, and T is the temperature (K). For $N_s > 0.1$ collisional forces dominate viscous forces (Iverson, 1997). The friction number is then defined as the Bagnold number divided by the Savage number, describing the ratio between frictional and viscous forces. According to experimental data of wet experimental debris flows of Parsons et al. (2001) and T. de Haas et al. (2015b) frictional forces dominate over viscous forces at $N_f > 100$ for the flow body and $N_f > 250$ for the flow front.

3 Results

3.1 General flow behaviour and morphology

Increased fluidisation of the material was observed for all experiments under Martian atmospheric pressures with CO_2 ice in the granular mixture. Compared to reference experiments without CO_2 ice, these experiments showed >2 times larger flow velocities and run-out, with typical flow velocities of 2 m/s for the small-scale flows and 3 m/s for the large-scale flows. For both the large-scale and the small-scale experiments, flow depths reached maximum values around 2 cm (Figure 3.a-b), and flow densities around 1000 kg/m^3. The relatively small flow depth in the large-scale experiments was caused by the controlled, and limited, outflow height in this setup. In both set-ups, the flow depth increased rapidly when the flow front arrived and dissipated more slowly when the tail passed. In experiments without CO_2, as soon as the flow front arrived at the outflow plain the flow stopped and the chute backfilled with sediment.

Both the small-scale and large-scale CO_2-driven granular flows show multiple surges (see Figure 3.a-b and the Supplementary videos). For all flows with CO_2 in the mixture, increased gas pressures were registered at the base of the flow (Figure 3.a-b). This gas pressure carried between 20–60% of the flow mass, independent of the experimental scale (Figure 3.c). When analysing the high-speed video of the experiment presented in Figure 3.a it becomes clear that the velocity of the granular flow is highest in the centre of the flow and that the flow itself is turbulent (see high-speed video in Supplementary videos).

The morphology of the outflow deposits of experiments with CO_2 in the granular mixture often contain multiple lobes formed by different surges (Figure 4). These lobes are stacked on top of each other (see for example Figure 4.c,l), and, in some cases, next to each other (see for example Figure 4.f,k). In both the small-scale and large-scale set-up levees form in experiments where a second surge of granular material deposits on top of an earlier surge (see Figure 4.b,f). With increased amount of CO_2 in the granular mixture the material flows further out onto the outflow plain (Figure 4.a–f). Increasing the chute slope by 5–10°also causes the material to flow further onto the outflow plain (Figure 4.g–l). In the large-scale experiments, a small increase in slope has a larger effect on the outflow length than doubling the CO_2 content (Figure 4.d–f and Figure 4.j–l). When no CO_2 is present in the granular mixture only a small sediment cone forms on the transition from the chute to the outflow plain.

3.2 Flow velocity, depth, and pore pressure

In the large-scale set-up, flow velocities in the lower half of the chute are constant (Supplementary Figure 5) and reach values around 3 m/s, independent of the CO_2 fraction (Figure 5.a). In the small-scale set-up, for high CO_2 fractions between 0.14 and 0.3, flow velocities around 2 m/s are recorded at the end of the chute, whereas for the lower CO_2 fractions the velocity slowly increases from 1 m/s to 2 m/s with increasing CO_2 fraction. When no CO_2 is present in the granular mixtures, no enhanced fluidisation is observed and the frontal velocity of the material is around 1 m/s in both set-ups. The same can be stated for granular flows with CO_2 in the mixture released under Earth atmospheric pressure. For both the large-scale and small-scale flows, an increase in the chute angle, from 20° to 30°, causes a small increase in flow velocity, from 2.2 to 3 m/s (Figure 5.b).

Maximum flow depth increases linearly with CO_2 mass fraction for both set-ups (Figure 5.c). This relation is steeper for the small-scale set-up. When increasing the chute angle, maximum flow depth decreases in the large-scale set-up from 22 to 14 mm, while staying around 15 mm in the small-scale set-up (Figure 5.d). Flow depths are stable in the lower half of the large-scale flume for all experiments (Supplementary Figure 5). In the small-scale flume, the flow depths are still increasing in the lower half of the flume, especially when the chute is on the steepest angle.

Increased basal pore pressures are observed in all experiments. Basal pore pressures increase with increasing CO_2 mass fraction and decrease with increasing chute slope (Figure 5.e-f). The differential pressure signal, which is the difference between the ambient pressure and the basal pressure, is more scattered for the small-scale experiments. This is likely caused by the combination of smaller, less stable flows, and a higher amount of deposition of granular material in the chute during the experiment compared to the large-scale set-up. Maximum added pressures in the large-scale set-up vary between 0.2 and 0.6 mbar, whereas they vary between 0 and 0.4 for the small-scale set-up.

The type of granular material used, either silver sand, builders sand, or the mixture, did not significantly influence the flow dynamics of the flows in the small-scale set-up (Supplementary Figure 6). Frontal velocities, maximum flow depths, and maximum basal pressure were the same for all sand types. The type of granular material used did influence the outflow deposit. CO_2-driven granular flows comprised of finer sands flowed out further.

3.3 Flow density, fluidisation and CO_2 sublimation during the flow

The density of the flow is calculated from the weight data from the load cell and the depth data from the laser distance sensor above the load cell. In addition, the load cell data and the data from the pore pressure sensors are combined to calculate the percentage of the material in the flows carried by the gas pressure. Here, we only present results from the large-scale experiments, because it was not possible to calculate flow density and degree of fluidisation for the experiments in the small-scale set-up due to the deposition of material on the load cell while the granular material was still flowing. Based on the combined data of the entire flow of all large-scale experiments, summarised in boxplots in Figure 6.a–b, we can state that our experimental CO_2-driven flows have a density around 1000 kg/m^3. This density is not dependent on the CO_2 fraction (Figure 6.a) but is slightly dependent on the chute angle (Figure 6.b). If the angle becomes steeper, the density decreases slightly. The fraction of the flow mass supported by the gas pressure ranges between 0.2–0.3 on average, with a small dependency on CO_2 mass fraction (Figure 6.c–d). For flows with a higher CO_2 fraction, a slightly higher percentage of the flow is supported by the gas pressure (Figure 6.c).

The data from the capacitance pressure sensor in the chamber of the large-scale set-up shows that for an experiment with a CO_2 mass of 0.59 kg at the beginning of the experiment (Supplementary Figure 4), only 42 grams of CO_2 sublimates during the flow (Figure 7.a). For an experiment with a CO_2 mass of 1.12 kg at the beginning of the experiment (Supplementary Figure 4), only 57 grams of CO_2 sublimates during the flow (Figure 7.b). For an experiment with a CO_2 mass of 2.13 kg at the beginning of the experiment (Supplementary Figure 4), only 92 grams of CO_2 sublimates during the flow (Figure 7.c). This means that for all experiments between 0.8–1.3% of the total flow mass (sand and CO_2 ice), and 0.5–0.9% of the volume (assuming a porosity of 0.4) sublimates. When normalized for chute length, width, and flow duration, the volume loss is 0.3%–0.55% per m^2/s, and the mass loss is 0.025–0.055 kg/m^2/s.

3.4 Dimensionless flow characteristics

To quantitatively compare the flow dynamics of the large-scale and small-scale granular flows, we characterized the flows using the dimensionless numbers discussed in the methods; the Bagnold, Savage, and friction numbers (Figure 8). Furthermore, this dimensionless analysis provides the opportunity to place the flow dynamics of the CO_2-driven granular flows into the context of other granular flows, such as debris flows and pyroclastic flows. In all of our experimental CO_2-driven granular flows, frictional forces dominated over collisional and viscous forces (Figure 8.c–f). In addition, the Bagnold numbers of our flows indicate that collisional forces dominated over viscous forces (Figure 8.a–b). The large-scale flows are relatively more collisional than the small-scale flows (Figure 8.a–d). Increasing the CO_2 mass fraction in the granular mixture does not have a large effect on the Bagnold or Savage numbers (Figure 8.a–d) . However, it does affect the relation between frictional and viscous forces, making viscous forces less important (Figure 8.e–f). An increase in the angle of the chute results in a larger relative influence of collisional forces (Figure 8.b,d).

4 Discussion

4.1 Initial and boundary conditions for CO_2-driven flows

Our experiments show that granular material can be fluidized by sublimating CO_2 ice under Martian atmospheric conditions (Figure 3 and Figure 5). This is enabled by the low Martian atmospheric pressure of around 8 mbar, which makes the gas flux from sublimation large enough to decrease intergranular friction between the grains and fluidize the granular material (Figure 5) (Cedillo-Flores et al., 2011; T. de Haas et al., 2019). Under terrestrial atmospheric pressure of around 1000 mbar, sublimation of CO_2 ice still occurs, but the gas flux from the ice into the atmosphere is not large enough to decrease intergranular friction and fluidize the granular material. From our experiments, it can be inferred that the fluidisation induced by the sublimation of CO_2 ice grains in a granular mixture can sustain a stable fluidized flow in a channel, i.e. the flume chute, as long as CO_2 ice is present and enough energy is available for sublimation. In our experiments, less than 10% of CO_2 ice in the mixture sublimated while in the chute, implying that the mixture could have likely flowed in a sustained fluidized way in a confined chute with a length of $\sim$10-20 metres.

The fluidisation of the material by the sublimation of CO_2 ice in the chute is reflected in the enhanced frontal flow velocities and increased basal pressures (Figure 5). In experiments under Martian atmospheric conditions, where CO_2 ice is present in the granular mixture, velocities between 2 and 3 m/s are reached, whereas frontal velocities in experiments without CO_2 ice, or with CO_2 ice under Earth atmospheric pressure, are only 1 m/s (Figure 5). Furthermore, the pressure data show that the gas pressure carries between 20–60% of the total flow mass in the experiments with CO_2 ice (Figure 3.c and Figure 6).

In the large-scale experiments, stable flow velocities around 3 m/s are reached in the lower part of the chute for all experiments, even for the experiments with the smallest amount of CO_2 ice in the mixture. This implies that for all the different CO_2 ice fractions tested, the rate of fluidisation is high and comparable, which is supported by only small differences in the amount of the flow carried by the pore pressure (Figure 6). Therefore, we hypothesise that granular material can be fluidized by the sublimation of even smaller amounts of CO_2 ice than we tested. In the small-scale experiments, we do see an increase in flow velocity and fluidisation rate for the smallest CO_2 ice fractions (Figure 5.a), which would imply a higher fluidisation rate for larger CO_2 ice fractions. However, we hypothesize that this trend is likely caused by the limited length of the chute compared to the distance over which the flow accelerated, instead of an actual relation between CO_2 fraction and velocity in our small-scale set-up. The longer chute length in our large-scale set-up allows the flow to reach a stable state where a balance exists between CO_2 ice sublimation, the reduction in friction because of the induced gas pressure, and the remaining friction, as we see in the large-scale set-up.

Our experiments also show that CO_2-driven granular flows are fluidized enough to flow on slopes below the angle of repose. CO_2-driven flows in experiments with chute angles of 20° still reach velocities 2 times higher than those of dry granular material without CO_2. In addition, the CO_2-driven flows continue to flow over the outflow plain of our set-ups, which have even lower slope angles, 10° and 12° for respectively the large-scale and small-scale set-ups. However, as the flow on these outflow plains is unconfined, the granular material spreads out laterally and ultimately halts (Figure 4). The lateral spreading decreases the flow depth and increases the relative amount of friction the flows have to overcome, both by increasing the area for gas escape and increasing the contact between the flow and the surface. These experimental observations on fluidisation on slopes below the angle of repose are important because they support the hypothesis that CO_2-driven flows on Mars can cause the changes we observe, like new depositional lobes on aprons with slopes as low as 10° to 15° (Diniega et al., 2010; Raack et al., 2020; Sinha & Ray, 2023).

The data from the pressure sensors in the chamber of the large-scale set-up highlight that the mass of CO_2 ice that needs to sublimate for the fluidisation process is small. For example, to fluidize 8 kg of sand in our experiments, as little as 43 gram of CO_2 ice needs to sublimate, equal to ~0.5% of the volume fraction of the flow (Figure 7). In other words, in our experiments, a mass loss of sublimating CO_2 ice between 0.025–0.055 kg/m^2/s is enough to create fluidized granular flows.

4.2 Heat transfer from the environment to the CO_2 ice

Our experiments clearly show that granular material can be fluidized by sublimating small amounts of CO_2 ice, less than 1% of the total flow weight, under Martian atmospheric conditions when sufficient energy is available for CO_2 ice sublimation. However, where that energy is coming from on Mars is debated. According to (Dundas et al., 2017; T. de Haas et al., 2019), this energy could be provided by the release of kinetic energy of a fall or from heat from warmer material in contact with the granular mixture of CO_2 ice and sediment. The sublimating ice would consequently increase pore pressures in the involved granular material, which would cause fluidisation and a two-phase granular flow. If all potential energy of a fall of 300 m, as earlier used by Dundas et al. (2017), would be transferred to heat according to:

$$E_p = mgL \tag{6}$$

with m as the mass of the material falling (kg), g the gravitational acceleration on Mars (3.71 m/s^2), and L being the fall height, the total available potential energy, E_{pot}, would equal to 1113 J per kg material. For our flume set-ups, the total potential kinetic energy is smaller, with 16.7 J/kg in the large-scale set-up and 5.9 J/kg for the small-scale set-up. However, the enthalpy of sublimation of CO_2 ice, which is the energy needed for the phase transition from ice to gas, is around 26–28 kJ/mol (Stephenson, 1987; Cedillo-Flores et al., 2011; Shakeel et al., 2018), which is equal to an energy of 590–636 kJ/kg, accounting for the molecular mass of CO_2 of 44.01 g/mol. Therefore, the amount of energy needed to sublimate CO_2 is much higher than is released from the complete conversion of potential energy to heat, both in our flumes and on Mars. Therefore, we hypothesize, as Dundas et al. (2017) did earlier, that the heat from the environment, thus from warmer material and surfaces in contact with the flow, is the main driver of sublimation instead of kinetic energy conversion.

Granular material at a slightly higher temperature than the CO_2 frost point could make several thousand J/kg available (Dundas et al., 2017). To put numbers to this, for our flumes the energy available in the aluminium bottom plate to sublimate CO_2 ice at the frost point temperature can be calculated as follows:

$$E_t = mc\Delta T \tag{7}$$

with m the mass of the aluminium, c the specific heat (902 J/kgK) and ΔT the temperature difference between the temperature of the chute bottom (20 °C, or 293 K) and the

CO_2 frost temperature (-120 °C, or 153 K). For our small-scale flume E_t is 67 kJ, and for our large-scale flume E_t is 324 kJ. If all this thermal energy is used to sublimate CO_2 ice, between 0.51 and 0.54 kg of CO_2 ice could sublimate in our large-scale set-up and between 0.1 and 0.11 kg of CO_2 ice could sublimate in our small-scale set-up. The predicted mass of CO_2 that could sublimate as a result of heat energy in our large-scale flume is similar to the actual observed mass of CO_2 ice that sublimated during the flows (Figure 7).

Equation 7 can also be used to estimate the amount of potential thermal energy available for sublimation at the bottom of a hypothetical gully on Mars. Taking two gullies in Hale crater, studied by T. de Haas et al. (2019), as an example; we state that our hypothetical Martian gully is incised in basaltic bedrock ($c = 600$ J/kg°C, $\rho_{basalt} = 3000$ kg/m^3), has a length of 600 m, a width of 15 m, and in the gully, the upper 1 mm of the surface regolith is heated up to a temperature of 20 °C, which is realistic for active gullies according to climate modelling (Roelofs et al., n.d.). In this gully system, the total potential thermal energy equals 2.27*10^6 kJ. If all this energy is used to sublimate CO_2 ice, between 3570 and 3840 kg of CO_2 at frost temperature could be sublimated. Suppose we combine the sublimating ice-to-sediment ratio in our experiments, of 0.5-0.9%, with this estimated CO_2-ice mass for extrapolation purposes. In that case, we can estimate that between ∼396000 – ∼769000 kg or ∼247 – ∼480 m^3 of unconsolidated granular material could be fluidized in this Martian gully when enough ice is available. Although this estimate is likely too conservative because it does not account for the weaker Martian gravity and the possible entrainment of warmer sediment, the prediction matches the back-calculated flow volumes of 415 and 263 m^3 in the smaller gullies in Hale crater (T. de Haas et al., 2019).

In general, our experimental granular flow results on thermal energy, flow volume, and the necessary mass of CO_2, agree with the back-calculated numbers for actual Martian flows (T. de Haas et al., 2019). Nonetheless, our predicted $E_{thermal}$ neglects important parameters and processes in thermodynamics. In the first place, it assumes that all heat is converted to energy for sublimation during the flow. This is unlikely because heat transfer does not happen instantaneously and is dependent on the type of heat transfer, the duration of the potential transfer, and the materials involved. The heat transfer process is further complicated by the newly-found turbulent behaviour of CO_2 driven flows, the presence of multiple materials, the unknown areas of contact between the cold ice and the warmer materials, and the possible entrainment of warmer material into the flow (T. de Haas et al., 2019). Furthermore, for experiments, this $E_{thermal}$ does not account for the constant heat input into our flume from heating pads installed underneath the aluminium bottom plate. Despite the still unresolved complications, the predicted thermal energy is multiple orders of magnitude larger than the potential energy transformed from a fall, both in our flumes as in our hypothetical gullies on Mars. The heat energy from the environment, either transferred by conduction, radiation, or convection, is, therefore, more likely to be the cause of the sublimation of the CO_2 ice in CO_2-driven granular flows on Mars. This implies that CO_2-driven granular flows can only occur in gullies on Mars at specific locations and during specific periods during the Martian year when CO_2-ice and warmer regolith simultaneously exist in the gully (Roelofs et al., n.d.).

4.3 Flow dynamics and morphology of CO_2 driven Martian flows in (terrestrial) context

To enable a fair comparison between the flows in the two different experimental set-ups, and compare our CO_2-driven flows with other two-phase granular flows we conducted dimensionless analysis. This analysis shows that the CO_2-driven flows in our experiments are supercritical two-phase flows (see Froude numbers in Supplementary Figure 7) in which frictional forces dominate, and collisional forces are more important than viscous forces (Figure 8). In experimental and real debris flows, frictional forces typically dominate (Iverson, 1997; Iverson & Denlinger, 2001; Roelofs et al., 2022, 2023) (Figure 9). In experimental dense pyroclastic density currents, frictional forces dominate, and viscous forces seem to be more important than collisional forces (Smith et al., 2020) (Figure 9). The latter could stem from the relatively small grain size between 45—90 μm used by (Smith et al., 2020) in their experiments. As far as we found, for only one natural pyroclastic density current the dimensionless numbers are known, and for that specific flow, the collisional forces seem to dominate over viscous forces (Rowley et al., 1981; Iverson & Denlinger, 2001) (Figure 9).

Despite the variation between the relative importance of certain forces between pyroclastic density currents, debris flows and our experimental CO_2-driven granular flows, these different multi-phase flows show similarity in dynamics, especially considering the variability within one flow group. The similarity becomes even more evident when comparing the dynamics of debris flows, dense pyroclastic density currents, and CO_2-driven flows with the dynamics of mud flows or natural rock avalanches (Figure 9). For both natural mud flows and rock avalanches, frictional forces are 10^2–10^6 higher than natural and experimental debris flows, dense pyroclastic density currents, and our CO_2-driven granular flows. In addition, in mud flows, the viscous forces become more dominant over collisional forces than for the other flows, and in rock avalanches, collisional forces become 10^3–10^7 more dominant over viscous forces.

The similarity in the relative influence of different forces in the flow between our CO_2-driven granular flows, and other fluidized multi-phase flows on Earth, is reflected in the similarity in the morphology of the deposits. The deposits of our experiments are lobate in shape, often show splitting of lobes, and sometimes have levees, similar to the hypothesized CO_2-driven granular flow deposits on Mars (Hugenholtz, 2008; Lanza et al., 2010; Levy et al., 2010; Johnsson et al., 2014; Sinha et al., 2018; Conway et al., 2019). These morphological elements are also observed in debris flow deposits (Hubert & Filipov, 1989; Blair & McPherson, 1998; de Haas et al., 2015a, 2018) and pyroclastic flow deposits (Rowley et al., 1981; Lube et al., 2007; Jessop et al., 2012), whereas they are less pronounced in mudflow deposits and absent in rock avalanche deposits (Figure 10). Not all of our outflow deposits contain different distinct lobes or levees, but nor do all recent deposits in gullies on Mars. A lack of levees might indicate a lack of clear grain size segregation, which is believed to contribute to levee formation (Jessop et al., 2012; Johnson et al., 2012; Baker et al., 2016). This could be caused by a more narrow grain size distribution or a relatively smaller influence of collisional forces over viscous forces. The latter can stem from a relatively small median grain size or high shear rates (see equation 2). Another factor that could influence the absence of levees in most of the lobes in our experimental work is the limited amount of surface friction and the inability of pore pressures to dissipate into the substrate and for particles to interact with the substrate. Earlier experimental work on terrestrial debris flows has shown that when experimental debris flows deposit on a layer of permeable sand the formation of levees is promoted (T. de Haas et al., 2015b).

4.4 Scaling and upscaling to Mars

From experiments with debris flows we know that small-scale flows experience larger effects of yield strength, viscous flow resistance, and grain inertia than field size flows (Iverson, 1997; Iverson & Denlinger, 2001; Iverson et al., 2010; Iverson, 2015). In addition, for small-scale experimental debris flows it has been proposed that they are insufficiently affected by pore-fluid pressure (Iverson, 1997; Iverson & Denlinger, 2001; Iverson et al., 2010). However, certain steps can be, and were, taken to overcome these scaling problems and use small-scale experiments for valid representation of real-world phenomena. For example, when scaling for momentum, a steeper slope in granular flow experiments can induce larger flow velocities to combat the effects of a smaller flow mass. Furthermore, it is important to evaluate the validity of experimental findings for the natural world by comparing flow dynamics expressed in dimensionless analysis. From the dimensionless analysis performed and discussed in the section above we can state that our CO_2-driven granular flows behave dynamically similar to debris flows and pyroclastic forms on Earth, both on an experimental and field scale (Figure 9). In addition, our experimental CO_2-driven granular flows show similar flow behaviour to those of back-calculated CO_2 driven flows in Hale crater (T. de Haas et al., 2019), with similar fractions of CO_2 needed for fluidisation, and similar flow velocities around 3 m/s in the steepest parts of the gullies and run-outs on slopes ranging between 13–19°.

The different sizes of the two experimental set-ups allow an assessment of the influence of scaling on CO_2-driven flows. From the dimensionless scaling in Figure 8, we can see that in our large-scale set-up, the collisional forces in the flow are of a higher importance than in the flows in the small-scale set-up. This difference is linked directly to the design of the opening mechanism in the large-scale flume, which limits the flow depth relative to the flow velocity more than in the small-scale flume. Additionally, we see that the friction number of our flows in the large-scale set-up is smaller than those in the small-scale set-up. Although significant differences in the dimensionless numbers between the large- and small-scale flows exist, they are small compared to differences in dimensionless numbers of experimental debris flows in the same flume but of different compositions (Roelofs et al., 2022, 2023) or of experimental pyroclastic density currents in the same flume but for different aeration states (Smith et al., 2020).

To summarize, the flow dynamics and morphology of our experimental CO_2-driven flows are comparable to a variety of natural two-phase flows (Figure 9, Figure 10, and Figure 4) and the influence of scale-effects on our experimental CO_2-driven flows seems to be relatively small. Classical scaling problems in debris flow experiments, related to viscous flow resistance, interstitial fluid, and pore pressures, are of a smaller concern in our CO_2-driven flow experiments because of the scale independence of the CO_2 sublimation process, pore pressure, and flow depth (T. de Haas et al., 2019; Roelofs et al., n.d.), and the low viscosity of the CO_2 gas. Therefore, our findings are of direct relevance to full-scale CO_2-driven flows on Mars.

On Mars the gravitational acceleration is 3.71 m/s^2, and thus 2.6 times smaller than on Earth. This could possibly influence the flow dynamics of CO_2 driven granular flows. We partly accounted for the smaller gravity on Mars by conducting our experiments on multiple slopes, and therefore studying how the changing gravitational component driving our flows would affect the results. However, the most important driver of CO_2-driven flows is the sublimation of the CO_2 frost, which is independent of gravity. The effect of gravity comes into the equation in the form of the weight of the particles in the flow and the speed with which they fall back to the surface. As earlier described by Roelofs et al. (n.d.), the extent to which the flow is suspended is given by a dimensionless group, which describes the ratio of the Darcy pressure $Hq\nu/\delta^2$ to the weight of the flow $Hg\rho_m$;

$$\frac{Hq\mu}{Hg\rho_m d^2} = \frac{q\mu}{g\rho_m \delta^2}. \tag{8}$$

where q is the volume flux of CO_2 in m/s. Here ρ_m and μ are the same for our experiments and Mars while g is different on Mars, but this can be compensated by increasing the grain diameter δ or decreasing the sublimation flux q.

The equation above implies that under Martian gravity only 0.38 of the volume flux of CO_2 is needed compared to Earth to fluidize a flow or that with the same amount of sublimating CO_2 ice significantly larger grains can be transported on Mars. Practically this means that under Martian gravity, if we were to repeat our large-scale experiments, we would be able to decrease the amount of CO_2 used to fluidize 8 kg of sediment over the length of our flume from 42 to 16 g, equal to a volume fraction of $\sim$0.002. This falls in the volume fraction range, 2×10^{-2}–2×10^{-5}, predicted to be needed for recent gully flows in Hale crater (T. de Haas et al., 2019). Furthermore, the sustained fluidisation under varying chute and outflow plain angles gives us the experimental evidence that under a range of gravitational accelerations sublimating CO_2 ice can produce two-phase granular flows.

4.5 Implications for Martian landscape evolution and granular flows in the solar system

From extensive analysis of remote sensing data we know that Martian gullies are active landscape features. Dundas et al. (2019); Pasquon et al. (2019); Dundas et al. (2022); Sinha and Ray (2023) observed erosion and transport of material in gullies, the formation of new terraces and erosion of channel segments, the migration of sinuous curves, channel abandonment, and lobate deposits. Dundas et al. (2019) also observed early stages of gully initiation, suggesting that the processes shaping and changing the gullies today are not merely modifying the pre-existing landforms, but are capable of actively shaping the landscape. Despite these observations, it remains debated what the original formation process of these landforms is. Our experimental results support the hypothesis by Diniega et al. (2010); Dundas et al. (2012, 2015, 2019, 2022) that current activity, by granular flow processes driven by CO_2 sublimation, are actively forming Martian gullies, and are not merely modifying older water-formed features, as suggested by Dickson et al. (2023).

The similarity in flow dynamics and morphology between our experimental CO_2-driven granular flows and natural two-phase granular flows on Earth supports their landscape-changing potential. On Earth, the erodible power of debris flows is suggested to be a primary force in cutting valleys in steep landscapes (Stock & Dietrich, 2003). Although the erodible power of CO_2-driven granular flows has yet to be experimentally explored, the observations of the Martian surface (Dundas et al., 2019, 2022; Sinha & Ray, 2023) and the observed dynamics of the experimental flows leave little doubt that erosion of material by CO_2-driven granular flows is possible. With the current state of remote observations and the lack of detailed in-situ sedimentological and geological investigations, it is impossible to completely rule out a water-driven origin of the Martian gullies. However, we need to be cautious about assuming a water-driven past for the Martian gullies when CO_2-related processes can explain present-day gully activity. As most gullies on Mars were formed during the Amazonian period on Mars, when little to no liquid water could exist on its surface, we deem it likely that the gullies on Mars have been modified and possibly formed by CO_2-related processes for the past 1-3 Ga.

For other planetary bodies in our solar system, our experimental results emphasize that the existence of gully-like landforms is not definite proof of flowing liquids. For example, the observed gully landforms on Vesta (Scully et al., 2015) and Mercury (Rothery et al., 2020) could also have a sublimation-related formation process, especially because of the lack of atmosphere of both bodies. Therefore, our results raise an important question on the use of Earth analogues for planetary science. Earth analogues have been essential in the exploration and understanding of planetary surfaces in our solar systems as well as the potential habitability of these planetary surfaces. Analogue studies are the backbone of our understanding of the processes that shaped the surfaces of rocky planets and bodies throughout our solar system. However, the pitfall of Earth analogue studies is the combined problems of unknown-unknowns and equifinality; the principle describing that different processes can result in the same outcome. Our experimental results could therefore be the start of a fundamental reinterpretation of planetary landforms previously thought to be formed by flowing liquids.

5 Conclusion

We experimentally investigated the feasibility of CO_2-ice sublimation as the driving force in fluidized granular flows on Mars. We conducted 68 experiments under Martian atmospheric conditions in two set-ups on different scales to explore under which boundary and initial conditions granular material can be fluidized by the sublimation of CO_2-ice.

Our experiments show that under Martian atmospheric pressure of 8 mbar, the sublimation of small quantities of CO_2-ice, $\sim$0.5% of the total flow volume, can fluidize large volumes of granular material on a range of different slopes, as long as enough thermal energy is present to initiate the sublimation of the CO_2-ice. Under Martian atmospheric pressure, the sublimation of CO_2-ice in a granular mixture increases the pore pressure within the flow by 0.2-0.6 mbar. This increased pressure carries a significant portion of the total weight of the flow, between 20–60%, which indicates a decrease in granular friction between the grains and a high degree of fluidisation of the mixture. The fluidisation of the material results in large flow velocities that exceed velocities in dry granular flows by a factor 2–3.

Dimensionless analysis of the CO_2-driven flows shows that they are dynamically similar to debris flows and dense pyroclastic density currents on Earth. The flows are supercritical and turbulent in behaviour, and frictional forces dominate over collisional and viscous forces. The similarity in flow dynamics is reflected in the similarity in deposit morphology. Our experimental CO_2 driven flows contain morphological elements, like levees and lobes, that are seen as key characteristics of debris flow and pyroclastic flow deposits. These features are also observed on the depositional aprons of active gullies on Mars. In addition, our findings on flow dynamics and morphology of CO_2 driven flows support the hypothesis that CO_2-driven processes are actively modifying and forming Martian gullies today. Therefore, CO_2-driven processes are not merely modifying older features, but can likely be used to explain the evolution of these landforms on Mars during the Amazonian, when little to no liquid water was present on the surface of Mars.

Furthermore, our calculations highlight the importance of thermal energy in driving the sublimation of CO_2-ice that propels the fluidisation of granular material. Direct thermal energy is a far more effective source of energy for sublimation than the conversion of kinetic and potential energy from a fall to heat. This implies that it is likely that CO_2-driven granular flows can only occur in gullies on Mars at specific locations and during specific periods during the Martian year when CO_2-ice and warmer regolith simultaneously exist in the gully.

Lastly, our experimental results emphasize that the existence of gully-like landforms on planetary bodies is not definite proof of flowing liquids. Gully landforms could also be formed by or at least be altered by sublimation-related processes.

6 Open Research

For all the experiments presented in this manuscript the data collected by the sensors in the flumes and the DEMs of Difference are available via Yoda (online repository of Utrecht University). The data and an instruction on how we processed the raw data can be found under this link: `https://public.yoda.uu.nl/geo/UU01/2T6YAU.html` DOI: 10.24416/UU01-2T6YAU

7 Acknowledgments

LR was supported by the Dutch Research Council (NWO) - grant OCENW.KLEIN.495 to TdH. The visits to the labs were funded by Europlanet - project number 20-EPN-015 to TdH, Europlanet - project number 20-EPN-023 to LR, and partly in-kind by the School of Physical Sciences of the Open University under the leadership of MRP through UK Space Agency Grant ST/X006549/1. We also acknowledge funding from the CNRS INSU

Programme Nationale de Planétologie. SJC is grateful for financial support of the French Space Agency CNES for her HiRISE and CaSSIS work.

Both the Mars Simulation Wind Tunnel laboratory and she Mars chamber of the HVI-lab at the Open University are members of Europlanet (2024) RI and have received funding from the European Union's Horizon 2020 research and innovation programme under grant agreement No 871149.

The authors thank the spacecraft and instrument engineering teams for the successful completion and operation of CaSSIS. CaSSIS is a project of the University of Bern funded through the Swiss Space Office via ESA's PRODEX programme. The instrument hardware development was also supported by the Italian Space Agency (ASI) (ASI-INAF agreement no. I/018/12/0), INAF/ Astronomical Observatory of Padova, and the Space Research Center (CBK) in Warsaw. Support from SGF (Budapest), the University of Arizona (LPL) and NASA are also gratefully acknowledged.

References

Baker, J., Gray, N., & Kokelaar, P. (2016). Particle size-segregation and spontaneous levee formation in geophysical granular flows. *International Journal of Erosion Control Engineering*, *9*(4), 174–178. doi: https://doi.org/10.13101/ijece.9.174

Bardera, R., Sor, S., & García-Magariño, A. (2020). Aerodynamics of mars 2020 rover wind sensors. In G. Pezzella & A. Viviani (Eds.), *Mars exploration* (chap. 5). Rijeka: IntechOpen. Retrieved from `https://doi.org/10.5772/intechopen.90912` doi: 10.5772/intechopen.90912

Blair, T. C., & McPherson, J. G. (1998, 09). Recent debris-flow processes and resultant form and facies of the Dolomite alluvial fan, Owens Valley, California. *Journal of Sedimentary Research*, *68*(5), 800-818. Retrieved from `https://doi.org/10.2110/jsr.68.800` doi: 10.2110/jsr.68.800

Cedillo-Flores, Y., Treiman, A. H., Lasue, J., & Clifford, S. M. (2011). Co2 gas fluidization in the initiation and formation of martian polar gullies. *Geophysical Research Letters*, *38*(21). Retrieved from `https://agupubs.onlinelibrary.wiley.com/doi/abs/10.1029/2011GL049403` doi: https://doi.org/10.1029/2011GL049403

Conway, S. J., de Haas, T., & Harrison, T. N. (2019). Martian gullies: A comprehensive review of observations, mechanisms and insights from earth analogues. *Geological Society, London, Special Publications*, *467*(1), 7–66. doi: https://doi.org/10.1144/SP467.14

Conway, S. J., Lamb, M. P., Balme, M. R., Towner, M. C., & Murray, J. B. (2011). Enhanced runout and erosion by overland flow at low pressure and sub-freezing conditions: Experiments and application to mars. *Icarus*, *211*(1), 443-457. Retrieved from `https://www.sciencedirect.com/science/article/pii/S0019103510003428` doi: https://doi.org/10.1016/j.icarus.2010.08.026

Costard, F., Forget, F., Mangold, N., & Peulvast, J. P. (2002). Formation of recent martian debris flows by melting of near-surface ground ice at high obliquity. *Science*, *295*(5552), 110-113. Retrieved from `https://www.science.org/doi/abs/10.1126/science.1066698` doi: 10.1126/science.1066698

Cottin, H., Kotler, J. M., Bartik, K., Cleaves, H. J., Cockell, C. S., De Vera, J.-P. P., … others (2017). Astrobiology and the possibility of life on earth and elsewhere…. *Space Science Reviews*, *209*, 1–42. doi: https://doi.org/10.1007/s11214-015-0196-1

de Haas, T., Densmore, A., Stoffel, M., Suwa, H., Imaizumi, F., Ballesteros-Cánovas, J., & Wasklewicz, T. (2018). Avulsions and the spatio-temporal evolution of debris-flow fans. *Earth-Science Reviews*, *177*, 53-75. Retrieved from `https://www.sciencedirect.com/science/article/pii/S0012825217302465` doi: https://doi.org/10.1016/j.earscirev.2017.11.007

de Haas, T., Kleinhans, M. G., Carbonneau, P. E., Rubensdotter, L., & Hauber, E. (2015a). Surface morphology of fans in the high-arctic periglacial environment of svalbard: Controls and processes. *Earth-Science Reviews*, *146*, 163-182. Retrieved from `https://www.sciencedirect.com/science/article/pii/S0012825215000641` doi: https://doi.org/10.1016/j.earscirev.2015.04.004

de Haas, T., Braat, L., Leuven, J. R., Lokhorst, I. R., & Kleinhans, M. G. (2015b). Effects of debris flow composition on runout, depositional mechanisms, and deposit morphology in laboratory experiments. *Journal of Geophysical Research: Earth Surface*, *120*(9), 1949–1972.

de Haas, T., Hauber, E., Conway, S., Van Steijn, H., Johnsson, A., & Kleinhans, M. (2015c). Earth-like aqueous debris-flow activity on mars at high orbital obliquity in the last million years. *Nature Communications*, *6*(1), 1–6. doi: https://doi.org/10.1038/ncomms8543

de Haas, T., McArdell, B. W., Conway, S. J., McElwaine, J. N., Kleinhans, M. G., Salese, F., & Grindrod, P. M. (2019). Initiation and flow conditions of contemporary flows in martian gullies. *Journal of Geophys-*

ical Research: Planets, *124*(8), 2246-2271. Retrieved from https://agupubs.onlinelibrary.wiley.com/doi/abs/10.1029/2018JE005899 doi: https://doi.org/10.1029/2018JE005899

de Haas, T. d., & Woerkom, T. v. (2016). Bed scour by debris flows: experimental investigation of effects of debris-flow composition. *Earth Surface Processes and Landforms*, *41*(13), 1951–1966. doi: https://doi.org/10.1002/esp.3963

Dickson, J. L., Palumbo, A. M., Head, J. W., Kerber, L., Fassett, C. I., & Kreslavsky, M. A. (2023). Gullies on mars could have formed by melting of water ice during periods of high obliquity. *Science*, *380*(6652), 1363-1367. Retrieved from https://www.science.org/doi/abs/10.1126/science.abk2464 doi: 10.1126/science.abk2464

Diniega, S., Bramson, A. M., Buratti, B., Buhler, P., Burr, D. M., Chojnacki, M., … Widmer, J. M. (2021). Modern mars' geomorphological activity, driven by wind, frost, and gravity. *Geomorphology*, *380*, 107627. Retrieved from https://www.sciencedirect.com/science/article/pii/S0169555X21000350 doi: https://doi.org/10.1016/j.geomorph.2021.107627

Diniega, S., Byrne, S., Bridges, N. T., Dundas, C. M., & McEwen, A. S. (2010, 11). Seasonality of present-day Martian dune-gully activity. *Geology*, *38*(11), 1047-1050. Retrieved from https://doi.org/10.1130/G31287.1 doi: 10.1130/G31287.1

Diniega, S., Hansen, C., McElwaine, J., Hugenholtz, C., Dundas, C., McEwen, A., & Bourke, M. (2013). A new dry hypothesis for the formation of martian linear gullies. *Icarus*, *225*(1), 526-537. Retrieved from https://www.sciencedirect.com/science/article/pii/S0019103513001668 doi: https://doi.org/10.1016/j.icarus.2013.04.006

Dundas, C. M., Conway, S. J., & Cushing, G. E. (2022). Martian gully activity and the gully sediment transport system. *Icarus*, 115133. Retrieved from https://www.sciencedirect.com/science/article/pii/S0019103522002408 doi: https://doi.org/10.1016/j.icarus.2022.115133

Dundas, C. M., Diniega, S., Hansen, C. J., Byrne, S., & McEwen, A. S. (2012). Seasonal activity and morphological changes in martian gullies. *Icarus*, *220*(1), 124-143. Retrieved from https://www.sciencedirect.com/science/article/pii/S0019103512001340 doi: https://doi.org/10.1016/j.icarus.2012.04.005

Dundas, C. M., Diniega, S., & McEwen, A. S. (2015). Long-term monitoring of martian gully formation and evolution with mro/hirise. *Icarus*, *251*, 244-263. Retrieved from https://www.sciencedirect.com/science/article/pii/S0019103514002668 (Dynamic Mars) doi: https://doi.org/10.1016/j.icarus.2014.05.013

Dundas, C. M., McEwen, A. S., Diniega, S., Byrne, S., & Martinez-Alonso, S. (2010). New and recent gully activity on mars as seen by hirise. *Geophysical Research Letters*, *37*(7). Retrieved from https://agupubs.onlinelibrary.wiley.com/doi/abs/10.1029/2009GL041351 doi: https://doi.org/10.1029/2009GL041351

Dundas, C. M., McEwen, A. S., Diniega, S., Hansen, C. J., Byrne, S., & McElwaine, J. N. (2017). The formation of gullies on mars today. *Geological Society, London, Special Publications*, *467*(1), 67–94. Retrieved from https://sp.lyellcollection.org/content/467/1/67 doi: 10.1144/SP467.5

Dundas, C. M., McEwen, A. S., Diniega, S., Hansen, C. J., Byrne, S., & McElwaine, J. N. (2019). scho. *Geological Society, London, Special Publications*, *467*(1), 67–94. Retrieved from https://sp.lyellcollection.org/content/467/1/67 doi: 10.1144/SP467.5

Hecht, M. H. (2002). Metastability of liquid water on mars. *Icarus*, *156*(2), 373-386. Retrieved from https://www.sciencedirect.com/science/article/pii/S0019103501967946 doi: https://doi.org/10.1006/icar.2001.6794

Hoffman, N. (2002). Active polar gullies on mars and the role of carbon dioxide. *Astrobiology*, *2*(3), 313–323. doi: https://doi.org/10.1089/153110702762027899

Holstein-Rathlou, C., Merrison, J., Iversen, J. J., Jakobsen, A. B., Nicolajsen, R., Nørnberg, P., ... Portyankina, G. (2014). An environmental wind tunnel facility for testing meteorological sensor systems. *Journal of Atmospheric and Oceanic Technology*, *31*(2), 447 - 457. Retrieved from `https://journals.ametsoc.org/view/journals/atot/31/2/jtech-d-13-00141_1.xml` doi: https://doi.org/10.1175/JTECH-D-13-00141.1

Hubert, J. F., & Filipov, A. J. (1989). Debris-flow deposits in alluvial fans on the west flank of the white mountains, owens valley, california, u.s.a. *Sedimentary Geology*, *61*(3), 177-205. Retrieved from `https://www.sciencedirect.com/science/article/pii/0037073889900572` doi: https://doi.org/10.1016/0037-0738(89)90057-2

Hugenholtz, C. H. (2008). Frosted granular flow: A new hypothesis for mass wasting in martian gullies. *Icarus*, *197*(1), 65-72. Retrieved from `https://www.sciencedirect.com/science/article/pii/S0019103508001796` doi: https://doi.org/10.1016/j.icarus.2008.04.010

Iverson, R. M. (1997). The physics of debris flows. *Reviews of geophysics*, *35*(3), 245–296.

Iverson, R. M. (2015). Scaling and design of landslide and debris-flow experiments. *Geomorphology*, *244*, 9-20. Retrieved from `https://www.sciencedirect.com/science/article/pii/S0169555X15001336` (Laboratory Experiments in Geomorphology 46th Annual Binghamton Geomorphology Symposium 18-20 September 2015) doi: https://doi.org/10.1016/j.geomorph.2015.02.033

Iverson, R. M., & Denlinger, R. P. (2001). Flow of variably fluidized granular masses across three-dimensional terrain: 1. coulomb mixture theory. *Journal of Geophysical Research: Solid Earth*, *106*(B1), 537–552.

Iverson, R. M., Logan, M., LaHusen, R. G., & Berti, M. (2010). The perfect debris flow? Aggregated results from 28 large-scale experiments. *Journal of Geophysical Research: Earth Surface*, *115*(F3). doi: https://doi.org/10.1029/2009JF001514

Jessop, D., Kelfoun, K., Labazuy, P., Mangeney, A., Roche, O., Tillier, J.-L., ... Thibault, G. (2012). Lidar derived morphology of the 1993 lascar pyroclastic flow deposits, and implication for flow dynamics and rheology. *Journal of Volcanology and Geothermal Research*, *245-246*, 81-97. Retrieved from `https://www.sciencedirect.com/science/article/pii/S0377027312002041` doi: https://doi.org/10.1016/j.jvolgeores.2012.06.030

Johnson, C. G., Kokelaar, B. P., Iverson, R. M., Logan, M., LaHusen, R. G., & Gray, J. M. N. T. (2012). Grain-size segregation and levee formation in geophysical mass flows. *Journal of Geophysical Research: Earth Surface*, *117*(F1). Retrieved from `https://agupubs.onlinelibrary.wiley.com/doi/abs/10.1029/2011JF002185` doi: https://doi.org/10.1029/2011JF002185

Johnsson, A., Reiss, D., Hauber, E., Hiesinger, H., & Zanetti, M. (2014). Evidence for very recent melt-water and debris flow activity in gullies in a young mid-latitude crater on mars. *Icarus*, *235*, 37-54. Retrieved from `https://www.sciencedirect.com/science/article/pii/S0019103514001225` doi: https://doi.org/10.1016/j.icarus.2014.03.005

Khuller, A. R., Christensen, P. R., Harrison, T. N., & Diniega, S. (2021). The distribution of frosts on mars: Links to present-day gully activity. *Journal of Geophysical Research: Planets*, *126*(3), e2020JE006577. Retrieved from `https://agupubs.onlinelibrary.wiley.com/doi/abs/10.1029/2020JE006577` (e2020JE006577 2020JE006577) doi: https://doi.org/10.1029/2020JE006577

Kieffer, H. H. (2007). Cold jets in the martian polar caps. *Journal of Geophysical Research: Planets*, *112*(E8). Retrieved from `https://agupubs.onlinelibrary.wiley.com/doi/abs/10.1029/2006JE002816` doi:

https://doi.org/10.1029/2006JE002816

Knauth, L., & Burt, D. M. (2002). Eutectic brines on mars: Origin and possible relation to young seepage features. *Icarus*, *158*(1), 267-271. Retrieved from https://www.sciencedirect.com/science/article/pii/S0019103502968661 doi: https://doi.org/10.1006/icar.2002.6866

Lanza, N., Meyer, G., Okubo, C., Newsom, H., & Wiens, R. (2010). Evidence for debris flow gully formation initiated by shallow subsurface water on mars. *Icarus*, *205*(1), 103-112. Retrieved from https://www.sciencedirect.com/science/article/pii/S001910350900164X (MRO/HiRISE Studies of Mars) doi: https://doi.org/10.1016/j.icarus.2009.04.014

Levy, J., Head, J., Dickson, J., Fassett, C., Morgan, G., & Schon, S. (2010). Identification of gully debris flow deposits in protonilus mensae, mars: Characterization of a water-bearing, energetic gully-forming process. *Earth and Planetary Science Letters*, *294*(3), 368-377. Retrieved from https://www.sciencedirect.com/science/article/pii/S0012821X09004580 (Mars Express after 6 Years in Orbit: Mars Geology from Three-Dimensional Mapping by the High Resolution Stereo Camera (HRSC) Experiment) doi: https://doi.org/10.1016/j.epsl.2009.08.002

Lube, G., Cronin, S. J., Platz, T., Freundt, A., Procter, J. N., Henderson, C., & Sheridan, M. F. (2007). Flow and deposition of pyroclastic granular flows: A type example from the 1975 ngauruhoe eruption, new zealand. *Journal of Volcanology and Geothermal Research*, *161*(3), 165-186. Retrieved from https://www.sciencedirect.com/science/article/pii/S0377027306004239 doi: https://doi.org/10.1016/j.jvolgeores.2006.12.003

Malin, M. C., & Edgett, K. S. (2000). Evidence for recent groundwater seepage and surface runoff on mars. *Science*, *288*(5475), 2330-2335. Retrieved from https://www.science.org/doi/abs/10.1126/science.288.5475.2330 doi: 10.1126/science.288.5475.2330

Parsons, J. D., Whipple, K. X., & Simoni, A. (2001). Experimental study of the grain-flow, fluid-mud transition in debris flows. *The Journal of Geology*, *109*(4), 427–447.

Pasquon, K., Conway, S., Vincendon, M., Massé, M., Raack, J., Noblet, A., … Lewis, S. R. (2023). Insights into the interaction between defrosting seasonal ices and gully activity from cassis and hirise observations in sisyphi cavi, mars. *Planetary and Space Science*, *235*, 105743. Retrieved from https://www.sciencedirect.com/science/article/pii/S0032063323001125 doi: https://doi.org/10.1016/j.pss.2023.105743

Pasquon, K., Gargani, J., Massé, M., Vincendon, M., Conway, S. J., Séjourné, A., … Guimpier, A. (2019). Present-day development of gully-channel sinuosity by carbon dioxide gas supported flows on mars. *Icarus*, *329*, 296-313. Retrieved from https://www.sciencedirect.com/science/article/pii/S0019103518304627 doi: https://doi.org/10.1016/j.icarus.2019.03.034

Pilorget, C., & Forget, F. (2016). Formation of gullies on mars by debris flows triggered by co2 sublimation. *Nature Geoscience*, *9*(1), 65–69. Retrieved from https://doi.org/10.1038/ngeo2619 doi: 10.1038/ngeo2619

Raack, J., Conway, S. J., Heyer, T., Bickel, V. T., Philippe, M., Hiesinger, H., … Massé, M. (2020). Present-day gully activity in sisyphi cavi, mars – flow-like features and block movements. *Icarus*, *350*, 113899. Retrieved from https://www.sciencedirect.com/science/article/pii/S0019103520302785 doi: https://doi.org/10.1016/j.icarus.2020.113899

Raack, J., Reiss, D., Appéré, T., Vincendon, M., Ruesch, O., & Hiesinger, H. (2015). Present-day seasonal gully activity in a south polar pit (sisyphi cavi) on mars. *Icarus*, *251*, 226-243. Retrieved from https://www.sciencedirect.com/science/article/pii/S0019103514001663 (Dynamic Mars) doi: https://doi.org/10.1016/j.icarus.2014.03.040

Richardson, M. I., & Mischna, M. A. (2005). Long-term evolution of transient liquid water on mars. *Journal of Geophysical Research: Planets*, *110*(E3). Retrieved from `https://agupubs.onlinelibrary.wiley.com/doi/abs/10.1029/2004JE002367` doi: https://doi.org/10.1029/2004JE002367

Roelofs, L., Colucci, P., & Haas, T. d. (2022). How debris-flow composition affects bed erosion quantity and mechanisms - an experimental assessment. *Earth Surface Processes and Landforms*.

Roelofs, L., Conway, S. J., de Haas, T., Dundas, C., Lewis, S. R., McElwaine, J., ... Patel, M. R. (n.d.). How, where, and when CO_2 drives current mass flows in martian gullies. *In Press at Communications Earth and Environment*.

Roelofs, L., Nota, E. W., Flipsen, T. C. W., Colucci, P., & de Haas, T. (2023). How bed composition affects erosion by debris flows—an experimental assessment. *Geophysical Research Letters*, *50*(14), e2023GL103294. Retrieved from `https://agupubs.onlinelibrary.wiley.com/doi/abs/10.1029/2023GL103294` (e2023GL103294 2023GL103294) doi: https://doi.org/10.1029/2023GL103294

Rothery, D. A., Massironi, M., Alemanno, G., Barraud, O., Besse, S., Bott, N., ... others (2020). Rationale for bepicolombo studies of mercury's surface and composition. *Space science reviews*, *216*(4), 1–46. Retrieved from `https://link.springer.com/article/10.1007/s11214-020-00694-7` doi: https://doi.org/10.1007/s11214-020-00694-7

Rowley, P. D., Kuntz, M. A., & Macleod, N. S. (1981). Pyroclastic-flow deposits. In *The 1980 eruptions of mount st. helens, washington* (p. 489-512). Washington: USGS. doi: 10.3133/pp1250

Scully, J. E., Russell, C. T., Yin, A., Jaumann, R., Carey, E., Castillo-Rogez, J., ... Le Corre, L. (2015). Geomorphological evidence for transient water flow on vesta. *Earth and Planetary Science Letters*, *411*, 151-163. Retrieved from `https://www.sciencedirect.com/science/article/pii/S0012821X14007572` doi: https://doi.org/10.1016/j.epsl.2014.12.004

Shakeel, H., Wei, H., & Pomeroy, J. (2018). Measurements of enthalpy of sublimation of ne, n2, o2, ar, co2, kr, xe, and h2o using a double paddle oscillator. *The Journal of Chemical Thermodynamics*, *118*, 127-138. Retrieved from `https://www.sciencedirect.com/science/article/pii/S0021961417303968` doi: https://doi.org/10.1016/j.jct.2017.11.004

Sinha, R. K., & Ray, D. (2023). Morphological changes currently occurring in sand-filled gully channels on mars: Implications for the role of substrates inside channels. *Icarus*, *390*, 115334. Retrieved from `https://www.sciencedirect.com/science/article/pii/S0019103522004262` doi: https://doi.org/10.1016/j.icarus.2022.115334

Sinha, R. K., Vijayan, S., Shukla, A. D., Das, P., & Bhattacharya, F. (2018). Gullies and debris-flows in ladakh himalaya, india: a potential martian analogue. *Geological Society, London, Special Publications*, *467*(1), 315–342. doi: https://doi.org/10.1144/SP467.9

Smith, G., Rowley, P., Williams, R., Giordano, G., Trolese, M., Silleni, A., ... Capon, S. (2020). A bedform phase diagram for dense granular currents. *Nature communications*, *11*(1), 2873. doi: https://doi.org/10.1038/s41467-020-16657-z

Stephenson, R. M. (1987). *Handbook of the thermodynamics of organic compounds.* Elsevier. doi: https://doi.org/10.1007/978-94-009-3173-2

Stock, J. D., & Dietrich, W. E. (2003). Valley incision by debris flows: Evidence of a topographic signature. *Water Resources Research*, *39*(4). doi: https://doi.org/10.1029/2001WR001057

Sylvest, M. E., Conway, S. J., Patel, M. R., Dixon, J. C., & Barnes, A. (2016). Mass wasting triggered by seasonal co2 sublimation under martian atmospheric conditions: Laboratory experiments. *Geophysical Research Letters*, *43*(24), 12,363-

12,370. Retrieved from https://agupubs.onlinelibrary.wiley.com/doi/abs/10.1002/2016GL071022 doi: https://doi.org/10.1002/2016GL071022

Sylvest, M. E., Dixon, J. C., Conway, S. J., Patel, M. R., McElwaine, J. N., Hagermann, A., & Barnes, A. (2019). Co2 sublimation in martian gullies: laboratory experiments at varied slope angle and regolith grain sizes. *Geological Society, London, Special Publications*, *467*(1), 343–371. Retrieved from https://www.lyellcollection.org/doi/full/10.1144/SP467.11 doi: https://doi.org/10.1144/SP467.11

Zhou, G. G., Li, S., Song, D., Choi, C. E., & Chen, X. (2019). Depositional mechanisms and morphology of debris flow: physical modelling. *Landslides*, *16*, 315–332. doi: https://doi.org/10.1007/s10346-018-1095-9

Figure 1. Three examples of Martian gullies with frost; a) gullies in Sisyphi Cavi (synthetic RGB CaSSIS images using the PAN and BLU channels, where defrosted surfaces appear red and frosted surfaces white, MY34_003464_256_1, Ls 242°) (Pasquon et al., 2023), b) gullies in an unnamed crater (HiRISE image, ESP_039114_1115, Ls 243°), c) gullies on Matara crater dune field (HiRISE image, ESP_063824_1340, Ls 160°). Colour strips in panels b) and c) are false colours, composed of near-infrared, red and blue-green wavelength signals.

Figure 2. Photos and schematic drawings of chambers (a-b) and flumes (c-f). The photo in panel (a) depicts the Mars chamber at the Hyper Velocity and Impact lab (HVI) of the Open University (UK), panel (b) shows the Mars Simulation Wind tunnel at Aarhus University (Denmark). Details of the small-scale flume set-up used in the Mars chamber of the HVI lab can be found in (c) and (e). Details of the large-scale set-up used in the Mars Simulation Wind tunnel in Aarhus can be found in (d) and (f). All dimensions are given in cm.

Figure 3. Example of flow depth, flow mass, and differential pore pressures (sensors 1 and 2) during an experiment for the large-scale set-up (a) and the small-scale set-up (b) with similar boundary conditions; initial CO_2 mass fraction of 0.23 and flume angle of 20°. The lower panel (c), depicts the mass fraction of the flow carried by the gas pressure for the experiments depicted in panels (a) and (b). As the data from the two pore pressure sensors slightly differs, this fraction is depicted as an envelope covering the range provided by the two sensors. The fraction carried by the gas pressure is a measure for the degree of fluidisation.

Figure 4. Digital elevation models (DEMs) for the outflow deposits of 12 experiments under Martian atmospheric pressures, 6 conducted in the large scale set-up, highlighted by thick black borders, and 6 conducted in the small scale set-up. The top two rows (a–f) show deposits of experiments with varying CO_2 mass fractions. The fractions depicted in the panels correspond to the mass fractions at the start of an experiment derived from Supplementary Figure 4. The bottom two rows (g–l) show deposits of experiments with different chute angles. For all depicted experiments, videos are present in the Supplementary material 8.

Figure 5. Frontal flow velocity (a-b), maximum flow depth (c-d), and maximum differential pore pressure for pore pressure sensor 1 (P1) and pore pressure sensor 2 (P2) (e-f), for the large-scale (L) and small-scale (S) experimental flows. All green and blue dots represent results from experiments conducted under Martian atmospheric pressure, whereas the yellow dots represent results from experiments conducted under Earth atmospheric pressure. The results of experiments with varying CO_2 mass fractions in the flow, but a constant chute angle of 30°, are presented in the left column. Note that the mass fractions presented here are the mass fractions at the start of an experiment derived from data presented in Supplementary Figure 4. The results of experiments conducted under different chute angles, but with a constant initial CO_2 mass fraction of 0.33, are presented in the right column.

Figure 6. Boxplots showing the distribution of the flow density (a-b) and the fraction of the flow carried by the gas pressure (c-d) for the large-scale experiments conducted with different CO_2 mass fractions (left column) and under different chute angles (right column). The data in a single boxplot combines the density or fraction carried by the gas pressure of the main flow over time (flow tails are disregarded) for all large-scale experiments performed under similar conditions (i.e. similar CO_2 mass fractions and chute angle). The dark blue dots represent the mean value during one experiment. The reported p-value in the subplots stems from an ANOVA test of these means. The p-values show that the results from the different experimental groups in panels (b) and (c) are marginally significant.

Figure 7. Flow depth and cumulative CO_2 mass loss for three experiments in the large-scale set-up, with a CO_2 mass at the beginning of the experiment of 0.59 kg (a), 1.12 kg (b), and 2.13 kg (c). All experiments were conducted under a chute slope of 30°. The cumulative CO_2 mass lost is determined based on data from a capacitance pressure sensor in the chamber, the measurement frequency is 1 Hz.

Figure 8. Bagnold (a-b), Savage (c-d), and friction (e-f) numbers for the granular flows in the large-scale and small-scale experiments conducted with different CO_2 mass fractions (left column) and under different chute angles (right column). The horizontal lines indicate the transition from one flow regime to the other (Iverson, 1997). For the Bagnold number (a-b), this is the transition between the collisional and the viscous flow regime. For the Savage number (c-d), this is the transition from the collisional to the frictional flow regime. For the friction number (e-f), this is the transition from the frictional to the viscous flow regime, the latter is not visible in the plot because the flows are far into the frictional flow regime.

Figure 9. Bagnold numbers plotted against Savage numbers for the experimental CO_2-driven flows presented in Figure 4, the experimental debris flows from Roelofs et al. (2022)[2], the experimental dense pyroclastic density currents from Smith et al. (2020)[3], three prototype natural debris flows from Iverson (1997)[4] and Iverson and Denlinger (2001)[5], a natural mud flow from Iverson (1997)[4], a rock avalanche from Iverson and Denlinger (2001)[5], and a pyroclastic density current from Mount St Helens from Iverson and Denlinger (2001)[5] and Rowley et al. (1981)[6]

Figure 10. Different natural granular flows and their key morphological features. (a) Debris flow fan with different lobate deposits with levees near Pinnisalm, Neustift im Stubaital, Austria. (b) Pyroclastic density current deposits from the eruption of Mount St Helens in 1980 on July 22, showing multiple channels with levees and lobes (Photo: Dan Miller and USGS, first published in Baker et al. (2016)). (c) Granular flow deposits on the slopes of Istok crater on Mars with levees and lobes (Photo: NASA - HiRISE PSP_006837_1345) (Johnsson et al., 2014; T. de Haas et al., 2015c) (d) Rock avalanche Hope Slide, Hope, British Columbia, Canada (Photo: John Clague). (e) Mud flow dominated Coldwater Canyon fan, California, USA, showing channels and dispersed lobes with thin levees.

Figure 1.

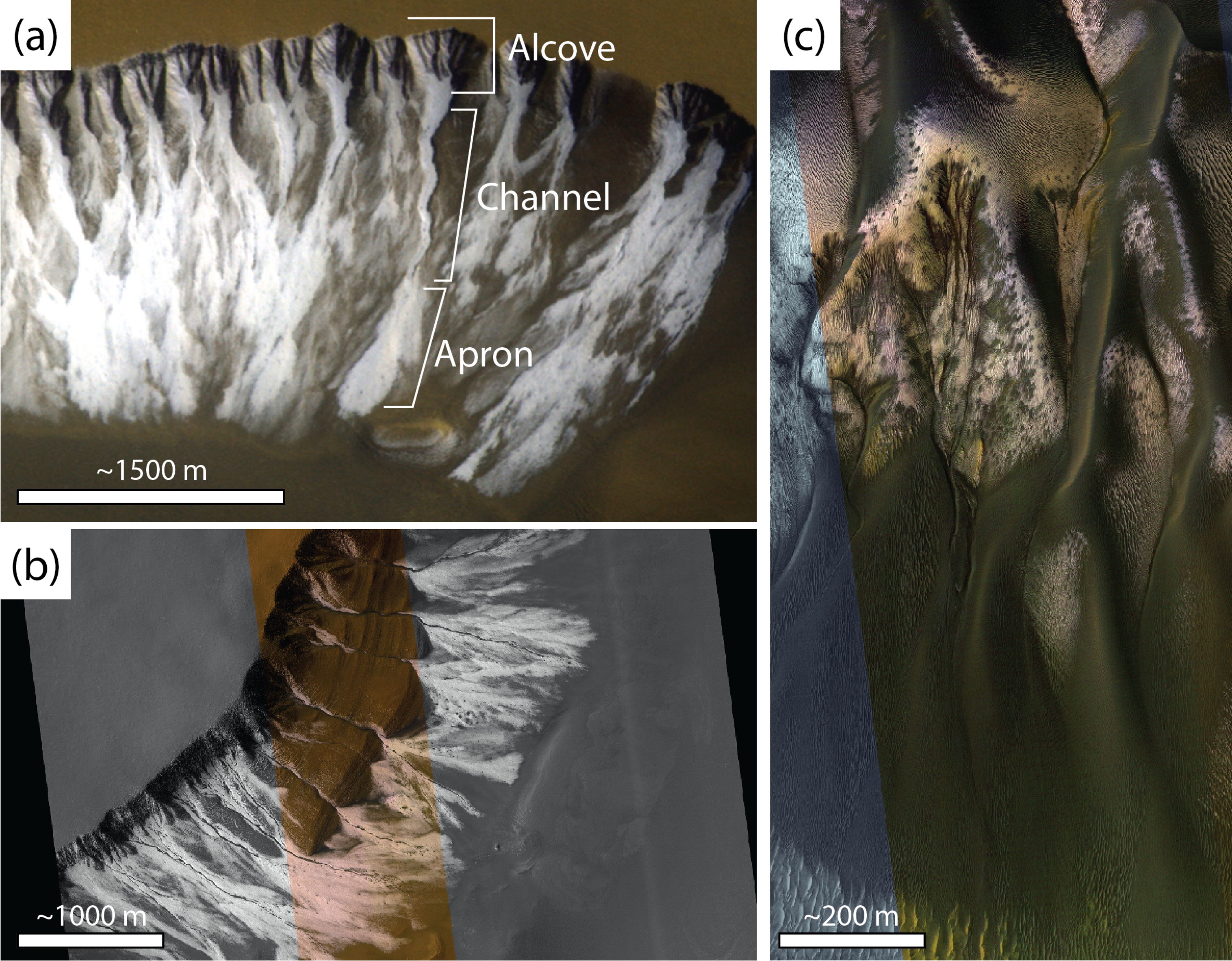
(a)
Alcove
Channel
Apron
~1500 m
(b)
~1000 m
(c)
~200 m

Figure 2.

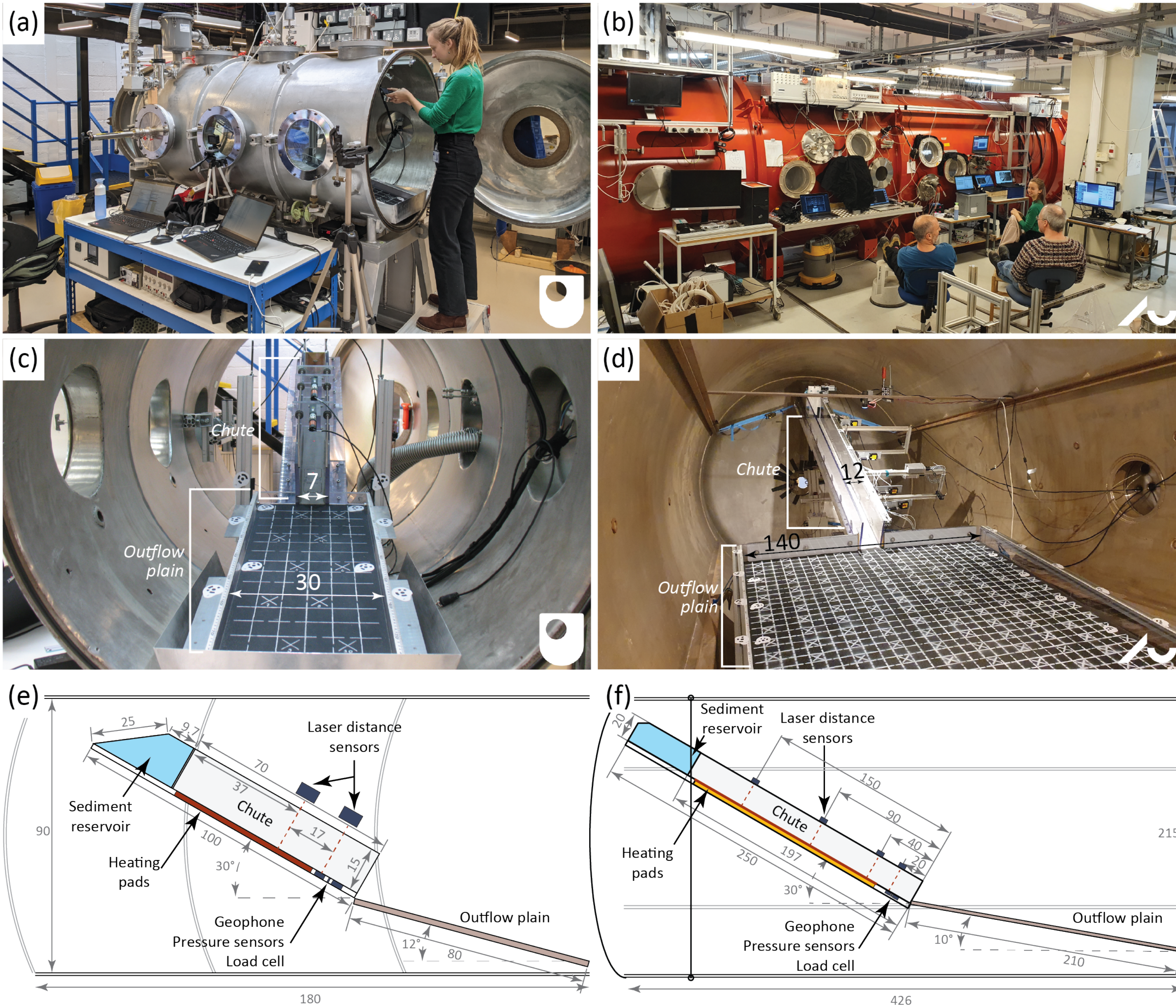
(a)
(b)
(c)
Chute
7
Outflow plain
30
(d)
Chute
12
140
Outflow plain
(e)
25
9.7
70
37
17
100
15
90
30°
12°
80
180
Laser distance sensors
Sediment reservoir
Chute
Heating pads
Geophone
Pressure sensors
Load cell
Outflow plain
(f)
20
Sediment reservoir
Laser distance sensors
150
90
40
20
250
197
215
30°
10°
210
426
Chute
Heating pads
Geophone
Pressure sensors
Load cell
Outflow plain

Figure 3.

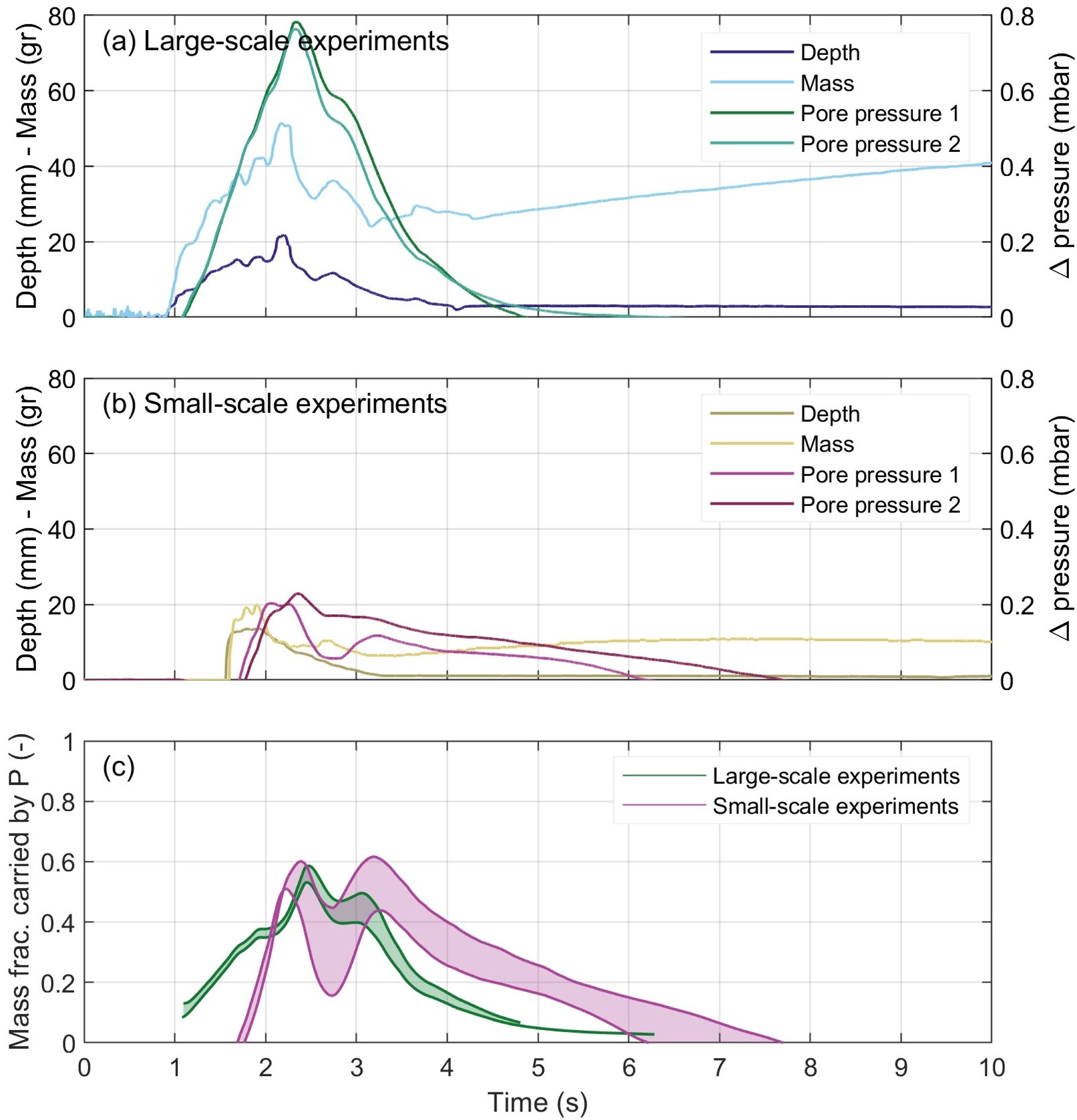

(a) Large-scale experiments
Depth
Mass
Pore pressure 1
Pore pressure 2
Depth (mm) - Mass (gr)
Δ pressure (mbar)
(b) Small-scale experiments
Depth
Mass
Pore pressure 1
Pore pressure 2
Depth (mm) - Mass (gr)
Δ pressure (mbar)
(c)
Large-scale experiments
Small-scale experiments
Mass frac. carried by P (-)
Time (s)

Figure 4.

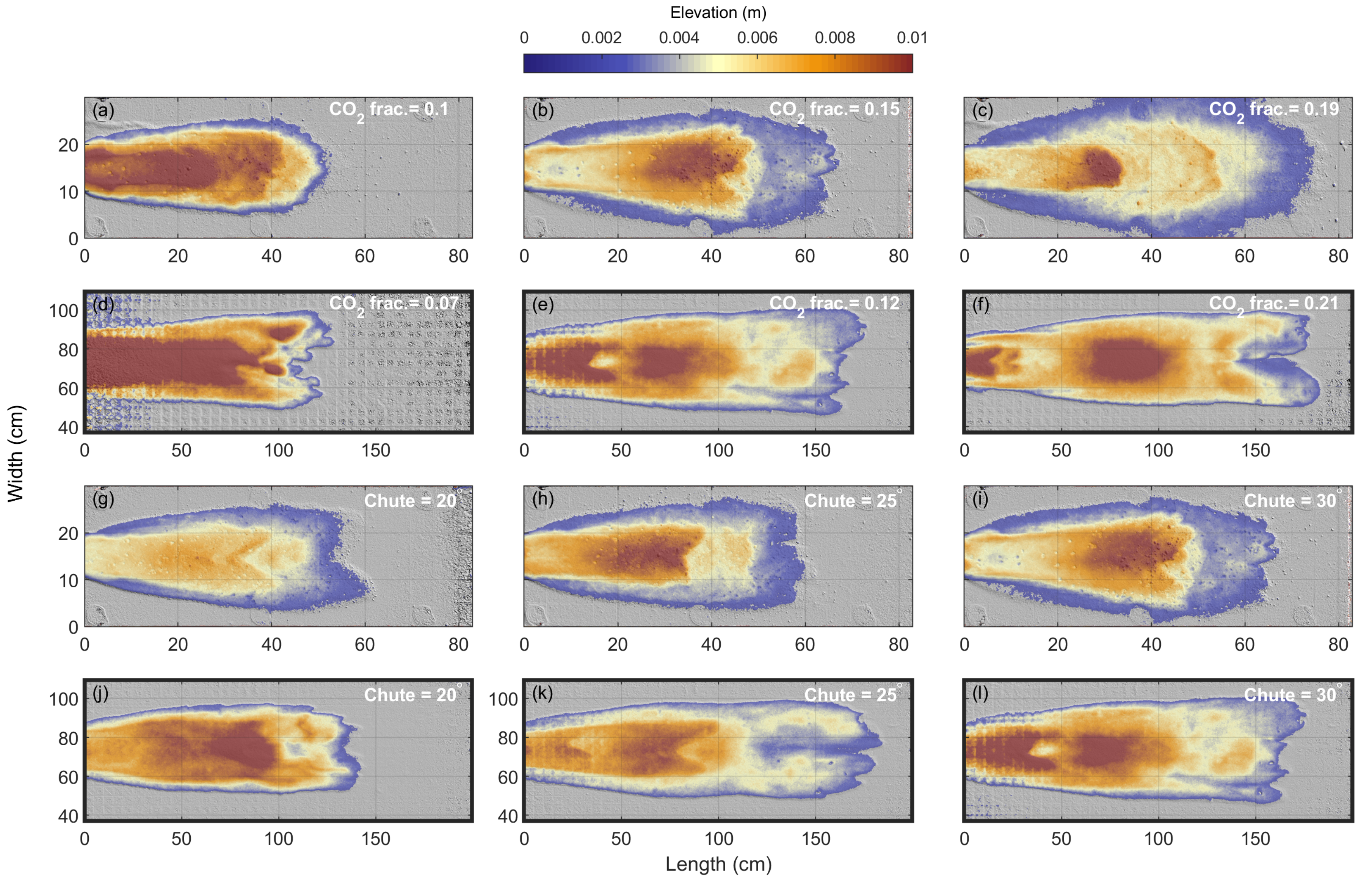

Elevation (m)
0
0.002
0.004
0.006
0.008
0.01
(a)
CO_2 frac.= 0.1
(b)
CO_2 frac.= 0.15
(c)
CO_2 frac.= 0.19
(d)
CO_2 frac.= 0.07
(e)
CO_2 frac.= 0.12
(f)
CO_2 frac.= 0.21
(g)
Chute = 20°
(h)
Chute = 25°
(i)
Chute = 30°
(j)
Chute = 20°
(k)
Chute = 25°
(l)
Chute = 30°
Width (cm)
Length (cm)

Figure 5.

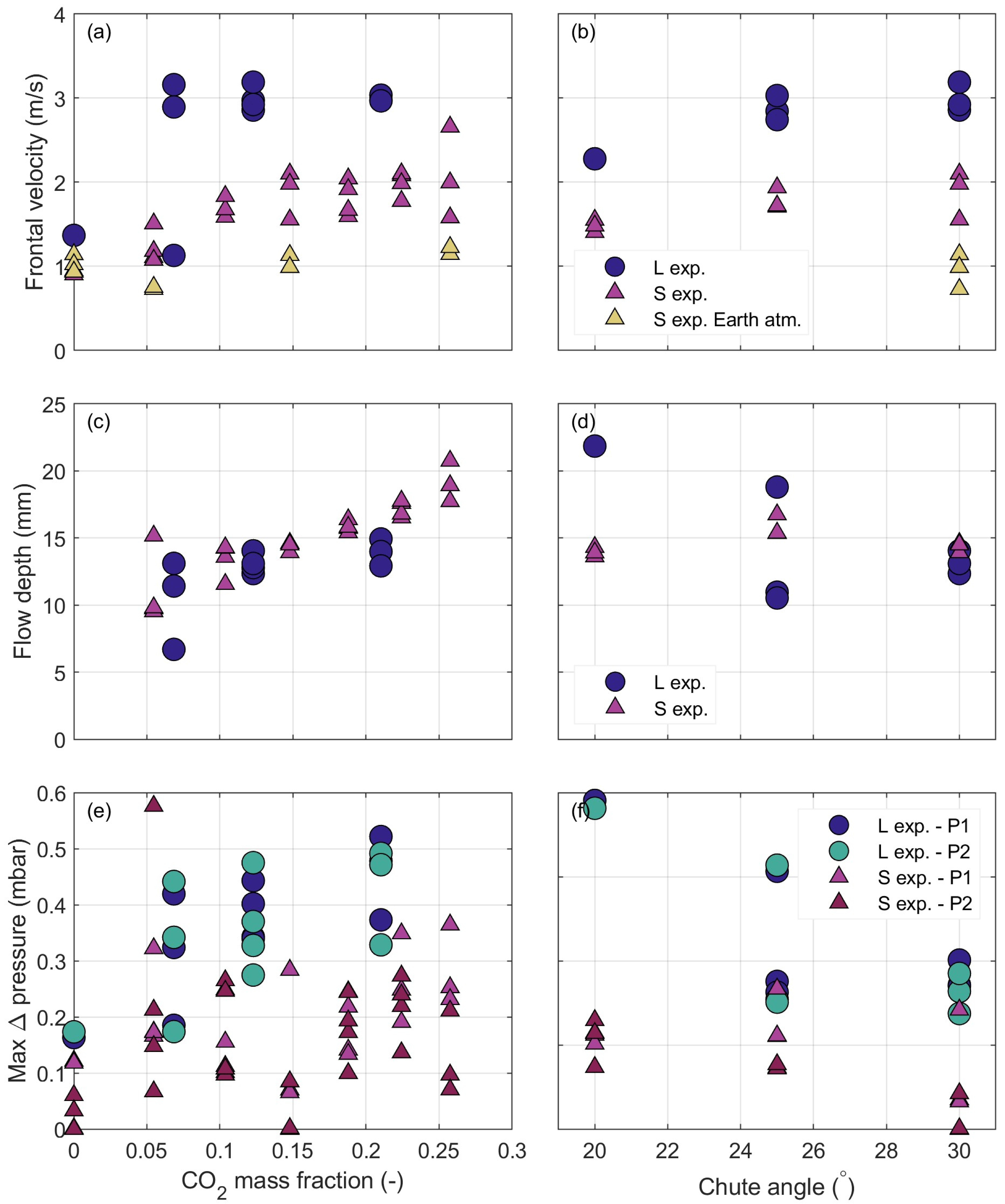

(a)
(b)
(c)
(d)
(e)
(f)
Frontal velocity (m/s)
Flow depth (mm)
Max Δ pressure (mbar)
CO2 mass fraction (-)
Chute angle (°)
L exp.
S exp.
S exp. Earth atm.
L exp. - P1
L exp. - P2
S exp. - P1
S exp. - P2
0
1
2
3
4
5
10
15
20
25
0.1
0.2
0.3
0.4
0.5
0.6
0.05
0.15
0.25
22
24
26
28
30

Figure 6.

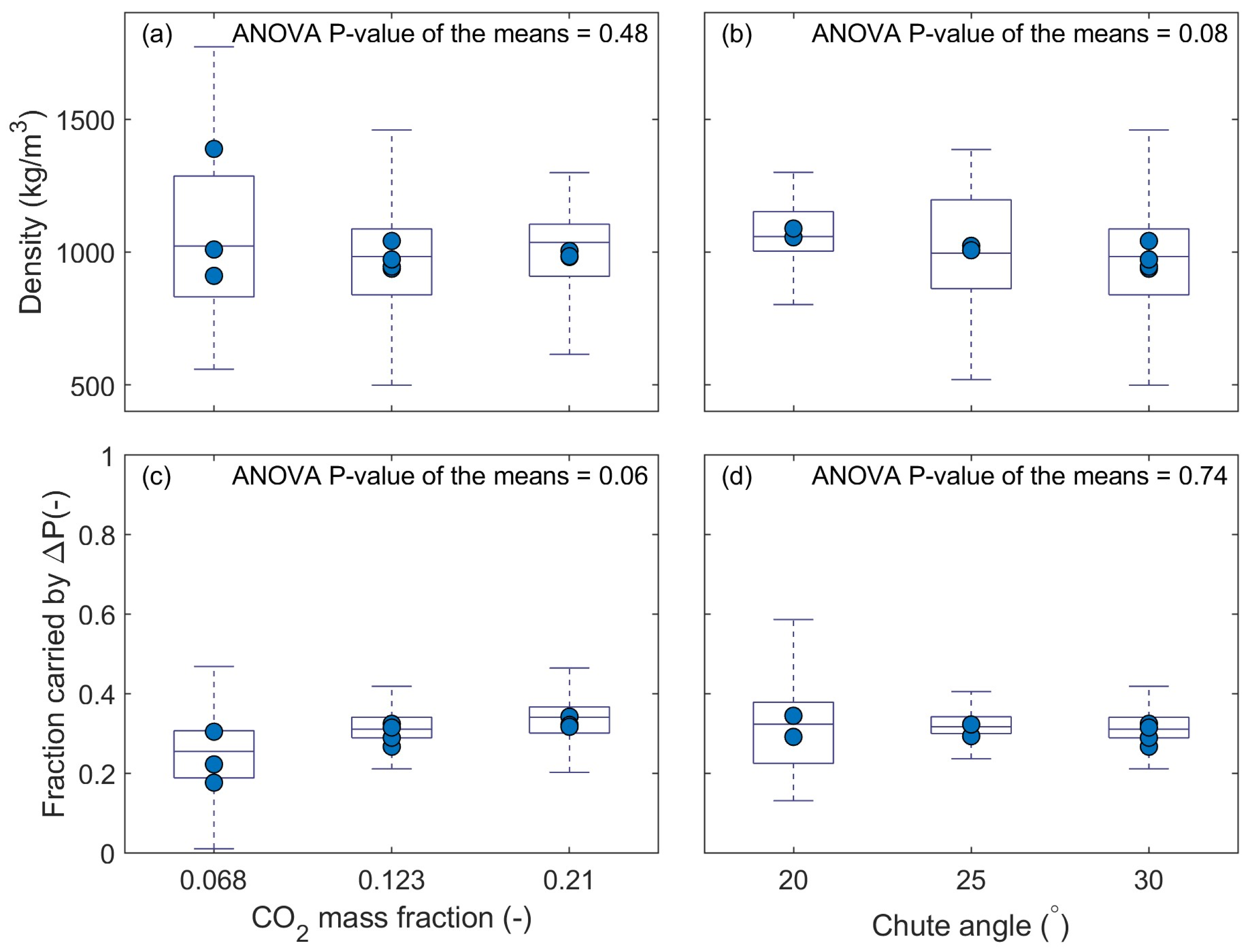

(a) ANOVA P-value of the means = 0.48
(b) ANOVA P-value of the means = 0.08
(c) ANOVA P-value of the means = 0.06
(d) ANOVA P-value of the means = 0.74
Density (kg/m3)
1500
1000
500
Fraction carried by ΔP(-)
1
0.8
0.6
0.4
0.2
0
0.068
0.123
0.21
CO2 mass fraction (-)
20
25
30
Chute angle (°)

Figure 7.

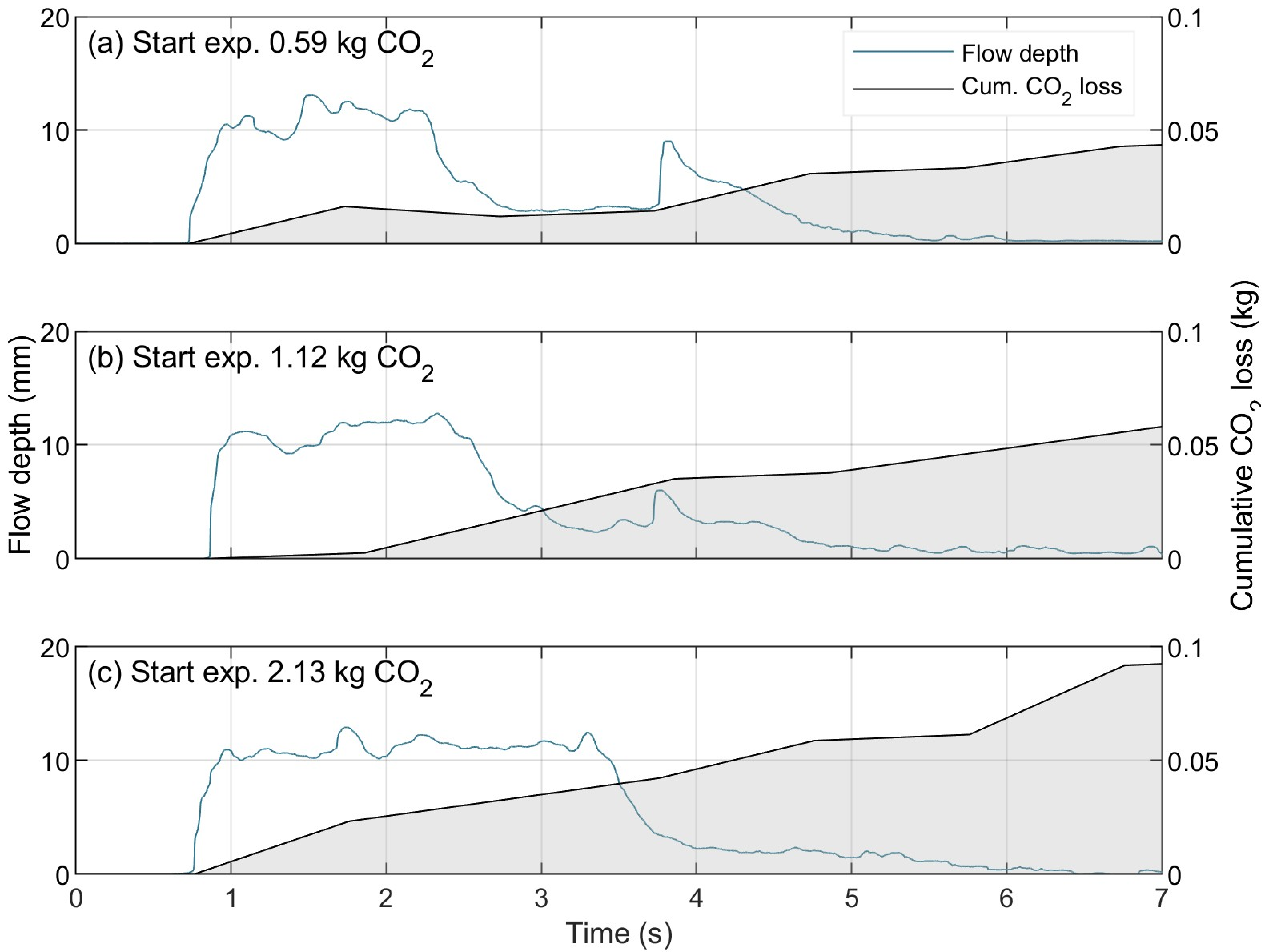

(a) Start exp. 0.59 kg CO2
Flow depth
Cum. CO2 loss
(b) Start exp. 1.12 kg CO2
(c) Start exp. 2.13 kg CO2
Flow depth (mm)
Cumulative CO2 loss (kg)
Time (s)

Figure 8.

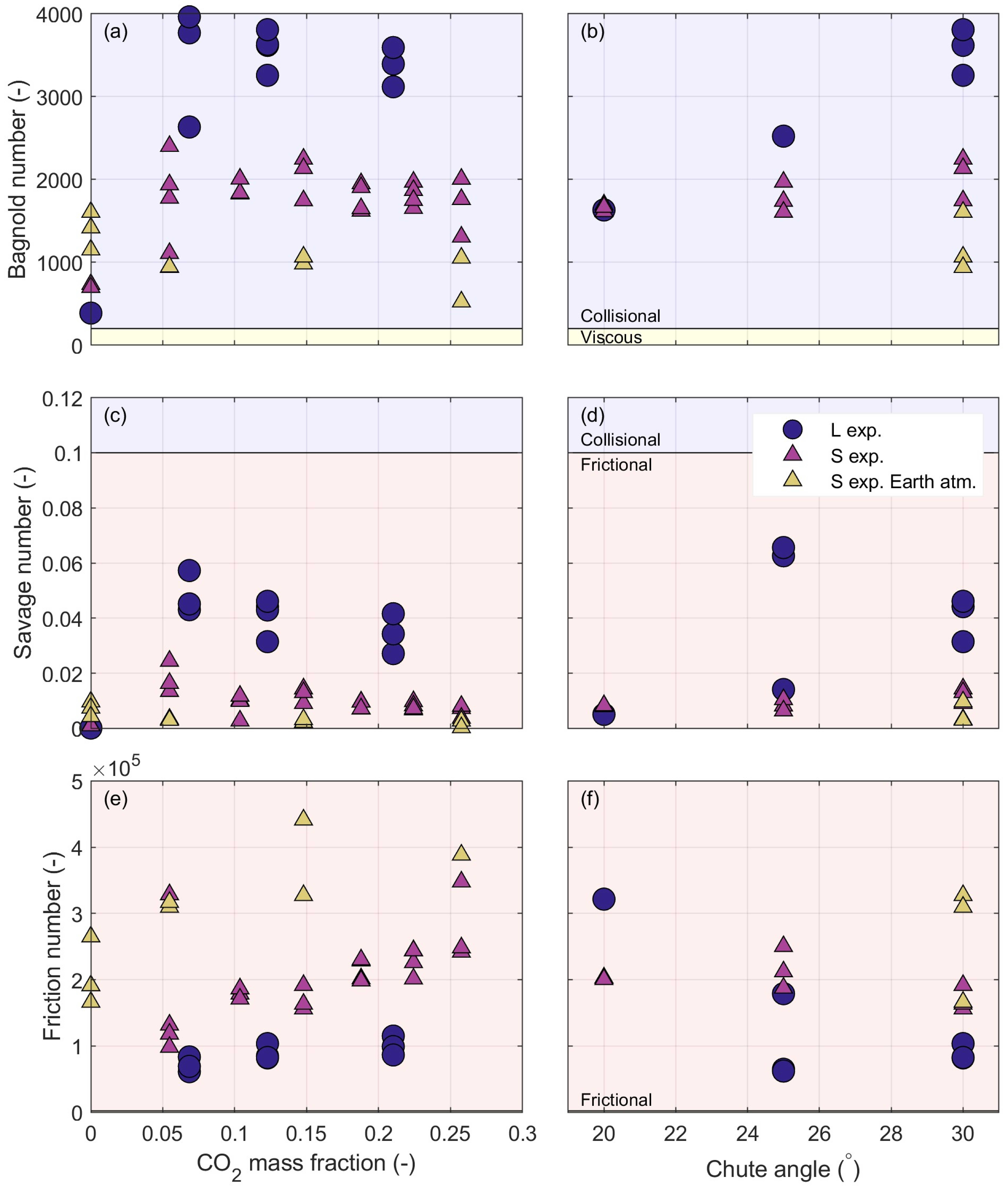

(a)
(b)
(c)
(d)
(e)
(f)
Bagnold number (-)
Savage number (-)
Friction number (-)
×10^5
Collisional
Viscous
Collisional
Frictional
Frictional
L exp.
S exp.
S exp. Earth atm.
CO2 mass fraction (-)
Chute angle (°)

Figure 9.

Collisional
Frictional
Viscous
Collisional
Savage number (-)
Bagnold number (-)
10^0
10^-2
10^-4
10^-6
10^-8
10^-10
10^2
10^4
10^6
10^8
Exp. CO2 flows - small
Exp. CO2 flows - large
Exp. DFs1
Natural DFs prototypes4,5
Exp. PDCs3
PDC Mount St Helens5,6
Natural mudflow4
Natural rock avalanche5

Figure 10.

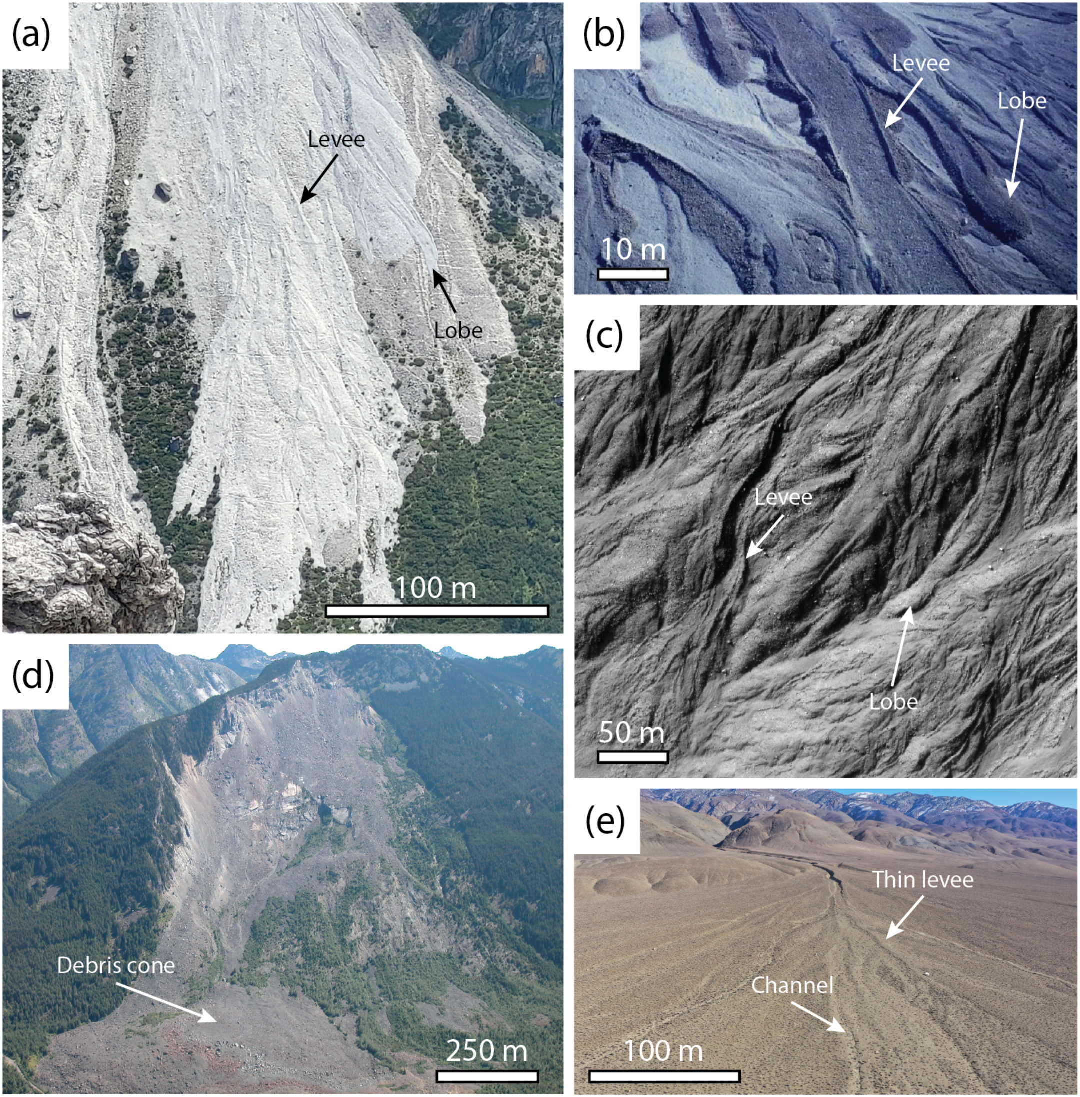
(a)
Levee
Lobe
100 m
(b)
Levee
Lobe
10 m
(c)
Levee
Lobe
50 m
(d)
Debris cone
250 m
(e)
Thin levee
Channel
100 m

The dynamics of CO_2-driven granular flows in gullies on Mars

Lonneke Roelofs [1], Susan J. Conway [2], Bas van Dam [1], Arjan van Eijk [1], Jonathan P. Merrison [3], Jens Jacob Iversen [3], Matthew Sylvest [4], Manish R. Patel [4], Henk Markies [1], Marcel van Maarseveen [1], Jim McElwaine [5], Maarten G. Kleinhans [1], Tjalling de Haas[1]

[1]Department of Physical Geography, Faculty of Geosciences, Utrecht University, Princetonlaan 8a, 3584 CB Utrecht,Netherlands
[2]Nantes Université, Univ Angers, Le Mans Université, CNRS, Laboratoire de Planétologie et Géosciences, LPG UMR 6112, 44000 Nantes, France
[3]Mars Simulation Laboratory, Aarhus University, Ny Munkegade, Bygning 520, 8000 Århus C, Denmark
[4]School of Physical Sciences, The Open University, Milton Keynes, United Kingdom
[5]Department of Earth Sciences, Durham University, Durham, United Kingdom

Key Points:

- The sublimation of small amounts of CO_2 ice can fluidize granular material on low slopes under Martian atmospheric pressure.
- The flow dynamics of CO_2-driven flows are similar to that of terrestrial fluidized two-phase flows, e.g. debris flows and dense pyroclastic flows.
- Experimental CO_2-driven granular flows create deposit morphologies similar to those observed in Martian gullies.

Corresponding author: Lonneke Roelofs, `l.roelofs@uu.nl`

Abstract

Martian gullies are landforms consisting of an erosional alcove, a channel, and a depositional apron. A significant proportion of Martian gullies at the mid-latitudes is active today. The seasonal sublimation of CO_2 ice has been suggested as a driver behind present-day gully activity. However, due to a lack of in-situ observations, the actual processes causing the observed changes remain unresolved. Here, we present results from flume experiments in environmental chambers in which we created CO_2-driven granular flows under Martian atmospheric conditions. Our experiments show that under Martian atmospheric pressure, large amounts of granular material can be fluidized by the sublimation of small quantities of CO_2 ice in the granular mixture (only 0.5% of the volume fraction of the flow) under slope angles as low as 10°. Dimensionless scaling of the CO_2-driven granular flows shows that they are dynamically similar to terrestrial two-phase granular flows, i.e. debris flows and pyroclastic flows. The similarity in flow dynamics explains the similarity in deposit morphology with levees and lobes, supporting the hypothesis that CO_2-driven granular flows on Mars are not merely modifying older landforms, but they are actively forming them. This has far-reaching implications for the processes thought to have formed these gullies over time. For other planetary bodies in our solar system, our experimental results suggest that the existence of gully-like landforms is not necessarily evidence for flowing liquids but that they could also be formed or modified by sublimation-driven flow processes.

Plain Language Summary

Martian gullies are landforms that look like landforms carved by aqueous debris flows on Earth. At the top, the gullies have an erosional alcove where material is eroded and at the bottom of the gully, a fan exists where the eroded material is deposited. For a long time, it was believed that these gullies were formed by liquid water, just like on Earth. However, the Martian gullies are active today, which cannot be reconciled with the low atmospheric pressure and resulting lack of liquid water on the surface of Mars. Data from satellites has shown that the activity in Martian gullies is correlated to a seasonal cycle of CO_2 ice deposition and sublimation. However, these observations are indirect, and therefore, we do not know whether and how CO_2 sublimation produces the observed changes in gullies. Here we show the results of flume experiments in environmental chambers in which we created CO_2-driven flows under Martian atmospheric conditions. The experiments show that granular material can be fluidized by sublimation of CO_2 ice. Furthermore, the experimental flow dynamics and morphology of the deposits are similar to debris flows and pyroclastic flows on Earth. This explains the similarity between the Martian gullies and the water-shaped gullies on Earth without the presence of liquid water on the surface of Mars today. These results also suggest that gully landforms on other planets can be formed by both sublimation-driven flows and fluid-driven flows.

1 Introduction

Despite the lack of stable liquid water on Mars today (Hecht, 2002; Richardson & Mischna, 2005), Mars is a geomorphologically active planet. Numerous studies in the last decades have documented a range of geomorphic activities (for an overview see (Diniega et al., 2021)). Among the most active landforms on Mars are Martian gullies (Figure 1). These landforms consist of an erosional alcove, a channel, and a depositional apron and resemble debris flow systems on Earth (Malin & Edgett, 2000; Costard et al., 2002; Conway et al., 2011; Johnsson et al., 2014; T. de Haas et al., 2015c). Since their discovery, Martian gullies have been a topic of scientific debate because of the possible link between their formation and liquid water (Malin & Edgett, 2000; Costard et al., 2002; T. de Haas et al., 2015c; Dickson et al., 2023), and thus planetary habitability (Hoffman, 2002; Cottin et al., 2017).

Present-day activity in gullies is observed in subsequent images as new depositional lobes on aprons, the carving of new channels, and the movement of meter-scale boulders (Dundas et al., 2010; Diniega et al., 2010; Dundas et al., 2015; Raack et al., 2020; Sinha & Ray, 2023). As this activity is observed on slopes as low as 10° (Dundas et al., 2019), the material needs to have been fluidized to a certain degree (T. de Haas et al., 2019) and thus dry granular processes cannot have been the cause of the change. In the last decade, the leading hypothesis behind the recent activity in these gullies has shifted from water-driven flows (with or without the involvement of brines) (e.g., Malin & Edgett, 2000; Costard et al., 2002; Knauth & Burt, 2002; Lanza et al., 2010; Levy et al., 2010; Conway et al., 2011; Johnsson et al., 2014; T. de Haas et al., 2015c) to flows driven by the sublimation of CO_2 frost (e.g., Diniega et al., 2010; Dundas et al., 2010, 2012, 2015; Raack et al., 2015, 2020; Pilorget & Forget, 2016; T. de Haas et al., 2019; Khuller et al., 2021; Dundas et al., 2022; Pasquon et al., 2023; Sinha & Ray, 2023). This shift is inspired by the lack of stable water on the Martian surface (Hecht, 2002; Richardson & Mischna, 2005) and a suite of remote sensing studies, showcasing the correlation between the spatial and temporal distribution of gully activity with that of CO_2 frost on the surface of Mars (Diniega et al., 2010; Dundas et al., 2010, 2012, 2015; Raack et al., 2015; Pasquon et al., 2019; Raack et al., 2020; Khuller et al., 2021; Dundas et al., 2022; Pasquon et al., 2023; Sinha & Ray, 2023) (for examples see Figure 1). The CO_2-driven granular flow hypothesis is supported by modelling studies advocating for the possibility of CO_2 gas to fluidize granular material under the thin Martian atmosphere when CO_2 sublimates (Pilorget & Forget, 2016; Cedillo-Flores et al., 2011; T. de Haas et al., 2019). Furthermore, experimental studies have proven that the sublimation of CO_2 ice in the thin Martian atmosphere can destabilize granular materials on slopes (Sylvest et al., 2016, 2019) and even fluidize small volumes of granular material on low angles (Roelofs et al., n.d.). The low atmospheric pressure of the Martian atmosphere is key in this process because of the large gas flux that is created when CO_2 ice sublimates and turns into CO_2 gas (Diniega et al., 2013; Sylvest et al., 2016; T. de Haas et al., 2019; Sylvest et al., 2019; Roelofs et al., n.d.). The gas flux, induced by the sublimation, depends on the ratio between the density of CO_2 ice and gas. In the thin Martian atmosphere (~800 Pa), the gas flux created by CO_2 sublimation is >100 larger than under Earth's atmosphere and thus likely sufficient to fluidize sediments (Cedillo-Flores et al., 2011; T. de Haas et al., 2019).

There are currently two "source-to-sink" hypotheses that attempt to explain how and why CO_2 ice sublimates near granular material on Mars, how this process mobilizes the granular material, and how it transports it over longer distances. The first hypothesis considers a layer of translucent CO_2 ice on top of a layer of regolith (Pilorget & Forget, 2016). This hypothesis is, in essence, the 'Kieffer model' explaining the formation of high-latitude defrosting spots (Kieffer, 2007) on a slope. According to this model, the translucency of CO_2 ice allows the solar radiation at the end of winter to heat up the underlying regolith during the day. This heat causes basal sublimation of the overlaying ice layer, building up the air pressure underneath the ice. This pressure can be large enough to lift the ice layer and eventually break it, forming jets of pressurized CO_2 gas (Hoffman, 2002; Kieffer, 2007). The gas flux created can potentially destabilize large amounts of slope material, also underneath the ice (Pilorget & Forget, 2016). However, the requirement of slab ice means that the latter mechanism is only applicable to Martian gullies at latitudes > 40°S where evidence for slab ice is observed (Dundas et al., 2017, 2019), whereas half of the observed active gully sites on the southern hemisphere are present at latitudes < 40°S (Dundas et al., 2022). Furthermore, this hypothesis does not explain how the pressurized flows underneath a layer of CO_2 ice would result in the deposition of new lobate deposits and the movement of meter-scale boulders.

The second hypothesis explains the observations of fluidized granular flow via two effects within a mix of sediment and CO_2 ice tumbling down a gully (Dundas et al., 2017). The initial mass movement can be triggered by many different processes, unrelated and related to CO_2 ice sublimation, for example, dry raveling, rock fall, marsquakes, meteor impacts or CO_2 sublimation-induced slumping (Sylvest et al., 2016, 2019). In the event that a mixture of CO_2 ice and granular material starts to move, the potential energy of the fall is converted to kinetic energy that must be dissipated as heat or latent heat loss in the form of sublimating CO_2 (Dundas et al., 2017; T. de Haas et al., 2019; Roelofs et al., n.d.). Furthermore, eroded and entrained sediment from the shallow subsurface or unfrosted areas could add additional heat to the mixture, enhancing sublimation (Hoffman, 2002; Dundas et al., 2017). The sublimation of the ice in the sediment-ice mixture is hypothesized to create a gas flux large enough to decrease intergranular friction and fluidize the mixture in such a way that it explains recent flows (T. de Haas et al., 2019; Roelofs et al., n.d.).

Details aside, all current theories on the CO_2-driven fluidization of granular material on Mars agree on two crucial points; (1) heat is needed to sublimate the CO_2, and (2) increased pore pressure, from the CO_2 gas, in the granular material is crucial to decrease intergranular friction and cause fluidisation. However, major research questions remain unanswered. First, it remains speculative whether and exactly how the sublimation of CO_2 ice is able to fluidize granular material. Second, it is unknown how much CO_2 ice needs to sublimate to explain the observed changes. Third, it is unclear how CO_2-driven granular flows on Mars create landforms that are practically identical to landforms created by water-driven debris flows on Earth. Active depositional aprons on both Earth and Mars show lobate deposits with clear levees, and contain meter-scale boulders that are transported through the gully system (T. de Haas et al., 2019; Raack et al., 2020; Dundas et al., 2022). The similarity in key elements in these landforms suggests similarity in the flow dynamics, but this remains unproven.

In this work, we experimentally study the fluidization of granular material by CO_2 ice sublimation under Martian conditions. We aim to (1) resolve the boundary conditions needed to fluidize granular material by CO_2 ice sublimation on Mars, (2) understand the fluid dynamics of CO_2-driven granular flows, and (3) understand the similarities between the CO_2-driven granular flow deposits on Mars and debris-flow deposits on Earth.

To overcome the lack of in-situ observations of CO_2-driven granular flows, we designed two experimental granular flow set-ups that were used to conduct experiments under Martian atmospheric pressure in environmental pressure chambers. In these experiments, granular flows driven by the sublimation of CO_2 in a mixture of sediment and CO_2 ice were created under different boundary conditions, i.e. CO_2 content and slope, and on two different scales to understand potential scale effects. The results of these experiments provide new insights into the flow dynamics of CO_2-driven granular flows on Mars and the resulting deposit morphologies. It is important to note that with our research we specifically aim at studying the transport and deposition processes of CO_2-driven granular flows, rather than the initiation mechanisms behind these flows.

2 Materials and Methods

To study if and how a mixture of CO_2-ice and granular material is fluidized under Martian atmospheric conditions we designed two experimental set-ups at two different scales based on terrestrial debris flow flumes (Iverson et al., 2010; T. de Haas et al., 2015b; Roelofs et al., 2022). The flumes were placed in two environmental chambers of different sizes to enable us to conduct experiments under Martian atmospheric conditions (Figure 2.a–b). Similar to terrestrial debris flow flumes, our flumes consisted of a steep and narrow chute ending on a larger outflow plain with a lower angle (Figure 2.c–f). The steep and narrow chute is used to study flow characteristics, e.g. flow depth, velocity, and pore pressures. Whereas the larger plain is used to study deposit morphology. The angle of the chute was varied during our experiments, whereas the angle of the outflow plain was kept constant (Figure 2.e–f). As is common practice in debris flow experiments, we stored the material that makes up the granular flow in a reservoir at the top of the flume before controlled release. Using flumes of two different sizes enabled us to study possible scaling issues known to influence the behaviour of experimental terrestrial debris flows (Iverson, 2015). The small-scale flume has a total length of 1.80 m and has a material reservoir that can store between 1.0 and 1.6 kg of material (Figure 2.e). The large-scale flume has a total length of 4.60 m and has a material reservoir that can store between 8.0 and 11.2 kg of material (Figure 2.f). This means that, while the large flume is only a factor 2.5 longer than the small flume, the granular flow it supports is 10 times larger.

The small-scale flume was used for conducting experiments in the Mars chamber of the Hyper Velocity and Impact lab (HVI-lab) at the Open University in Milton Keynes in the United Kingdom in the autumn of 2021. The large-scale flume was used for conducting experiments in the Mars Simulation Wind Tunnel at Aarhus University in Denmark in the autumn of 2022. To compare results between the flumes, experiments were performed with similar initial and boundary conditions. In this manuscript, 46 experiments conducted in the small-scale set-up in the Mars chamber of the Open University are presented, and 15 experiments conducted in the large-scale set-up in the Mars Simulation Wind Tunnel are presented.

2.1 Chamber and flume details

The Mars chamber of the HVI-lab at the Open University is a cylindrical low-pressure chamber with a length of 2 m and an inner diameter of 0.9 m (Conway et al., 2011; Sylvest et al., 2016) (Figure 2.a). The chamber can replicate Martian atmospheric conditions and a range of different temperatures.

The Mars Simulation Wind Tunnel at Aarhus University is a cylindrical low-pressure wind tunnel, originally designed to simulate eolian transport processes on Mars (Holstein-Rathlou et al., 2014) (Figure 2.b). The chamber has a total length of 8 m and an inner diameter of 2.15 m. In both chambers, electrical and mechanical feedthroughs exist to enable the operation of the experimental set-up in the chamber from the outside. Both chambers have multiple porthole windows that allow for videography of the experiments.

Both the large-scale and the small-scale flume were mostly constructed out of Lexan, a transparent polycarbonate resin thermoplastic, that can deform considerably without cracking or breaking. The transparency of the Lexan was an important design prerequisite because it allowed us to study the granular flow from the side of the chute. The bottom of the chute was created out of aluminium, with heating pads installed underneath it that controlled the temperature of the chute bottom, which was kept at 20 °C during the experiments. On the edges of the outflow plain, markers were attached that were used for creating 3D models of the outflow morphologies using photogrammetry with Agisoft Metashape software. The outflow plains of the flumes were further covered with antislip material (3M Safety-Walk 500 series, equal to 80 grit sandpaper with 0.2 mm median sand diameter) to mimic natural roughness. To achieve the same for the chute bottom, the aluminium was sandblasted. The sediment and ice reservoirs on top of the flumes were constructed out of copper for the small set-up, and out of aluminium for the large set-up, because of their relatively low deformation under low temperatures. The reservoirs in both flumes are opened by means of mechanically operated trap doors. In the small-scale flume the entire reservoir opened at once, whereas in the large-scale flume, the opening height was set at 5 cm. This difference in design allowed a more constant and stable flow of granular material in the large-scale experiments, providing better insight into the flow dynamics.

In both flumes, the same sensors were used to study the flow dynamics. In the downstream part of the chute, four sensors were installed underneath the chute bottom plate (Figure 2.e-f); a geophone (Geospace GS-20DX), two relative gas pressure sensors (Honeywell TruStability HSCDRRD006MGAA5), and a load cell (HBM PW6D – 3 kg). The geophone and the load cell were attached to individual load plates of 5 by 5 cm. The geophone recorded seismic vibrations during the experiment, the pressure sensors recorded the gas pressure at the bottom of a flow relative to the ambient pressure, and the load cell recorded the weight of the granular material as the flow passed. Above the flume, multiple laser distance sensors (Baumer OADM 20U2480/S14C) were installed that recorded the flow depth at sub-mm accuracy. In the small-scale set-up two laser distance sensors were used, whereas in the large-scale set-up, four laser distance sensors were used. With the time difference of the arrival of the flow front at the different laser distance sensors, reconstructed from the flow depth data, flow velocity was calculated. In both set-ups, the last laser distance sensor was installed above the load cell (Figure 2e-f). This allowed us to reconstruct the density of the flow, ρ_m, according to:

$$\rho_m = \frac{M}{AH} \tag{1}$$

where M is the mass recorded by the load cell (kg), A is the area of the load cell (m^2), and H is the flow depth (m). Furthermore, by combining the load cell data and the data from the pore pressure sensors, the percentage of the material in the flows carried by the gas pressure could be quantified. The latter is a measure of the degree of fluidisation. For more detailed photos of the chambers, the flumes and the sensors see Supplementary Figure 1.

The amount of CO_2 ice sublimating during the flow in the large-scale set-up could be calculated from the data produced by a capacitance pressure sensor in the Mars Simulation Wind Tunnel. By adding the pressure drawdown caused by the pumping to the observed pressure increase during the experiment we reconstructed the amount of CO_2 released into the chamber during the flow for three individual experiments with varying amounts of CO_2 ice in the granular mixture (Figure 7).

Multiple video cameras were installed in and around both chambers. For the small-scale set-up, every experiment was recorded with a Go-Pro camera from the side and a camcorder from the front. For the large-scale set-up, every experiment was recorded with two webcams in the chamber that looked at the chute from the side, and one high-speed camera that filmed the flow at the transition from the chute to the outflow plain at a frame rate of 600 Hz.

2.2 Materials used and experimental routine

Two materials form the ingredients of the granular mixture in our experiments; sand and CO_2 ice. The sand for the experiments is a mixture of fine-grained sand (silver sand of marine origin, D_{50} of 270 μm) and coarse-grained sand (builders sand of fluvial origin, D_{50} of 490 μm), combined in a specific ratio (0.6–0.4) to create a broad grain size distribution (D_{50} of 310 μm, Supplementary Figure 2) that minimizes gas permeability relative to a mono-disperse sand, and thus slows down the gas escape rate. Experiments conducted with only silver sand or only builders sand behave similarly overall, although finer mixtures flow further onto the outflow plain. Results of these experiments are presented in the Supplementary Material (see Supplementary Figure 6). The sand was predried in the oven and cleared of any excess moisture in the environmental chambers by putting it in a vacuum prior to the experiments.

The CO_2 ice used for our experiments was ordered in pellet form from commercial parties close to the labs. The CO_2 ice pellets were then crushed to the size of the coarsest sand grains. For the small-scale experiments, this was done by hand with the use of a mortar and pestle. For the large-scale experiments, the ice was crushed with the KitchenAid 5KGM grain mill. Despite the difference in methods, the resulting CO_2 ice grains are similar in size and shape (see Supplementary Figure 3.c-d). To limit the contamination of the CO_2 ice with water, the CO_2 ice was stored in closed polystyrene foam containers in a sealed freezer (Supplementary Figure 3.a-b), and the ice was refreshed at least once a week.

For every experiment, CO_2 ice would be freshly crushed and mixed with a specific amount of sand. To control the amount of CO_2 ice at the start of an experiment, the combined weight was monitored during the mixing process. The loss of CO_2 due to sublimation was compensated by adding more crushed CO_2 ice. Once the desired weight ratio of sediment and CO_2 ice was reached, the mixture was poured into the sediment-ice reservoir in the flume. After this, the chamber was closed and depressurized to an atmospheric pressure of $\sim$8 mbar, a process that took between 12–15 min in the Mars Chamber at the Open University and between 20–25 min in the Mars Simulation Wind Tunnel at Aarhus University. At this pressure, the mixture was released into the flume, while the sensor data was logged and the videos recorded the passing of the granular flow.

2.3 Explored parameter-space

To determine the conditions under which CO_2-driven granular flows can occur on Mars, experiments were conducted under different initial and boundary conditions. For both the experiments in the small-scale and the large-scale set-up, the CO_2-sediment ratio was systematically varied, as well as the slope of the chute. The CO_2-sediment ratio was varied between 0 and 0.6 in the small-scale experiments and varied between 0 and 0.4 for the large-scale experiments (Table 1), while keeping the flume chute at a stable angle of 30°. Note that the mass ratio here is the ratio between the mass of the CO_2 and the sediment before depressurization of the chamber. During depressurization the CO_2 sublimates, which causes the mass ratio to change. We quantified this change for both the small- and large-scale setup by doing initial tests tracking the weight of the mixture inside the sediment-ice reservoir while depressurizing the chamber. The results of these tests can be found in Supplementary Figure 4. In the subsequent sections of this manuscript, we switch from using the initial CO_2-sediment mass ratios to using the mass fraction of CO_2 at the start of an experiment derived from these tests.

Table 1. Parameters explored in the experiments and the tested values. All parameters and values reported in this table are tested in the small-scale setup. The values of the parameters in bold font and teal colour are the ones also tested in the large-scale setup. For more details on the grain-size distributions see Supplementary Figure 2. For a full list of all experiments see Supplementary material.

Variable	Unit	Standard value	Tested values
CO_2-sediment ratio	(kg/kg)	0.3	**0**, 0.1, **0.2**, **0.3**, **0.4**, 0.5, 0.6
Chute angle	°	30	**20**, **25**, **30**
Sediment type		Sand mixture	**Sand mixture**, Fine, Coarse
Atmospheric pressure	mbar	8	**8**, 1000

The angle of the chute was varied between 20 and 30 degrees in both the small-scale and the large-scale experiments (Table 1), while keeping the initial CO_2-sediment mass ratio at 0.3. In the small-scale experiments, we did additional tests with different sediment types and under Earth atmospheric pressure (Table 1). To account for the effects of natural variability, each experimental setting was repeated at least twice, and when time allowed three times. A complete list of all experiments and their initial and boundary conditions can be found in the Supplementary material 8.

2.4 Flow characterization

To characterize the dynamics of the CO_2-driven granular flows and objectively compare the flows of different sizes three dimensionless numbers are used; the Bagnold, Savage, and friction numbers. These numbers are used in both debris flow (Iverson, 1997; Iverson & Denlinger, 2001; Roelofs et al., 2022, 2023) and pyroclastic literature (Smith et al., 2020) and therefore also allow for comparison between the CO_2-driven granular flows, and terrestrial debris flows and pyroclastic flows. The numbers describe the relationship between the motion-resisting forces in granular flows; collisional forces, frictional forces, and viscous forces (Iverson, 1997; Parsons et al., 2001; Iverson et al., 2010). The relative importance of these forces plays a big role in both erosional (T. d. de Haas & Woerkom, 2016; Roelofs et al., 2022) and depositional processes (T. de Haas et al., 2015b; Zhou et al., 2019) and is, therefore, an important tool in understanding how certain flows lead to certain morphological features. The Bagnold number describes the ratio between collisional and viscous forces (Iverson, 1997):

$$Nb = \frac{v_s \rho_s \delta^2 \gamma}{v_f \mu} \tag{2}$$

wherein v_s is the volumetric solids fraction, ρ_s is the density of the sediment grains, δ is the D_50 grain size of the sediment (m), v_f is the volumetric fluid fraction, μ is the dynamic viscosity of CO_2 gas under Martian atmospheric conditions, which is $9.82{*}10^{-6} Ns/m^2$ (Bardera et al., 2020), and γ is the flow shear rate $(1/s)$:

$$\gamma = \frac{u}{H} \tag{3}$$

wherein u is the is the flow velocity (m/s). According to Iverson (1997), collisional forces dominate at $N_b > 200$.

The Savage number quantifies the ratio between collisional and frictional forces:

$$N_s = \frac{\rho_s \delta^2 \gamma^2}{(\rho_s - \rho_f) g H \tan\phi} \tag{4}$$

wherein g is the gravitational acceleration (m/s^2), ρ_f is the density of the fluid, in our case this is the density of the CO_2 gas at 8 mbar, and ϕ is the internal angle of friction, assumed to be 42° (Parsons et al., 2001; T. de Haas et al., 2015b). The density of the CO_2 gas at a certain pressure can be calculated from the ideal gas law:

$$\rho_f = \frac{P M_m}{RT} \tag{5}$$

wherein P is the atmospheric pressure (Pa), M_m is the molar mass of CO_2, R is the universal gas constant, and T is the temperature (K). For $N_s > 0.1$ collisional forces dominate viscous forces (Iverson, 1997). The friction number is then defined as the Bagnold number divided by the Savage number, describing the ratio between frictional and viscous forces. According to experimental data of wet experimental debris flows of Parsons et al. (2001) and T. de Haas et al. (2015b) frictional forces dominate over viscous forces at $N_f > 100$ for the flow body and $N_f > 250$ for the flow front.

3 Results

3.1 General flow behaviour and morphology

Increased fluidisation of the material was observed for all experiments under Martian atmospheric pressures with CO_2 ice in the granular mixture. Compared to reference experiments without CO_2 ice, these experiments showed >2 times larger flow velocities and run-out, with typical flow velocities of 2 m/s for the small-scale flows and 3 m/s for the large-scale flows. For both the large-scale and the small-scale experiments, flow depths reached maximum values around 2 cm (Figure 3.a-b), and flow densities around 1000 kg/m^3. The relatively small flow depth in the large-scale experiments was caused by the controlled, and limited, outflow height in this setup. In both set-ups, the flow depth increased rapidly when the flow front arrived and dissipated more slowly when the tail passed. In experiments without CO_2, as soon as the flow front arrived at the outflow plain the flow stopped and the chute backfilled with sediment.

Both the small-scale and large-scale CO_2-driven granular flows show multiple surges (see Figure 3.a-b and the Supplementary videos). For all flows with CO_2 in the mixture, increased gas pressures were registered at the base of the flow (Figure 3.a-b). This gas pressure carried between 20–60% of the flow mass, independent of the experimental scale (Figure 3.c). When analysing the high-speed video of the experiment presented in Figure 3.a it becomes clear that the velocity of the granular flow is highest in the centre of the flow and that the flow itself is turbulent (see high-speed video in Supplementary videos).

The morphology of the outflow deposits of experiments with CO_2 in the granular mixture often contain multiple lobes formed by different surges (Figure 4). These lobes are stacked on top of each other (see for example Figure 4.c,l), and, in some cases, next to each other (see for example Figure 4.f,k). In both the small-scale and large-scale set-up levees form in experiments where a second surge of granular material deposits on top of an earlier surge (see Figure 4.b,f). With increased amount of CO_2 in the granular mixture the material flows further out onto the outflow plain (Figure 4.a–f). Increasing the chute slope by 5–10°also causes the material to flow further onto the outflow plain (Figure 4.g–l). In the large-scale experiments, a small increase in slope has a larger effect on the outflow length than doubling the CO_2 content (Figure 4.d–f and Figure 4.j–l). When no CO_2 is present in the granular mixture only a small sediment cone forms on the transition from the chute to the outflow plain.

3.2 Flow velocity, depth, and pore pressure

In the large-scale set-up, flow velocities in the lower half of the chute are constant (Supplementary Figure 5) and reach values around 3 m/s, independent of the CO_2 fraction (Figure 5.a). In the small-scale set-up, for high CO_2 fractions between 0.14 and 0.3, flow velocities around 2 m/s are recorded at the end of the chute, whereas for the lower CO_2 fractions the velocity slowly increases from 1 m/s to 2 m/s with increasing CO_2 fraction. When no CO_2 is present in the granular mixtures, no enhanced fluidisation is observed and the frontal velocity of the material is around 1 m/s in both set-ups. The same can be stated for granular flows with CO_2 in the mixture released under Earth atmospheric pressure. For both the large-scale and small-scale flows, an increase in the chute angle, from 20° to 30°, causes a small increase in flow velocity, from 2.2 to 3 m/s (Figure 5.b).

Maximum flow depth increases linearly with CO_2 mass fraction for both set-ups (Figure 5.c). This relation is steeper for the small-scale set-up. When increasing the chute angle, maximum flow depth decreases in the large-scale set-up from 22 to 14 mm, while staying around 15 mm in the small-scale set-up (Figure 5.d). Flow depths are stable in the lower half of the large-scale flume for all experiments (Supplementary Figure 5). In the small-scale flume, the flow depths are still increasing in the lower half of the flume, especially when the chute is on the steepest angle.

Increased basal pore pressures are observed in all experiments. Basal pore pressures increase with increasing CO_2 mass fraction and decrease with increasing chute slope (Figure 5.e-f). The differential pressure signal, which is the difference between the ambient pressure and the basal pressure, is more scattered for the small-scale experiments. This is likely caused by the combination of smaller, less stable flows, and a higher amount of deposition of granular material in the chute during the experiment compared to the large-scale set-up. Maximum added pressures in the large-scale set-up vary between 0.2 and 0.6 mbar, whereas they vary between 0 and 0.4 for the small-scale set-up.

The type of granular material used, either silver sand, builders sand, or the mixture, did not significantly influence the flow dynamics of the flows in the small-scale set-up (Supplementary Figure 6). Frontal velocities, maximum flow depths, and maximum basal pressure were the same for all sand types. The type of granular material used did influence the outflow deposit. CO_2-driven granular flows comprised of finer sands flowed out further.

3.3 Flow density, fluidisation and CO_2 sublimation during the flow

The density of the flow is calculated from the weight data from the load cell and the depth data from the laser distance sensor above the load cell. In addition, the load cell data and the data from the pore pressure sensors are combined to calculate the percentage of the material in the flows carried by the gas pressure. Here, we only present results from the large-scale experiments, because it was not possible to calculate flow density and degree of fluidisation for the experiments in the small-scale set-up due to the deposition of material on the load cell while the granular material was still flowing. Based on the combined data of the entire flow of all large-scale experiments, summarised in boxplots in Figure 6.a–b, we can state that our experimental CO_2-driven flows have a density around 1000 kg/m^3. This density is not dependent on the CO_2 fraction (Figure 6.a) but is slightly dependent on the chute angle (Figure 6.b). If the angle becomes steeper, the density decreases slightly. The fraction of the flow mass supported by the gas pressure ranges between 0.2–0.3 on average, with a small dependency on CO_2 mass fraction (Figure 6.c–d). For flows with a higher CO_2 fraction, a slightly higher percentage of the flow is supported by the gas pressure (Figure 6.c).

The data from the capacitance pressure sensor in the chamber of the large-scale set-up shows that for an experiment with a CO_2 mass of 0.59 kg at the beginning of the experiment (Supplementary Figure 4), only 42 grams of CO_2 sublimates during the flow (Figure 7.a). For an experiment with a CO_2 mass of 1.12 kg at the beginning of the experiment (Supplementary Figure 4), only 57 grams of CO_2 sublimates during the flow (Figure 7.b). For an experiment with a CO_2 mass of 2.13 kg at the beginning of the experiment (Supplementary Figure 4), only 92 grams of CO_2 sublimates during the flow (Figure 7.c). This means that for all experiments between 0.8–1.3% of the total flow mass (sand and CO_2 ice), and 0.5–0.9% of the volume (assuming a porosity of 0.4) sublimates. When normalized for chute length, width, and flow duration, the volume loss is 0.3%–0.55% per m^2/s, and the mass loss is 0.025–0.055 kg/m^2/s.

3.4 Dimensionless flow characteristics

To quantitatively compare the flow dynamics of the large-scale and small-scale granular flows, we characterized the flows using the dimensionless numbers discussed in the methods; the Bagnold, Savage, and friction numbers (Figure 8). Furthermore, this dimensionless analysis provides the opportunity to place the flow dynamics of the CO_2-driven granular flows into the context of other granular flows, such as debris flows and pyroclastic flows. In all of our experimental CO_2-driven granular flows, frictional forces dominated over collisional and viscous forces (Figure 8.c–f). In addition, the Bagnold numbers of our flows indicate that collisional forces dominated over viscous forces (Figure 8.a–b). The large-scale flows are relatively more collisional than the small-scale flows (Figure 8.a–d). Increasing the CO_2 mass fraction in the granular mixture does not have a large effect on the Bagnold or Savage numbers (Figure 8.a–d) . However, it does affect the relation between frictional and viscous forces, making viscous forces less important (Figure 8.e–f). An increase in the angle of the chute results in a larger relative influence of collisional forces (Figure 8.b,d).

4 Discussion

4.1 Initial and boundary conditions for CO_2-driven flows

Our experiments show that granular material can be fluidized by sublimating CO_2 ice under Martian atmospheric conditions (Figure 3 and Figure 5). This is enabled by the low Martian atmospheric pressure of around 8 mbar, which makes the gas flux from sublimation large enough to decrease intergranular friction between the grains and fluidize the granular material (Figure 5) (Cedillo-Flores et al., 2011; T. de Haas et al., 2019). Under terrestrial atmospheric pressure of around 1000 mbar, sublimation of CO_2 ice still occurs, but the gas flux from the ice into the atmosphere is not large enough to decrease intergranular friction and fluidize the granular material. From our experiments, it can be inferred that the fluidisation induced by the sublimation of CO_2 ice grains in a granular mixture can sustain a stable fluidized flow in a channel, i.e. the flume chute, as long as CO_2 ice is present and enough energy is available for sublimation. In our experiments, less than 10% of CO_2 ice in the mixture sublimated while in the chute, implying that the mixture could have likely flowed in a sustained fluidized way in a confined chute with a length of $\sim$10-20 metres.

The fluidisation of the material by the sublimation of CO_2 ice in the chute is reflected in the enhanced frontal flow velocities and increased basal pressures (Figure 5). In experiments under Martian atmospheric conditions, where CO_2 ice is present in the granular mixture, velocities between 2 and 3 m/s are reached, whereas frontal velocities in experiments without CO_2 ice, or with CO_2 ice under Earth atmospheric pressure, are only 1 m/s (Figure 5). Furthermore, the pressure data show that the gas pressure carries between 20–60% of the total flow mass in the experiments with CO_2 ice (Figure 3.c and Figure 6).

In the large-scale experiments, stable flow velocities around 3 m/s are reached in the lower part of the chute for all experiments, even for the experiments with the smallest amount of CO_2 ice in the mixture. This implies that for all the different CO_2 ice fractions tested, the rate of fluidisation is high and comparable, which is supported by only small differences in the amount of the flow carried by the pore pressure (Figure 6). Therefore, we hypothesise that granular material can be fluidized by the sublimation of even smaller amounts of CO_2 ice than we tested. In the small-scale experiments, we do see an increase in flow velocity and fluidisation rate for the smallest CO_2 ice fractions (Figure 5.a), which would imply a higher fluidisation rate for larger CO_2 ice fractions. However, we hypothesize that this trend is likely caused by the limited length of the chute compared to the distance over which the flow accelerated, instead of an actual relation between CO_2 fraction and velocity in our small-scale set-up. The longer chute length in our large-scale set-up allows the flow to reach a stable state where a balance exists between CO_2 ice sublimation, the reduction in friction because of the induced gas pressure, and the remaining friction, as we see in the large-scale set-up.

Our experiments also show that CO_2-driven granular flows are fluidized enough to flow on slopes below the angle of repose. CO_2-driven flows in experiments with chute angles of 20° still reach velocities 2 times higher than those of dry granular material without CO_2. In addition, the CO_2-driven flows continue to flow over the outflow plain of our set-ups, which have even lower slope angles, 10° and 12° for respectively the large-scale and small-scale set-ups. However, as the flow on these outflow plains is unconfined, the granular material spreads out laterally and ultimately halts (Figure 4). The lateral spreading decreases the flow depth and increases the relative amount of friction the flows have to overcome, both by increasing the area for gas escape and increasing the contact between the flow and the surface. These experimental observations on fluidisation on slopes below the angle of repose are important because they support the hypothesis that CO_2-driven flows on Mars can cause the changes we observe, like new depositional lobes on aprons with slopes as low as 10° to 15° (Diniega et al., 2010; Raack et al., 2020; Sinha & Ray, 2023).

The data from the pressure sensors in the chamber of the large-scale set-up highlight that the mass of CO_2 ice that needs to sublimate for the fluidisation process is small. For example, to fluidize 8 kg of sand in our experiments, as little as 43 gram of CO_2 ice needs to sublimate, equal to ∼0.5% of the volume fraction of the flow (Figure 7). In other words, in our experiments, a mass loss of sublimating CO_2 ice between 0.025–0.055 kg/m^2/s is enough to create fluidized granular flows.

4.2 Heat transfer from the environment to the CO_2 ice

Our experiments clearly show that granular material can be fluidized by sublimating small amounts of CO_2 ice, less than 1% of the total flow weight, under Martian atmospheric conditions when sufficient energy is available for CO_2 ice sublimation. However, where that energy is coming from on Mars is debated. According to (Dundas et al., 2017; T. de Haas et al., 2019), this energy could be provided by the release of kinetic energy of a fall or from heat from warmer material in contact with the granular mixture of CO_2 ice and sediment. The sublimating ice would consequently increase pore pressures in the involved granular material, which would cause fluidisation and a two-phase granular flow. If all potential energy of a fall of 300 m, as earlier used by Dundas et al. (2017), would be transferred to heat according to:

$$E_p = mgL \tag{6}$$

with m as the mass of the material falling (kg), g the gravitational acceleration on Mars (3.71 m/s^2), and L being the fall height, the total available potential energy, E_{pot}, would equal to 1113 J per kg material. For our flume set-ups, the total potential kinetic energy is smaller, with 16.7 J/kg in the large-scale set-up and 5.9 J/kg for the small-scale set-up. However, the enthalpy of sublimation of CO_2 ice, which is the energy needed for the phase transition from ice to gas, is around 26–28 kJ/mol (Stephenson, 1987; Cedillo-Flores et al., 2011; Shakeel et al., 2018), which is equal to an energy of 590–636 kJ/kg, accounting for the molecular mass of CO_2 of 44.01 g/mol. Therefore, the amount of energy needed to sublimate CO_2 is much higher than is released from the complete conversion of potential energy to heat, both in our flumes and on Mars. Therefore, we hypothesize, as Dundas et al. (2017) did earlier, that the heat from the environment, thus from warmer material and surfaces in contact with the flow, is the main driver of sublimation instead of kinetic energy conversion.

Granular material at a slightly higher temperature than the CO_2 frost point could make several thousand J/kg available (Dundas et al., 2017). To put numbers to this, for our flumes the energy available in the aluminium bottom plate to sublimate CO_2 ice at the frost point temperature can be calculated as follows:

$$E_t = mc\Delta T \tag{7}$$

with m the mass of the aluminium, c the specific heat (902 J/kgK) and ΔT the temperature difference between the temperature of the chute bottom (20 °C, or 293 K) and the

CO_2 frost temperature (−120 °C, or 153 K). For our small-scale flume E_t is 67 kJ, and for our large-scale flume E_t is 324 kJ. If all this thermal energy is used to sublimate CO_2 ice, between 0.51 and 0.54 kg of CO_2 ice could sublimate in our large-scale set-up and between 0.1 and 0.11 kg of CO_2 ice could sublimate in our small-scale set-up. The predicted mass of CO_2 that could sublimate as a result of heat energy in our large-scale flume is similar to the actual observed mass of CO_2 ice that sublimated during the flows (Figure 7).

Equation 7 can also be used to estimate the amount of potential thermal energy available for sublimation at the bottom of a hypothetical gully on Mars. Taking two gullies in Hale crater, studied by T. de Haas et al. (2019), as an example; we state that our hypothetical Martian gully is incised in basaltic bedrock (c = 600 J/kg°C, ρ_{basalt} = 3000 kg/m^3), has a length of 600 m, a width of 15 m, and in the gully, the upper 1 mm of the surface regolith is heated up to a temperature of 20 °C, which is realistic for active gullies according to climate modelling (Roelofs et al., n.d.). In this gully system, the total potential thermal energy equals 2.27*10^6 kJ. If all this energy is used to sublimate CO_2 ice, between 3570 and 3840 kg of CO_2 at frost temperature could be sublimated. Suppose we combine the sublimating ice-to-sediment ratio in our experiments, of 0.5-0.9%, with this estimated CO_2-ice mass for extrapolation purposes. In that case, we can estimate that between ∼396000 – ∼769000 kg or ∼247 – ∼480 m^3 of unconsolidated granular material could be fluidized in this Martian gully when enough ice is available. Although this estimate is likely too conservative because it does not account for the weaker Martian gravity and the possible entrainment of warmer sediment, the prediction matches the back-calculated flow volumes of 415 and 263 m^3 in the smaller gullies in Hale crater (T. de Haas et al., 2019).

In general, our experimental granular flow results on thermal energy, flow volume, and the necessary mass of CO_2, agree with the back-calculated numbers for actual Martian flows (T. de Haas et al., 2019). Nonetheless, our predicted $E_{thermal}$ neglects important parameters and processes in thermodynamics. In the first place, it assumes that all heat is converted to energy for sublimation during the flow. This is unlikely because heat transfer does not happen instantaneously and is dependent on the type of heat transfer, the duration of the potential transfer, and the materials involved. The heat transfer process is further complicated by the newly-found turbulent behaviour of CO_2 driven flows, the presence of multiple materials, the unknown areas of contact between the cold ice and the warmer materials, and the possible entrainment of warmer material into the flow (T. de Haas et al., 2019). Furthermore, for experiments, this $E_{thermal}$ does not account for the constant heat input into our flume from heating pads installed underneath the aluminium bottom plate. Despite the still unresolved complications, the predicted thermal energy is multiple orders of magnitude larger than the potential energy transformed from a fall, both in our flumes as in our hypothetical gullies on Mars. The heat energy from the environment, either transferred by conduction, radiation, or convection, is, therefore, more likely to be the cause of the sublimation of the CO_2 ice in CO_2-driven granular flows on Mars. This implies that CO_2-driven granular flows can only occur in gullies on Mars at specific locations and during specific periods during the Martian year when CO_2-ice and warmer regolith simultaneously exist in the gully (Roelofs et al., n.d.).

4.3 Flow dynamics and morphology of CO_2 driven Martian flows in (terrestrial) context

To enable a fair comparison between the flows in the two different experimental setups, and compare our CO_2-driven flows with other two-phase granular flows we conducted dimensionless analysis. This analysis shows that the CO_2-driven flows in our experiments are supercritical two-phase flows (see Froude numbers in Supplementary Figure 7) in which frictional forces dominate, and collisional forces are more important than viscous forces (Figure 8). In experimental and real debris flows, frictional forces typically dominate (Iverson, 1997; Iverson & Denlinger, 2001; Roelofs et al., 2022, 2023) (Figure 9). In experimental dense pyroclastic density currents, frictional forces dominate, and viscous forces seem to be more important than collisional forces (Smith et al., 2020) (Figure 9). The latter could stem from the relatively small grain size between 45—90 μm used by (Smith et al., 2020) in their experiments. As far as we found, for only one natural pyroclastic density current the dimensionless numbers are known, and for that specific flow, the collisional forces seem to dominate over viscous forces (Rowley et al., 1981; Iverson & Denlinger, 2001) (Figure 9).

Despite the variation between the relative importance of certain forces between pyroclastic density currents, debris flows and our experimental CO_2-driven granular flows, these different multi-phase flows show similarity in dynamics, especially considering the variability within one flow group. The similarity becomes even more evident when comparing the dynamics of debris flows, dense pyroclastic density currents, and CO_2-driven flows with the dynamics of mud flows or natural rock avalanches (Figure 9). For both natural mud flows and rock avalanches, frictional forces are 10^2–10^6 higher than natural and experimental debris flows, dense pyroclastic density currents, and our CO_2-driven granular flows. In addition, in mud flows, the viscous forces become more dominant over collisional forces than for the other flows, and in rock avalanches, collisional forces become 10^3–10^7 more dominant over viscous forces.

The similarity in the relative influence of different forces in the flow between our CO_2-driven granular flows, and other fluidized multi-phase flows on Earth, is reflected in the similarity in the morphology of the deposits. The deposits of our experiments are lobate in shape, often show splitting of lobes, and sometimes have levees, similar to the hypothesized CO_2-driven granular flow deposits on Mars (Hugenholtz, 2008; Lanza et al., 2010; Levy et al., 2010; Johnsson et al., 2014; Sinha et al., 2018; Conway et al., 2019). These morphological elements are also observed in debris flow deposits (Hubert & Filipov, 1989; Blair & McPherson, 1998; de Haas et al., 2015a, 2018) and pyroclastic flow deposits (Rowley et al., 1981; Lube et al., 2007; Jessop et al., 2012), whereas they are less pronounced in mudflow deposits and absent in rock avalanche deposits (Figure 10). Not all of our outflow deposits contain different distinct lobes or levees, but nor do all recent deposits in gullies on Mars. A lack of levees might indicate a lack of clear grain size segregation, which is believed to contribute to levee formation (Jessop et al., 2012; Johnson et al., 2012; Baker et al., 2016). This could be caused by a more narrow grain size distribution or a relatively smaller influence of collisional forces over viscous forces. The latter can stem from a relatively small median grain size or high shear rates (see equation 2). Another factor that could influence the absence of levees in most of the lobes in our experimental work is the limited amount of surface friction and the inability of pore pressures to dissipate into the substrate and for particles to interact with the substrate. Earlier experimental work on terrestrial debris flows has shown that when experimental debris flows deposit on a layer of permeable sand the formation of levees is promoted (T. de Haas et al., 2015b).

4.4 Scaling and upscaling to Mars

From experiments with debris flows we know that small-scale flows experience larger effects of yield strength, viscous flow resistance, and grain inertia than field size flows (Iverson, 1997; Iverson & Denlinger, 2001; Iverson et al., 2010; Iverson, 2015). In addition, for small-scale experimental debris flows it has been proposed that they are insufficiently affected by pore-fluid pressure (Iverson, 1997; Iverson & Denlinger, 2001; Iverson et al., 2010). However, certain steps can be, and were, taken to overcome these scaling problems and use small-scale experiments for valid representation of real-world phenomena. For example, when scaling for momentum, a steeper slope in granular flow experiments can induce larger flow velocities to combat the effects of a smaller flow mass. Furthermore, it is important to evaluate the validity of experimental findings for the natural world by comparing flow dynamics expressed in dimensionless analysis. From the dimensionless analysis performed and discussed in the section above we can state that our CO_2-driven granular flows behave dynamically similar to debris flows and pyroclastic forms on Earth, both on an experimental and field scale (Figure 9). In addition, our experimental CO_2-driven granular flows show similar flow behaviour to those of back-calculated CO_2 driven flows in Hale crater (T. de Haas et al., 2019), with similar fractions of CO_2 needed for fluidisation, and similar flow velocities around 3 m/s in the steepest parts of the gullies and run-outs on slopes ranging between 13–19°.

The different sizes of the two experimental set-ups allow an assessment of the influence of scaling on CO_2-driven flows. From the dimensionless scaling in Figure 8, we can see that in our large-scale set-up, the collisional forces in the flow are of a higher importance than in the flows in the small-scale set-up. This difference is linked directly to the design of the opening mechanism in the large-scale flume, which limits the flow depth relative to the flow velocity more than in the small-scale flume. Additionally, we see that the friction number of our flows in the large-scale set-up is smaller than those in the small-scale set-up. Although significant differences in the dimensionless numbers between the large- and small-scale flows exist, they are small compared to differences in dimensionless numbers of experimental debris flows in the same flume but of different compositions (Roelofs et al., 2022, 2023) or of experimental pyroclastic density currents in the same flume but for different aeration states (Smith et al., 2020).

To summarize, the flow dynamics and morphology of our experimental CO_2-driven flows are comparable to a variety of natural two-phase flows (Figure 9, Figure 10, and Figure 4) and the influence of scale-effects on our experimental CO_2-driven flows seems to be relatively small. Classical scaling problems in debris flow experiments, related to viscous flow resistance, interstitial fluid, and pore pressures, are of a smaller concern in our CO_2-driven flow experiments because of the scale independence of the CO_2 sublimation process, pore pressure, and flow depth (T. de Haas et al., 2019; Roelofs et al., n.d.), and the low viscosity of the CO_2 gas. Therefore, our findings are of direct relevance to full-scale CO_2-driven flows on Mars.

On Mars the gravitational acceleration is 3.71 m/s^2, and thus 2.6 times smaller than on Earth. This could possibly influence the flow dynamics of CO_2 driven granular flows. We partly accounted for the smaller gravity on Mars by conducting our experiments on multiple slopes, and therefore studying how the changing gravitational component driving our flows would affect the results. However, the most important driver of CO_2-driven flows is the sublimation of the CO_2 frost, which is independent of gravity. The effect of gravity comes into the equation in the form of the weight of the particles in the flow and the speed with which they fall back to the surface. As earlier described by Roelofs et al. (n.d.), the extent to which the flow is suspended is given by a dimensionless group, which describes the ratio of the Darcy pressure $Hq\nu/\delta^2$ to the weight of the flow $Hg\rho_m$;

$$\frac{Hq\mu}{Hg\rho_m d^2} = \frac{q\mu}{g\rho_m \delta^2}. \tag{8}$$

where q is the volume flux of CO_2 in m/s. Here ρ_m and μ are the same for our experiments and Mars while g is different on Mars, but this can be compensated by increasing the grain diameter δ or decreasing the sublimation flux q.

The equation above implies that under Martian gravity only 0.38 of the volume flux of CO_2 is needed compared to Earth to fluidize a flow or that with the same amount of sublimating CO_2 ice significantly larger grains can be transported on Mars. Practically this means that under Martian gravity, if we were to repeat our large-scale experiments, we would be able to decrease the amount of CO_2 used to fluidize 8 kg of sediment over the length of our flume from 42 to 16 g, equal to a volume fraction of ∼0.002. This falls in the volume fraction range, 2×10^{-2}–2×10^{-5}, predicted to be needed for recent gully flows in Hale crater (T. de Haas et al., 2019). Furthermore, the sustained fluidisation under varying chute and outflow plain angles gives us the experimental evidence that under a range of gravitational accelerations sublimating CO_2 ice can produce two-phase granular flows.

4.5 Implications for Martian landscape evolution and granular flows in the solar system

From extensive analysis of remote sensing data we know that Martian gullies are active landscape features. Dundas et al. (2019); Pasquon et al. (2019); Dundas et al. (2022); Sinha and Ray (2023) observed erosion and transport of material in gullies, the formation of new terraces and erosion of channel segments, the migration of sinuous curves, channel abandonment, and lobate deposits. Dundas et al. (2019) also observed early stages of gully initiation, suggesting that the processes shaping and changing the gullies today are not merely modifying the pre-existing landforms, but are capable of actively shaping the landscape. Despite these observations, it remains debated what the original formation process of these landforms is. Our experimental results support the hypothesis by Diniega et al. (2010); Dundas et al. (2012, 2015, 2019, 2022) that current activity, by granular flow processes driven by CO_2 sublimation, are actively forming Martian gullies, and are not merely modifying older water-formed features, as suggested by Dickson et al. (2023).

The similarity in flow dynamics and morphology between our experimental CO_2-driven granular flows and natural two-phase granular flows on Earth supports their landscape-changing potential. On Earth, the erodible power of debris flows is suggested to be a primary force in cutting valleys in steep landscapes (Stock & Dietrich, 2003). Although the erodible power of CO_2-driven granular flows has yet to be experimentally explored, the observations of the Martian surface (Dundas et al., 2019, 2022; Sinha & Ray, 2023) and the observed dynamics of the experimental flows leave little doubt that erosion of material by CO_2-driven granular flows is possible. With the current state of remote observations and the lack of detailed in-situ sedimentological and geological investigations, it is impossible to completely rule out a water-driven origin of the Martian gullies. However, we need to be cautious about assuming a water-driven past for the Martian gullies when CO_2-related processes can explain present-day gully activity. As most gullies on Mars were formed during the Amazonian period on Mars, when little to no liquid water could exist on its surface, we deem it likely that the gullies on Mars have been modified and possibly formed by CO_2-related processes for the past 1-3 Ga.

For other planetary bodies in our solar system, our experimental results emphasize that the existence of gully-like landforms is not definite proof of flowing liquids. For example, the observed gully landforms on Vesta (Scully et al., 2015) and Mercury (Rothery et al., 2020) could also have a sublimation-related formation process, especially because of the lack of atmosphere of both bodies. Therefore, our results raise an important question on the use of Earth analogues for planetary science. Earth analogues have been essential in the exploration and understanding of planetary surfaces in our solar systems as well as the potential habitability of these planetary surfaces. Analogue studies are the backbone of our understanding of the processes that shaped the surfaces of rocky planets and bodies throughout our solar system. However, the pitfall of Earth analogue studies is the combined problems of unknown-unknowns and equifinality; the principle describing that different processes can result in the same outcome. Our experimental results could therefore be the start of a fundamental reinterpretation of planetary landforms previously thought to be formed by flowing liquids.

5 Conclusion

We experimentally investigated the feasibility of CO_2-ice sublimation as the driving force in fluidized granular flows on Mars. We conducted 68 experiments under Martian atmospheric conditions in two set-ups on different scales to explore under which boundary and initial conditions granular material can be fluidized by the sublimation of CO_2-ice.

Our experiments show that under Martian atmospheric pressure of 8 mbar, the sublimation of small quantities of CO_2-ice, ∼0.5% of the total flow volume, can fluidize large volumes of granular material on a range of different slopes, as long as enough thermal energy is present to initiate the sublimation of the CO_2-ice. Under Martian atmospheric pressure, the sublimation of CO_2-ice in a granular mixture increases the pore pressure within the flow by 0.2-0.6 mbar. This increased pressure carries a significant portion of the total weight of the flow, between 20–60%, which indicates a decrease in granular friction between the grains and a high degree of fluidisation of the mixture. The fluidisation of the material results in large flow velocities that exceed velocities in dry granular flows by a factor 2–3.

Dimensionless analysis of the CO_2-driven flows shows that they are dynamically similar to debris flows and dense pyroclastic density currents on Earth. The flows are supercritical and turbulent in behaviour, and frictional forces dominate over collisional and viscous forces. The similarity in flow dynamics is reflected in the similarity in deposit morphology. Our experimental CO_2 driven flows contain morphological elements, like levees and lobes, that are seen as key characteristics of debris flow and pyroclastic flow deposits. These features are also observed on the depositional aprons of active gullies on Mars. In addition, our findings on flow dynamics and morphology of CO_2 driven flows support the hypothesis that CO_2-driven processes are actively modifying and forming Martian gullies today. Therefore, CO_2-driven processes are not merely modifying older features, but can likely be used to explain the evolution of these landforms on Mars during the Amazonian, when little to no liquid water was present on the surface of Mars.

Furthermore, our calculations highlight the importance of thermal energy in driving the sublimation of CO_2-ice that propels the fluidisation of granular material. Direct thermal energy is a far more effective source of energy for sublimation than the conversion of kinetic and potential energy from a fall to heat. This implies that it is likely that CO_2-driven granular flows can only occur in gullies on Mars at specific locations and during specific periods during the Martian year when CO_2-ice and warmer regolith simultaneously exist in the gully.

Lastly, our experimental results emphasize that the existence of gully-like landforms on planetary bodies is not definite proof of flowing liquids. Gully landforms could also be formed by or at least be altered by sublimation-related processes.

6 Open Research

For all the experiments presented in this manuscript the data collected by the sensors in the flumes and the DEMs of Difference are available via Yoda (online repository of Utrecht University). The data and an instruction on how we processed the raw data can be found under this link: `https://public.yoda.uu.nl/geo/UU01/2T6YAU.html` DOI: 10.24416/UU01-2T6YAU

7 Acknowledgments

LR was supported by the Dutch Research Council (NWO) - grant OCENW.KLEIN.495 to TdH. The visits to the labs were funded by Europlanet - project number 20-EPN-015 to TdH, Europlanet - project number 20-EPN-023 to LR, and partly in-kind by the School of Physical Sciences of the Open University under the leadership of MRP through UK Space Agency Grant ST/X006549/1. We also acknowledge funding from the CNRS INSU

Programme Nationale de Planétologie. SJC is grateful for financial support of the French Space Agency CNES for her HiRISE and CaSSIS work.

Both the Mars Simulation Wind Tunnel laboratory and she Mars chamber of the HVI-lab at the Open University are members of Europlanet (2024) RI and have received funding from the European Union's Horizon 2020 research and innovation programme under grant agreement No 871149.

The authors thank the spacecraft and instrument engineering teams for the successful completion and operation of CaSSIS. CaSSIS is a project of the University of Bern funded through the Swiss Space Office via ESA's PRODEX programme. The instrument hardware development was also supported by the Italian Space Agency (ASI) (ASI-INAF agreement no. I/018/12/0), INAF/ Astronomical Observatory of Padova, and the Space Research Center (CBK) in Warsaw. Support from SGF (Budapest), the University of Arizona (LPL) and NASA are also gratefully acknowledged.

References

Baker, J., Gray, N., & Kokelaar, P. (2016). Particle size-segregation and spontaneous levee formation in geophysical granular flows. *International Journal of Erosion Control Engineering*, *9*(4), 174–178. doi: https://doi.org/10.13101/ijece.9.174

Bardera, R., Sor, S., & García-Magariño, A. (2020). Aerodynamics of mars 2020 rover wind sensors. In G. Pezzella & A. Viviani (Eds.), *Mars exploration* (chap. 5). Rijeka: IntechOpen. Retrieved from `https://doi.org/10.5772/intechopen.90912` doi: 10.5772/intechopen.90912

Blair, T. C., & McPherson, J. G. (1998, 09). Recent debris-flow processes and resultant form and facies of the Dolomite alluvial fan, Owens Valley, California. *Journal of Sedimentary Research*, *68*(5), 800-818. Retrieved from `https://doi.org/10.2110/jsr.68.800` doi: 10.2110/jsr.68.800

Cedillo-Flores, Y., Treiman, A. H., Lasue, J., & Clifford, S. M. (2011). Co2 gas fluidization in the initiation and formation of martian polar gullies. *Geophysical Research Letters*, *38*(21). Retrieved from `https://agupubs.onlinelibrary.wiley.com/doi/abs/10.1029/2011GL049403` doi: https://doi.org/10.1029/2011GL049403

Conway, S. J., de Haas, T., & Harrison, T. N. (2019). Martian gullies: A comprehensive review of observations, mechanisms and insights from earth analogues. *Geological Society, London, Special Publications*, *467*(1), 7–66. doi: https://doi.org/10.1144/SP467.14

Conway, S. J., Lamb, M. P., Balme, M. R., Towner, M. C., & Murray, J. B. (2011). Enhanced runout and erosion by overland flow at low pressure and sub-freezing conditions: Experiments and application to mars. *Icarus*, *211*(1), 443-457. Retrieved from `https://www.sciencedirect.com/science/article/pii/S0019103510003428` doi: https://doi.org/10.1016/j.icarus.2010.08.026

Costard, F., Forget, F., Mangold, N., & Peulvast, J. P. (2002). Formation of recent martian debris flows by melting of near-surface ground ice at high obliquity. *Science*, *295*(5552), 110-113. Retrieved from `https://www.science.org/doi/abs/10.1126/science.1066698` doi: 10.1126/science.1066698

Cottin, H., Kotler, J. M., Bartik, K., Cleaves, H. J., Cockell, C. S., De Vera, J.-P. P., … others (2017). Astrobiology and the possibility of life on earth and elsewhere…. *Space Science Reviews*, *209*, 1–42. doi: https://doi.org/10.1007/s11214-015-0196-1

de Haas, T., Densmore, A., Stoffel, M., Suwa, H., Imaizumi, F., Ballesteros-Cánovas, J., & Wasklewicz, T. (2018). Avulsions and the spatio-temporal evolution of debris-flow fans. *Earth-Science Reviews*, *177*, 53-75. Retrieved from `https://www.sciencedirect.com/science/article/pii/S0012825217302465` doi: https://doi.org/10.1016/j.earscirev.2017.11.007

de Haas, T., Kleinhans, M. G., Carbonneau, P. E., Rubensdotter, L., & Hauber, E. (2015a). Surface morphology of fans in the high-arctic periglacial environment of svalbard: Controls and processes. *Earth-Science Reviews*, *146*, 163-182. Retrieved from `https://www.sciencedirect.com/science/article/pii/S0012825215000641` doi: https://doi.org/10.1016/j.earscirev.2015.04.004

de Haas, T., Braat, L., Leuven, J. R., Lokhorst, I. R., & Kleinhans, M. G. (2015b). Effects of debris flow composition on runout, depositional mechanisms, and deposit morphology in laboratory experiments. *Journal of Geophysical Research: Earth Surface*, *120*(9), 1949–1972.

de Haas, T., Hauber, E., Conway, S., Van Steijn, H., Johnsson, A., & Kleinhans, M. (2015c). Earth-like aqueous debris-flow activity on mars at high orbital obliquity in the last million years. *Nature Communications*, *6*(1), 1–6. doi: https://doi.org/10.1038/ncomms8543

de Haas, T., McArdell, B. W., Conway, S. J., McElwaine, J. N., Kleinhans, M. G., Salese, F., & Grindrod, P. M. (2019). Initiation and flow conditions of contemporary flows in martian gullies. *Journal of Geophys-*

ical Research: Planets, *124*(8), 2246-2271. Retrieved from https://agupubs.onlinelibrary.wiley.com/doi/abs/10.1029/2018JE005899 doi: https://doi.org/10.1029/2018JE005899

de Haas, T. d., & Woerkom, T. v. (2016). Bed scour by debris flows: experimental investigation of effects of debris-flow composition. *Earth Surface Processes and Landforms*, *41*(13), 1951–1966. doi: https://doi.org/10.1002/esp.3963

Dickson, J. L., Palumbo, A. M., Head, J. W., Kerber, L., Fassett, C. I., & Kreslavsky, M. A. (2023). Gullies on mars could have formed by melting of water ice during periods of high obliquity. *Science*, *380*(6652), 1363-1367. Retrieved from https://www.science.org/doi/abs/10.1126/science.abk2464 doi: 10.1126/science.abk2464

Diniega, S., Bramson, A. M., Buratti, B., Buhler, P., Burr, D. M., Chojnacki, M., … Widmer, J. M. (2021). Modern mars' geomorphological activity, driven by wind, frost, and gravity. *Geomorphology*, *380*, 107627. Retrieved from https://www.sciencedirect.com/science/article/pii/S0169555X21000350 doi: https://doi.org/10.1016/j.geomorph.2021.107627

Diniega, S., Byrne, S., Bridges, N. T., Dundas, C. M., & McEwen, A. S. (2010, 11). Seasonality of present-day Martian dune-gully activity. *Geology*, *38*(11), 1047-1050. Retrieved from https://doi.org/10.1130/G31287.1 doi: 10.1130/G31287.1

Diniega, S., Hansen, C., McElwaine, J., Hugenholtz, C., Dundas, C., McEwen, A., & Bourke, M. (2013). A new dry hypothesis for the formation of martian linear gullies. *Icarus*, *225*(1), 526-537. Retrieved from https://www.sciencedirect.com/science/article/pii/S0019103513001668 doi: https://doi.org/10.1016/j.icarus.2013.04.006

Dundas, C. M., Conway, S. J., & Cushing, G. E. (2022). Martian gully activity and the gully sediment transport system. *Icarus*, 115133. Retrieved from https://www.sciencedirect.com/science/article/pii/S0019103522002408 doi: https://doi.org/10.1016/j.icarus.2022.115133

Dundas, C. M., Diniega, S., Hansen, C. J., Byrne, S., & McEwen, A. S. (2012). Seasonal activity and morphological changes in martian gullies. *Icarus*, *220*(1), 124-143. Retrieved from https://www.sciencedirect.com/science/article/pii/S0019103512001340 doi: https://doi.org/10.1016/j.icarus.2012.04.005

Dundas, C. M., Diniega, S., & McEwen, A. S. (2015). Long-term monitoring of martian gully formation and evolution with mro/hirise. *Icarus*, *251*, 244-263. Retrieved from https://www.sciencedirect.com/science/article/pii/S0019103514002668 (Dynamic Mars) doi: https://doi.org/10.1016/j.icarus.2014.05.013

Dundas, C. M., McEwen, A. S., Diniega, S., Byrne, S., & Martinez-Alonso, S. (2010). New and recent gully activity on mars as seen by hirise. *Geophysical Research Letters*, *37*(7). Retrieved from https://agupubs.onlinelibrary.wiley.com/doi/abs/10.1029/2009GL041351 doi: https://doi.org/10.1029/2009GL041351

Dundas, C. M., McEwen, A. S., Diniega, S., Hansen, C. J., Byrne, S., & McElwaine, J. N. (2017). The formation of gullies on mars today. *Geological Society, London, Special Publications*, *467*(1), 67–94. Retrieved from https://sp.lyellcollection.org/content/467/1/67 doi: 10.1144/SP467.5

Dundas, C. M., McEwen, A. S., Diniega, S., Hansen, C. J., Byrne, S., & McElwaine, J. N. (2019). scho. *Geological Society, London, Special Publications*, *467*(1), 67–94. Retrieved from https://sp.lyellcollection.org/content/467/1/67 doi: 10.1144/SP467.5

Hecht, M. H. (2002). Metastability of liquid water on mars. *Icarus*, *156*(2), 373-386. Retrieved from https://www.sciencedirect.com/science/article/pii/S0019103501967946 doi: https://doi.org/10.1006/icar.2001.6794

Hoffman, N. (2002). Active polar gullies on mars and the role of carbon dioxide. *Astrobiology*, *2*(3), 313–323. doi: https://doi.org/10.1089/153110702762027899

Holstein-Rathlou, C., Merrison, J., Iversen, J. J., Jakobsen, A. B., Nicolajsen, R., Nørnberg, P., ... Portyankina, G. (2014). An environmental wind tunnel facility for testing meteorological sensor systems. *Journal of Atmospheric and Oceanic Technology*, *31*(2), 447 - 457. Retrieved from `https://journals.ametsoc.org/view/journals/atot/31/2/jtech-d-13-00141_1.xml` doi: https://doi.org/10.1175/JTECH-D-13-00141.1

Hubert, J. F., & Filipov, A. J. (1989). Debris-flow deposits in alluvial fans on the west flank of the white mountains, owens valley, california, u.s.a. *Sedimentary Geology*, *61*(3), 177-205. Retrieved from `https://www.sciencedirect.com/science/article/pii/0037073889900572` doi: https://doi.org/10.1016/0037-0738(89)90057-2

Hugenholtz, C. H. (2008). Frosted granular flow: A new hypothesis for mass wasting in martian gullies. *Icarus*, *197*(1), 65-72. Retrieved from `https://www.sciencedirect.com/science/article/pii/S0019103508001796` doi: https://doi.org/10.1016/j.icarus.2008.04.010

Iverson, R. M. (1997). The physics of debris flows. *Reviews of geophysics*, *35*(3), 245–296.

Iverson, R. M. (2015). Scaling and design of landslide and debris-flow experiments. *Geomorphology*, *244*, 9-20. Retrieved from `https://www.sciencedirect.com/science/article/pii/S0169555X15001336` (Laboratory Experiments in Geomorphology 46th Annual Binghamton Geomorphology Symposium 18-20 September 2015) doi: https://doi.org/10.1016/j.geomorph.2015.02.033

Iverson, R. M., & Denlinger, R. P. (2001). Flow of variably fluidized granular masses across three-dimensional terrain: 1. coulomb mixture theory. *Journal of Geophysical Research: Solid Earth*, *106*(B1), 537–552.

Iverson, R. M., Logan, M., LaHusen, R. G., & Berti, M. (2010). The perfect debris flow? Aggregated results from 28 large-scale experiments. *Journal of Geophysical Research: Earth Surface*, *115*(F3). doi: https://doi.org/10.1029/2009JF001514

Jessop, D., Kelfoun, K., Labazuy, P., Mangeney, A., Roche, O., Tillier, J.-L., ... Thibault, G. (2012). Lidar derived morphology of the 1993 lascar pyroclastic flow deposits, and implication for flow dynamics and rheology. *Journal of Volcanology and Geothermal Research*, *245-246*, 81-97. Retrieved from `https://www.sciencedirect.com/science/article/pii/S0377027312002041` doi: https://doi.org/10.1016/j.jvolgeores.2012.06.030

Johnson, C. G., Kokelaar, B. P., Iverson, R. M., Logan, M., LaHusen, R. G., & Gray, J. M. N. T. (2012). Grain-size segregation and levee formation in geophysical mass flows. *Journal of Geophysical Research: Earth Surface*, *117*(F1). Retrieved from `https://agupubs.onlinelibrary.wiley.com/doi/abs/10.1029/2011JF002185` doi: https://doi.org/10.1029/2011JF002185

Johnsson, A., Reiss, D., Hauber, E., Hiesinger, H., & Zanetti, M. (2014). Evidence for very recent melt-water and debris flow activity in gullies in a young mid-latitude crater on mars. *Icarus*, *235*, 37-54. Retrieved from `https://www.sciencedirect.com/science/article/pii/S0019103514001225` doi: https://doi.org/10.1016/j.icarus.2014.03.005

Khuller, A. R., Christensen, P. R., Harrison, T. N., & Diniega, S. (2021). The distribution of frosts on mars: Links to present-day gully activity. *Journal of Geophysical Research: Planets*, *126*(3), e2020JE006577. Retrieved from `https://agupubs.onlinelibrary.wiley.com/doi/abs/10.1029/2020JE006577` (e2020JE006577 2020JE006577) doi: https://doi.org/10.1029/2020JE006577

Kieffer, H. H. (2007). Cold jets in the martian polar caps. *Journal of Geophysical Research: Planets*, *112*(E8). Retrieved from `https://agupubs.onlinelibrary.wiley.com/doi/abs/10.1029/2006JE002816` doi:

https://doi.org/10.1029/2006JE002816
Knauth, L., & Burt, D. M. (2002). Eutectic brines on mars: Origin and possible relation to young seepage features. *Icarus*, *158*(1), 267-271. Retrieved from https://www.sciencedirect.com/science/article/pii/S0019103502968661 doi: https://doi.org/10.1006/icar.2002.6866
Lanza, N., Meyer, G., Okubo, C., Newsom, H., & Wiens, R. (2010). Evidence for debris flow gully formation initiated by shallow subsurface water on mars. *Icarus*, *205*(1), 103-112. Retrieved from https://www.sciencedirect.com/science/article/pii/S001910350900164X (MRO/HiRISE Studies of Mars) doi: https://doi.org/10.1016/j.icarus.2009.04.014
Levy, J., Head, J., Dickson, J., Fassett, C., Morgan, G., & Schon, S. (2010). Identification of gully debris flow deposits in protonilus mensae, mars: Characterization of a water-bearing, energetic gully-forming process. *Earth and Planetary Science Letters*, *294*(3), 368-377. Retrieved from https://www.sciencedirect.com/science/article/pii/S0012821X09004580 (Mars Express after 6 Years in Orbit: Mars Geology from Three-Dimensional Mapping by the High Resolution Stereo Camera (HRSC) Experiment) doi: https://doi.org/10.1016/j.epsl.2009.08.002
Lube, G., Cronin, S. J., Platz, T., Freundt, A., Procter, J. N., Henderson, C., & Sheridan, M. F. (2007). Flow and deposition of pyroclastic granular flows: A type example from the 1975 ngauruhoe eruption, new zealand. *Journal of Volcanology and Geothermal Research*, *161*(3), 165-186. Retrieved from https://www.sciencedirect.com/science/article/pii/S0377027306004239 doi: https://doi.org/10.1016/j.jvolgeores.2006.12.003
Malin, M. C., & Edgett, K. S. (2000). Evidence for recent groundwater seepage and surface runoff on mars. *Science*, *288*(5475), 2330-2335. Retrieved from https://www.science.org/doi/abs/10.1126/science.288.5475.2330 doi: 10.1126/science.288.5475.2330
Parsons, J. D., Whipple, K. X., & Simoni, A. (2001). Experimental study of the grain-flow, fluid-mud transition in debris flows. *The Journal of Geology*, *109*(4), 427–447.
Pasquon, K., Conway, S., Vincendon, M., Massé, M., Raack, J., Noblet, A., ... Lewis, S. R. (2023). Insights into the interaction between defrosting seasonal ices and gully activity from cassis and hirise observations in sisyphi cavi, mars. *Planetary and Space Science*, *235*, 105743. Retrieved from https://www.sciencedirect.com/science/article/pii/S0032063323001125 doi: https://doi.org/10.1016/j.pss.2023.105743
Pasquon, K., Gargani, J., Massé, M., Vincendon, M., Conway, S. J., Séjourné, A., ... Guimpier, A. (2019). Present-day development of gully-channel sinuosity by carbon dioxide gas supported flows on mars. *Icarus*, *329*, 296-313. Retrieved from https://www.sciencedirect.com/science/article/pii/S0019103518304627 doi: https://doi.org/10.1016/j.icarus.2019.03.034
Pilorget, C., & Forget, F. (2016). Formation of gullies on mars by debris flows triggered by co2 sublimation. *Nature Geoscience*, *9*(1), 65–69. Retrieved from https://doi.org/10.1038/ngeo2619 doi: 10.1038/ngeo2619
Raack, J., Conway, S. J., Heyer, T., Bickel, V. T., Philippe, M., Hiesinger, H., ... Massé, M. (2020). Present-day gully activity in sisyphi cavi, mars – flow-like features and block movements. *Icarus*, *350*, 113899. Retrieved from https://www.sciencedirect.com/science/article/pii/S0019103520302785 doi: https://doi.org/10.1016/j.icarus.2020.113899
Raack, J., Reiss, D., Appéré, T., Vincendon, M., Ruesch, O., & Hiesinger, H. (2015). Present-day seasonal gully activity in a south polar pit (sisyphi cavi) on mars. *Icarus*, *251*, 226-243. Retrieved from https://www.sciencedirect.com/science/article/pii/S0019103514001663 (Dynamic Mars) doi: https://doi.org/10.1016/j.icarus.2014.03.040

Richardson, M. I., & Mischna, M. A. (2005). Long-term evolution of transient liquid water on mars. *Journal of Geophysical Research: Planets*, *110*(E3). Retrieved from https://agupubs.onlinelibrary.wiley.com/doi/abs/10.1029/2004JE002367 doi: https://doi.org/10.1029/2004JE002367

Roelofs, L., Colucci, P., & Haas, T. d. (2022). How debris-flow composition affects bed erosion quantity and mechanisms - an experimental assessment. *Earth Surface Processes and Landforms*.

Roelofs, L., Conway, S. J., de Haas, T., Dundas, C., Lewis, S. R., McElwaine, J., ... Patel, M. R. (n.d.). How, where, and when CO_2 drives current mass flows in martian gullies. *In Press at Communications Earth and Environment*.

Roelofs, L., Nota, E. W., Flipsen, T. C. W., Colucci, P., & de Haas, T. (2023). How bed composition affects erosion by debris flows—an experimental assessment. *Geophysical Research Letters*, *50*(14), e2023GL103294. Retrieved from https://agupubs.onlinelibrary.wiley.com/doi/abs/10.1029/2023GL103294 (e2023GL103294 2023GL103294) doi: https://doi.org/10.1029/2023GL103294

Rothery, D. A., Massironi, M., Alemanno, G., Barraud, O., Besse, S., Bott, N., ... others (2020). Rationale for bepicolombo studies of mercury's surface and composition. *Space science reviews*, *216*(4), 1–46. Retrieved from https://link.springer.com/article/10.1007/s11214-020-00694-7 doi: https://doi.org/10.1007/s11214-020-00694-7

Rowley, P. D., Kuntz, M. A., & Macleod, N. S. (1981). Pyroclastic-flow deposits. In *The 1980 eruptions of mount st. helens, washington* (p. 489-512). Washington: USGS. doi: 10.3133/pp1250

Scully, J. E., Russell, C. T., Yin, A., Jaumann, R., Carey, E., Castillo-Rogez, J., ... Le Corre, L. (2015). Geomorphological evidence for transient water flow on vesta. *Earth and Planetary Science Letters*, *411*, 151-163. Retrieved from https://www.sciencedirect.com/science/article/pii/S0012821X14007572 doi: https://doi.org/10.1016/j.epsl.2014.12.004

Shakeel, H., Wei, H., & Pomeroy, J. (2018). Measurements of enthalpy of sublimation of ne, n2, o2, ar, co2, kr, xe, and h2o using a double paddle oscillator. *The Journal of Chemical Thermodynamics*, *118*, 127-138. Retrieved from https://www.sciencedirect.com/science/article/pii/S0021961417303968 doi: https://doi.org/10.1016/j.jct.2017.11.004

Sinha, R. K., & Ray, D. (2023). Morphological changes currently occurring in sand-filled gully channels on mars: Implications for the role of substrates inside channels. *Icarus*, *390*, 115334. Retrieved from https://www.sciencedirect.com/science/article/pii/S0019103522004262 doi: https://doi.org/10.1016/j.icarus.2022.115334

Sinha, R. K., Vijayan, S., Shukla, A. D., Das, P., & Bhattacharya, F. (2018). Gullies and debris-flows in ladakh himalaya, india: a potential martian analogue. *Geological Society, London, Special Publications*, *467*(1), 315–342. doi: https://doi.org/10.1144/SP467.9

Smith, G., Rowley, P., Williams, R., Giordano, G., Trolese, M., Silleni, A., ... Capon, S. (2020). A bedform phase diagram for dense granular currents. *Nature communications*, *11*(1), 2873. doi: https://doi.org/10.1038/s41467-020-16657-z

Stephenson, R. M. (1987). *Handbook of the thermodynamics of organic compounds*. Elsevier. doi: https://doi.org/10.1007/978-94-009-3173-2

Stock, J. D., & Dietrich, W. E. (2003). Valley incision by debris flows: Evidence of a topographic signature. *Water Resources Research*, *39*(4). doi: https://doi.org/10.1029/2001WR001057

Sylvest, M. E., Conway, S. J., Patel, M. R., Dixon, J. C., & Barnes, A. (2016). Mass wasting triggered by seasonal co2 sublimation under martian atmospheric conditions: Laboratory experiments. *Geophysical Research Letters*, *43*(24), 12,363-

12,370. Retrieved from https://agupubs.onlinelibrary.wiley.com/doi/abs/10.1002/2016GL071022 doi: https://doi.org/10.1002/2016GL071022

Sylvest, M. E., Dixon, J. C., Conway, S. J., Patel, M. R., McElwaine, J. N., Hagermann, A., & Barnes, A. (2019). Co2 sublimation in martian gullies: laboratory experiments at varied slope angle and regolith grain sizes. *Geological Society, London, Special Publications*, *467*(1), 343–371. Retrieved from https://www.lyellcollection.org/doi/full/10.1144/SP467.11 doi: https://doi.org/10.1144/SP467.11

Zhou, G. G., Li, S., Song, D., Choi, C. E., & Chen, X. (2019). Depositional mechanisms and morphology of debris flow: physical modelling. *Landslides*, *16*, 315–332. doi: https://doi.org/10.1007/s10346-018-1095-9

Figure 1. Three examples of Martian gullies with frost; a) gullies in Sisyphi Cavi (synthetic RGB CaSSIS images using the PAN and BLU channels, where defrosted surfaces appear red and frosted surfaces white, MY34_003464_256_1, Ls 242°) (Pasquon et al., 2023), b) gullies in an unnamed crater (HiRISE image, ESP_039114_1115, Ls 243°), c) gullies on Matara crater dune field (HiRISE image, ESP_063824_1340, Ls 160°). Colour strips in panels b) and c) are false colours, composed of near-infrared, red and blue-green wavelength signals.

Figure 2. Photos and schematic drawings of chambers (a-b) and flumes (c-f). The photo in panel (a) depicts the Mars chamber at the Hyper Velocity and Impact lab (HVI) of the Open University (UK), panel (b) shows the Mars Simulation Wind tunnel at Aarhus University (Denmark). Details of the small-scale flume set-up used in the Mars chamber of the HVI lab can be found in (c) and (e). Details of the large-scale set-up used in the Mars Simulation Wind tunnel in Aarhus can be found in (d) and (f). All dimensions are given in cm.

Figure 3. Example of flow depth, flow mass, and differential pore pressures (sensors 1 and 2) during an experiment for the large-scale set-up (a) and the small-scale set-up (b) with similar boundary conditions; initial CO_2 mass fraction of 0.23 and flume angle of 20°. The lower panel (c), depicts the mass fraction of the flow carried by the gas pressure for the experiments depicted in panels (a) and (b). As the data from the two pore pressure sensors slightly differs, this fraction is depicted as an envelope covering the range provided by the two sensors. The fraction carried by the gas pressure is a measure for the degree of fluidisation.

Figure 4. Digital elevation models (DEMs) for the outflow deposits of 12 experiments under Martian atmospheric pressures, 6 conducted in the large scale set-up, highlighted by thick black borders, and 6 conducted in the small scale set-up. The top two rows (a–f) show deposits of experiments with varying CO_2 mass fractions. The fractions depicted in the panels correspond to the mass fractions at the start of an experiment derived from Supplementary Figure 4. The bottom two rows (g–l) show deposits of experiments with different chute angles. For all depicted experiments, videos are present in the Supplementary material 8.

Figure 5. Frontal flow velocity (a-b), maximum flow depth (c-d), and maximum differential pore pressure for pore pressure sensor 1 (P1) and pore pressure sensor 2 (P2) (e-f), for the large-scale (L) and small-scale (S) experimental flows. All green and blue dots represent results from experiments conducted under Martian atmospheric pressure, whereas the yellow dots represent results from experiments conducted under Earth atmospheric pressure. The results of experiments with varying CO_2 mass fractions in the flow, but a constant chute angle of 30°, are presented in the left column. Note that the mass fractions presented here are the mass fractions at the start of an experiment derived from data presented in Supplementary Figure 4. The results of experiments conducted under different chute angles, but with a constant initial CO_2 mass fraction of 0.33, are presented in the right column.

Figure 6. Boxplots showing the distribution of the flow density (a-b) and the fraction of the flow carried by the gas pressure (c-d) for the large-scale experiments conducted with different CO_2 mass fractions (left column) and under different chute angles (right column). The data in a single boxplot combines the density or fraction carried by the gas pressure of the main flow over time (flow tails are disregarded) for all large-scale experiments performed under similar conditions (i.e. similar CO_2 mass fractions and chute angle). The dark blue dots represent the mean value during one experiment. The reported p-value in the subplots stems from an ANOVA test of these means. The p-values show that the results from the different experimental groups in panels (b) and (c) are marginally significant.

Figure 7. Flow depth and cumulative CO_2 mass loss for three experiments in the large-scale set-up, with a CO_2 mass at the beginning of the experiment of 0.59 kg (a), 1.12 kg (b), and 2.13 kg (c). All experiments were conducted under a chute slope of 30°. The cumulative CO_2 mass lost is determined based on data from a capacitance pressure sensor in the chamber, the measurement frequency is 1 Hz.

Figure 8. Bagnold (a-b), Savage (c-d), and friction (e-f) numbers for the granular flows in the large-scale and small-scale experiments conducted with different CO_2 mass fractions (left column) and under different chute angles (right column). The horizontal lines indicate the transition from one flow regime to the other (Iverson, 1997). For the Bagnold number (a-b), this is the transition between the collisional and the viscous flow regime. For the Savage number (c-d), this is the transition from the collisional to the frictional flow regime. For the friction number (e-f), this is the transition from the frictional to the viscous flow regime, the latter is not visible in the plot because the flows are far into the frictional flow regime.

Figure 9. Bagnold numbers plotted against Savage numbers for the experimental CO_2-driven flows presented in Figure 4, the experimental debris flows from Roelofs et al. (2022)[2], the experimental dense pyroclastic density currents from Smith et al. (2020)[3], three prototype natural debris flows from Iverson (1997)[4] and Iverson and Denlinger (2001)[5], a natural mud flow from Iverson (1997)[4], a rock avalanche from Iverson and Denlinger (2001)[5], and a pyroclastic density current from Mount St Helens from Iverson and Denlinger (2001)[5] and Rowley et al. (1981)[6]

Figure 10. Different natural granular flows and their key morphological features. (a) Debris flow fan with different lobate deposits with levees near Pinnisalm, Neustift im Stubaital, Austria. (b) Pyroclastic density current deposits from the eruption of Mount St Helens in 1980 on July 22, showing multiple channels with levees and lobes (Photo: Dan Miller and USGS, first published in Baker et al. (2016)). (c) Granular flow deposits on the slopes of Istok crater on Mars with levees and lobes (Photo: NASA - HiRISE PSP_006837_1345) (Johnsson et al., 2014; T. de Haas et al., 2015c) (d) Rock avalanche Hope Slide, Hope, British Columbia, Canada (Photo: John Clague). (e) Mud flow dominated Coldwater Canyon fan, California, USA, showing channels and dispersed lobes with thin levees.

8 Supplementary Material

- Supplementary Table 1 - List of experiments and experimental settings (SupplementaryMaterialExperimentListOUAU.xlsx)

Supplementary Information - "The dynamics of CO2-driven granular flows in gullies on Mars
List of experiments and experimental settings
Compiled by Lonneke Roelofs - December 2023
l.roelofs@uu.nl

Notes:
Only experiments presented in the manuscript are presented here.
Experiments were numbered based on the order of execution but are organised here in logical order concerning the tested parameter space.
Not all experiments that were executed are presented in the manuscript, therefore some numbers are "missing" in this list.
The small-scale and large-scale experiments were numbered seperately.

Small scale experiments - Open University, Milton Keynes, United Kingdom

date	exp nr.	CO2 ice volume (m3)	CO2 ice weight (kg)	Sediment volume (m^3)	Sediment weight (kg)	Volume frac CO2	Total volume (m3)	Total weight (kg)	Chamber pressure (mbar)	Temp chute bottom (	Flume angle (degrees)	Silver sand (kg)	Builders sand (kg)	Slope chute (de	Slope outflow plain (deg)	Notes
Different CO2 fractions																
28-9-2021	18	0.00000	0.00	0.00038	1	0.00	0.00038	1.0	7-8.3	20	30	0.6	0.4	30	12	
6-10-2021	51	0.00000	0.00	0.00038	1	0.00	0.00038	1.0	7-8.3	20	30	0.6	0.4	30	12	Triggered record to early, so no channel data
6-10-2021	52	0.00000	0.00	0.00038	1	0.00	0.00038	1.0	7-8.3	20	30	0.6	0.4	30	12	
24-9-2021	9	0.00006	0.10	0.00038	1	0.14	0.00044	1.1	7-8.3	20	30	0.6	0.4	30	12	
24-9-2021	10	0.00006	0.10	0.00038	1	0.14	0.00044	1.1	7-8.3	20	30	0.6	0.4	30	12	
27-9-2021	11	0.00006	0.10	0.00038	1	0.14	0.00044	1.1	7-8.3	20	30	0.6	0.4	30	12	
28-9-2021	20	0.00006	0.10	0.00038	1	0.14	0.00044	1.1	7-8.3	20	30	0.6	0.4	30	12	
15-10-2021	73	0.00013	0.20	0.00038	1	0.25	0.00050	1.2	7-8.3	20	30	0.6	0.4	30	12	Slope heaters were off, and no frontal movie
15-10-2021	74	0.00013	0.20	0.00038	1	0.25	0.00050	1.2	7-8.3	20	30	0.6	0.4	30	12	
15-10-2021	75	0.00013	0.20	0.00038	1	0.25	0.00050	1.2	7-8.3	20	30	0.6	0.4	30	12	
15-10-2021	76	0.00013	0.20	0.00038	1	0.25	0.00050	1.2	7-8.3	20	30	0.6	0.4	30	12	
29-9-2021	22	0.00019	0.30	0.00038	1	0.33	0.00056	1.3	7-8.3	20	30	0.6	0.4	30	12	
24-9-2021	7	0.00019	0.30	0.00038	1	0.33	0.00056	1.3	7-8.3	20	30	0.6	0.4	30	12	
24-9-2021	8	0.00019	0.30	0.00038	1	0.33	0.00056	1.3	7-8.3	20	30	0.6	0.4	30	12	
15-10-2021	77	0.00025	0.40	0.00038	1	0.40	0.00063	1.4	7-8.3	20	30	0.6	0.4	30	12	
15-10-2021	78	0.00025	0.40	0.00038	1	0.40	0.00063	1.4	7-8.3	20	30	0.6	0.4	30	12	Forgot to take photos, so no T1
18-10-2021	79	0.00025	0.40	0.00038	1	0.40	0.00063	1.4	7-8.3	20	30	0.6	0.4	30	12	
18-10-2021	80	0.00025	0.40	0.00038	1	0.40	0.00063	1.4	7-8.3	20	30	0.6	0.4	30	12	
18-10-2021	81	0.00031	0.50	0.00038	1	0.45	0.00069	1.5	7-8.3	20	30	0.6	0.4	30	12	
18-10-2021	82	0.00031	0.50	0.00038	1	0.45	0.00069	1.5	7-8.3	20	30	0.6	0.4	30	12	
18-10-2021	83	0.00031	0.50	0.00038	1	0.45	0.00069	1.5	7-8.3	20	30	0.6	0.4	30	12	
18-10-2021	84	0.00031	0.50	0.00038	1	0.45	0.00069	1.5	7-8.3	20	30	0.6	0.4	30	12	
27-9-2021	12	0.00038	0.60	0.00038	1	0.50	0.00075	1.6	7-8.3	20	30	0.6	0.4	30	12	
27-9-2021	13	0.00038	0.60	0.00038	1	0.50	0.00075	1.6	7-8.3	20	30	0.6	0.4	30	12	
27-9-2021	14	0.00038	0.60	0.00038	1	0.50	0.00075	1.6	7-8.3	20	30	0.6	0.4	30	12	
Different chute slopes																
30-9-2021	27	0.00019	0.30	0.00038	1	0.33	0.00056	1.3	7-8.3	20	20	0.6	0.4	20	12	No videos from front
30-9-2021	28	0.00019	0.30	0.00038	1	0.33	0.00056	1.3	7-8.3	20	20	0.6	0.4	20	12	
30-9-2021	29	0.00019	0.30	0.00038	1	0.33	0.00056	1.3	7-8.3	20	20	0.6	0.4	20	12	
5-10-2021	40	0.00019	0.30	0.00038	1	0.33	0.00056	1.3	7-8.3	20	25	0.6	0.4	25	12	
5-10-2021	41	0.00019	0.30	0.00038	1	0.33	0.00056	1.3	7-8.3	20 surf		0.6	0.4	25	12	
5-10-2021	42	0.00019	0.30	0.00038	1	0.33	0.00056	1.3	7-8.3	20	25	0.6	0.4	25	12	
Earth atmospheric conditions																
28-9-2021	16	0.00000	0.00	0.00038	1	0.00	0.00038	1.0	1022	20	30	0.6	0.4	30	12	
28-9-2021	17	0.00000	0.00	0.00038	1	0.00	0.00038	1.0	1022	20	30	0.6	0.4	30	12	
29-9-2021	21	0.00000	0.00	0.00038	1	0.00	0.00038	1.0	1022	20	30	0.6	0.4	30	12	
29-9-2021	23	0.00006	0.10	0.00038	1	0.14	0.00044	1.1	1022	20	30	0.6	0.4	30	12	
29-9-2021	24	0.00006	0.10	0.00038	1	0.14	0.00044	1.1	1022	20	30	0.6	0.4	30	12	
28-9-2021	15	0.00019	0.30	0.00038	1	0.33	0.00056	1.3	1022	20	30	0.6	0.4	30	12	
28-9-2021	19	0.00019	0.30	0.00038	1	0.33	0.00056	1.3	1022	20	30	0.6	0.4	30	12	
29-9-2021	25	0.00038	0.60	0.00038	1	0.50	0.00075	1.6	1022	20	30	0.6	0.4	30	12	
29-9-2021	26	0.00038	0.60	0.00038	1	0.50	0.00075	1.6	1022	20	30	0.6	0.4	30	12	
Other sediments																
8-10-2021	57	0.00019	0.30	0.00038	1	0.33	0.00056	1.3	7-8.3	20	30	0	1	30	12	
8-10-2021	60	0.00019	0.30	0.00038	1	0.33	0.00056	1.3	7-8.3	20	30	0	1	30	12	
11-10-2021	61	0.00019	0.30	0.00038	1	0.33	0.00056	1.3	7-8.3	20	30	0	1	30	12	
7-10-2021	56	0.00019	0.30	0.00038	1	0.33	0.00056	1.3	7-8.3	20	30	1	0	30	12	
8-10-2021	58	0.00019	0.30	0.00038	1	0.33	0.00056	1.3	7-8.3	20	30	1	0	30	12	
8-10-2021	59	0.00019	0.30	0.00038	1	0.33	0.00056	1.3	7-8.3	20	30	1	0	30	12	

Large scale experiments - Aarhus University, Aarhus, Denmark

date	exp nr.	CO2 ice volume (m3)	CO2 ice weight (kg)	Sediment volume (m^3)	Sediment weight (kg)	Volume frac CO2	Total volume (m3)	Total weight (kg)	Chamber pressure (mbar)	Temp chute bottom (	Flume angle (degrees)	Silver sand (kg)	Builders sand (kg)	Slope chute (de	Slope outflow plain (deg)	Notes
Different CO2 fractions																
11-10-2022	15	0.0000	0	0.00302	8	0.00	0.00302	8.0	8	20	30	4.8	3.2	30	10	
6-10-2022	5	0.0010	1.6	0.00302	8	0.25	0.00402	9.6	8	20	30	4.8	3.2	30	10	
13-10-2022	21	0.0010	1.6	0.00302	8	0.25	0.00402	9.6	8	20	30	4.8	3.2	30	10	
17-10-2022	25	0.0010	1.6	0.00302	8	0.25	0.00402	9.6	8	20	30	4.8	3.2	30	10	
13-10-2022	20	0.0015	2.4	0.00302	8	0.33	0.00452	10.4	8	20	30	4.8	3.2	30	10	
17-10-2022	24	0.0015	2.4	0.00302	8	0.33	0.00452	10.4	8	20	30	4.8	3.2	30	10	
17-10-2022	26	0.0015	2.4	0.00302	8	0.33	0.00452	10.4	8	20	30	4.8	3.2	30	10	
5-10-2022	2	0.0015	2.4	0.00302	8	0.33	0.00452	10.4	8	20	30	4.8	3.2	30	10	No high speed footage
7-10-2022	7	0.0020	3.2	0.00302	8	0.40	0.00502	11.2	8	20	30	4.8	3.2	30	10	
7-10-2022	8	0.0020	3.2	0.00302	8	0.40	0.00502	11.2	8	20	30	4.8	3.2	30	10	
14-10-2022	23	0.0020	3.2	0.00302	8	0.40	0.00502	11.2	8	20	30	4.8	3.2	30	10	
Different chute slopes																
18-10-2022	28	0.0015	2.4	0.00302	8	0.33	0.00452	10.4	8	20	20	4.8	3.2	20	10	
12-10-2022	18	0.0015	2.4	0.00302	8	0.33	0.00452	10.4	8	20	25	4.8	3.2	25	10	
13-10-2022	19	0.0015	2.4	0.00302	8	0.33	0.00452	10.4	8	20	25	4.8	3.2	25	10	
17-10-2022	27	0.0015	2.4	0.00302	8	0.33	0.00452	10.4	8	20	25	4.8	3.2	25	10	

- **Supplementary videos**
- Can be downloaded under this link:
- https://filesender.surf.nl/?s=download&token=110d4f61-f624-406b-a23c-3cb3a66b5ef0

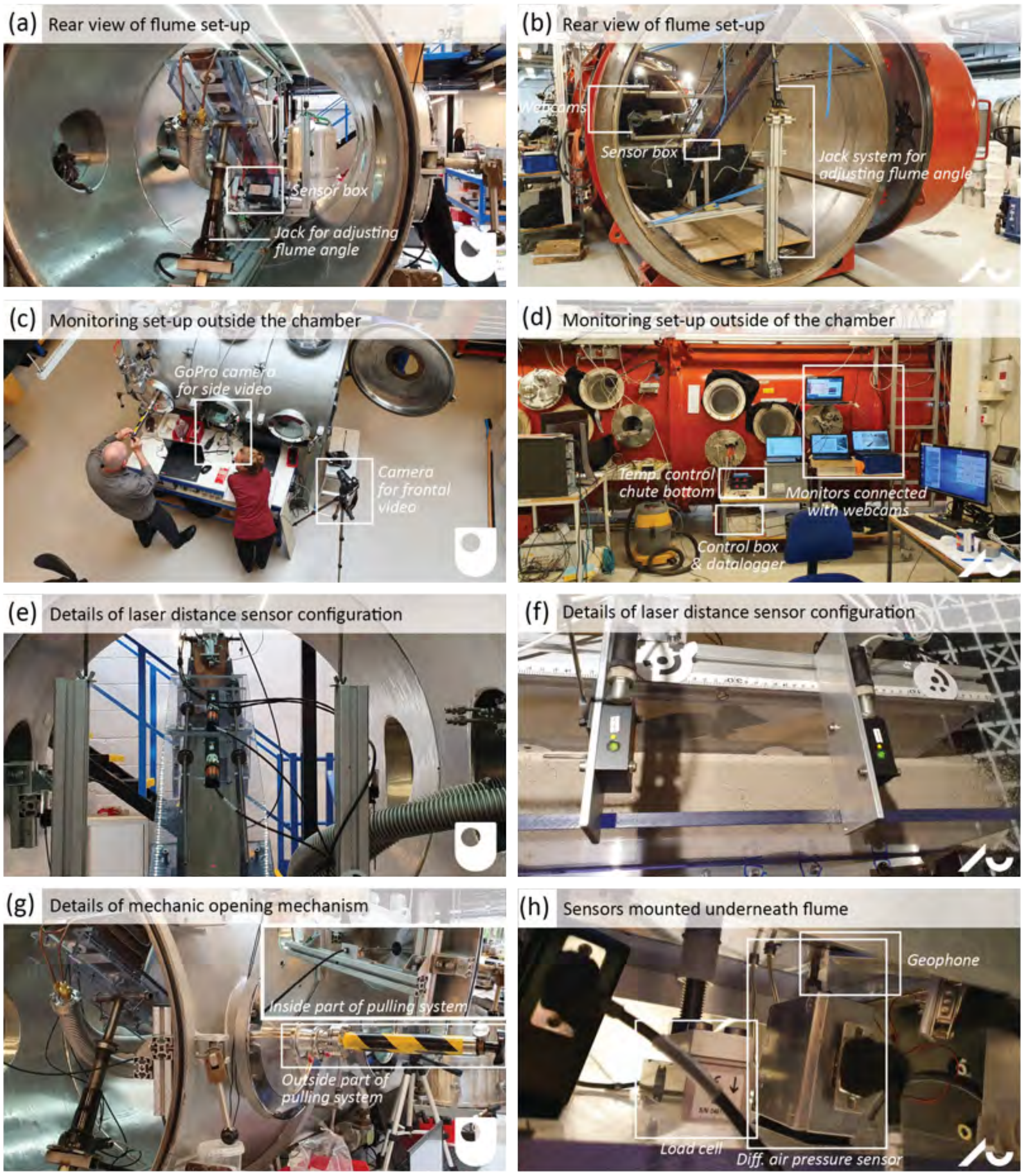

Supplementary Figure 1. Photos showing important details of the flumes. The details of the small-scale experiments conducted in the Mars chamber at the Hyper Velocity and Impact lab (HVI) of the Open University (UK) are shown in panels (a), (c), (e), and (g). The details of the large-scale experiments conducted in the Mars Simulation Wind tunnel at Aarhus University (Denmark) are shown in panels (b), (d), (f), and (h). Note that the sensors depicted in panel (h) are used in both flumes.

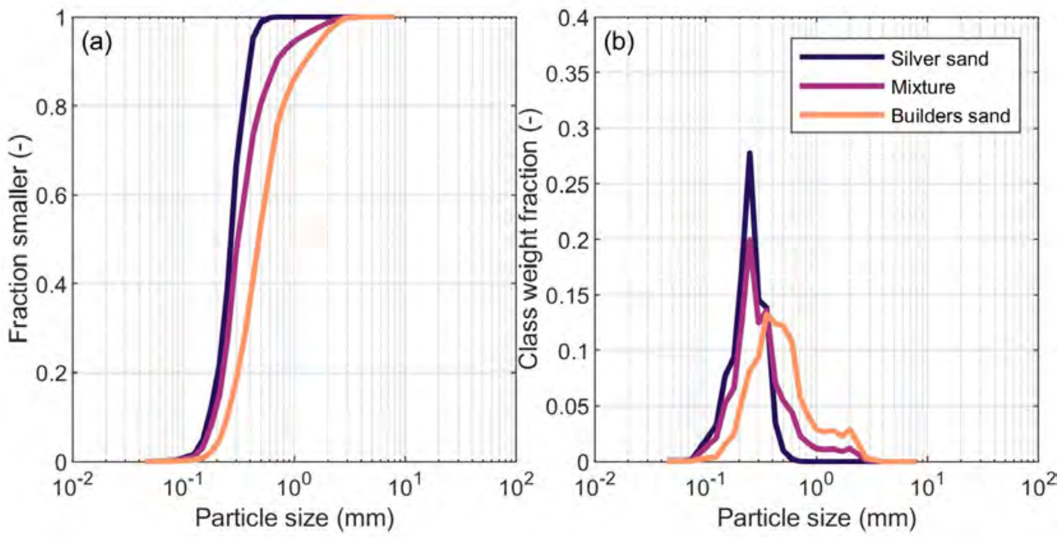

Supplementary Figure 2. Grain size distributions of the three different sands used; (a) frequency distribution, (b) cumulative particle-size distribution. Note that the mixture is used for all experiments in the main manuscript, this mixture comprises for 60% of silver sand and 40% builders sand.

Supplementary Figure 3. Photos showing important details of the experimental routine, from storing the CO_2 ice (a-b) to the loading of the material before an experiment (g-h). The experimental routine for the small-scale and large-scale experiments are mostly similar. The most important differences are depicted in this figure. For the small-scale experiments, the CO_2 ice was crushed by hand (c), whereas for the large-scale experiments a grain mill was used (d). The resulting grain size of the ice is similar for both methods (see insets of (c) and (d)). In the small-scale experiments, the sediment-ice mixture was poured into the reservoir and the reservoir was loaded into the flume, whereas in the large-scale experiments, the sediment-ice mixture was directly poured into a reservoir permanently connected to the flume.

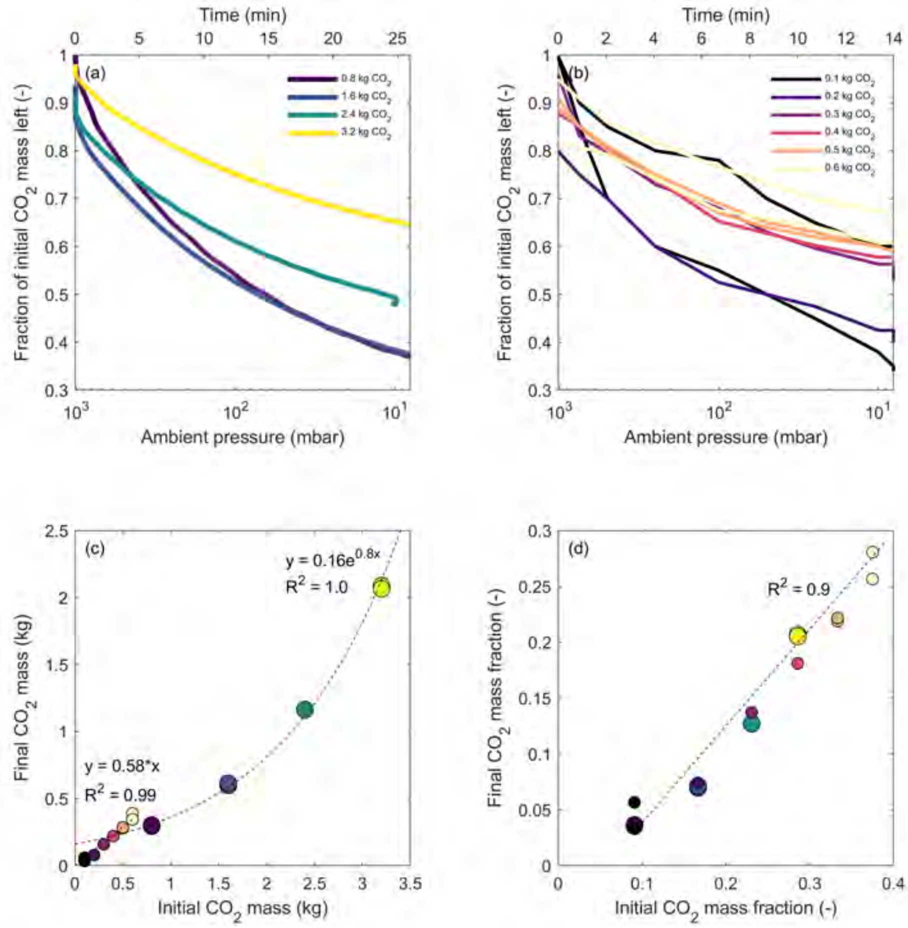

Supplementary Figure 4. Results of the CO_2 sublimation tests. With these tests, we quantified the loss of CO_2 during depressurization and determined the amount of CO_2 ice in the sediment-ice reservoir at the start of an experiment. In panels (a) and (b) the fraction of CO_2 relative to the initial CO_2 mass is given over time and pressure, for the large-scale set-up and the small-scale set-up respectively. In panel (c) the final CO_2 mass in the sediment-ice reservoir, when reaching a chamber pressure of 8 mbar, is plotted against the initial CO_2 mass. Panel (d) shows the final CO_2 mass fraction against the initial CO_2 mass fraction. Note that for the large-scale set-up, we used a digital lab scale and automatically recorded the weight at a frequency of 1 Hz, whereas for the small-scale set-up, we used simple analog kitchen scales and wrote down the remaining weight every minute.

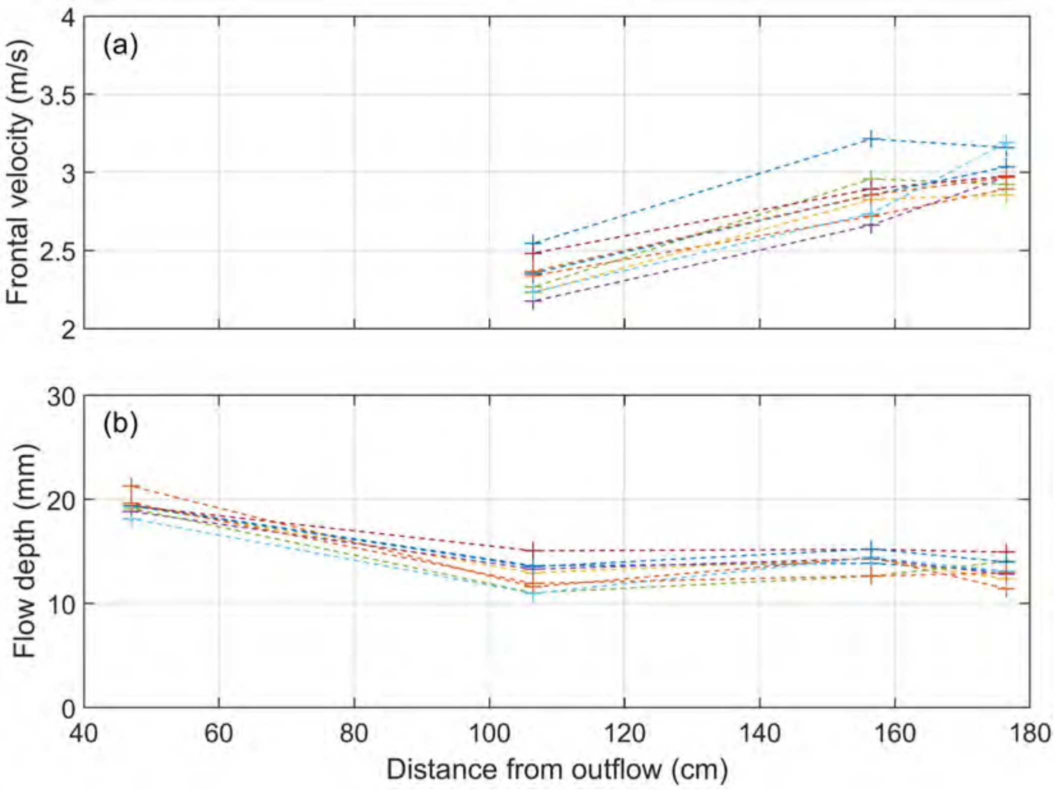

Supplementary Figure 5. Frontal flow velocity (a) and maximum flow depth (b) for the large-scale experiments over the distance along the flume, seen from the outflow point. The experiments shown are conducted under a chute angle of 30° with varying CO_2 mass fractions. Colors correspond to individual experiments. Note that the flow velocity is calculated from the difference in arrival times of the flow front at two consecutive locations. Therefore, the flow velocity depicted here is an average velocity over a certain distance. For the locations in the flume where the flow is still accelerating, this means that the depicted velocity is likely lower than the actual velocity at that location in the flume. This is the case for the flow velocities depicted at 106.5 cm from the outflow point.

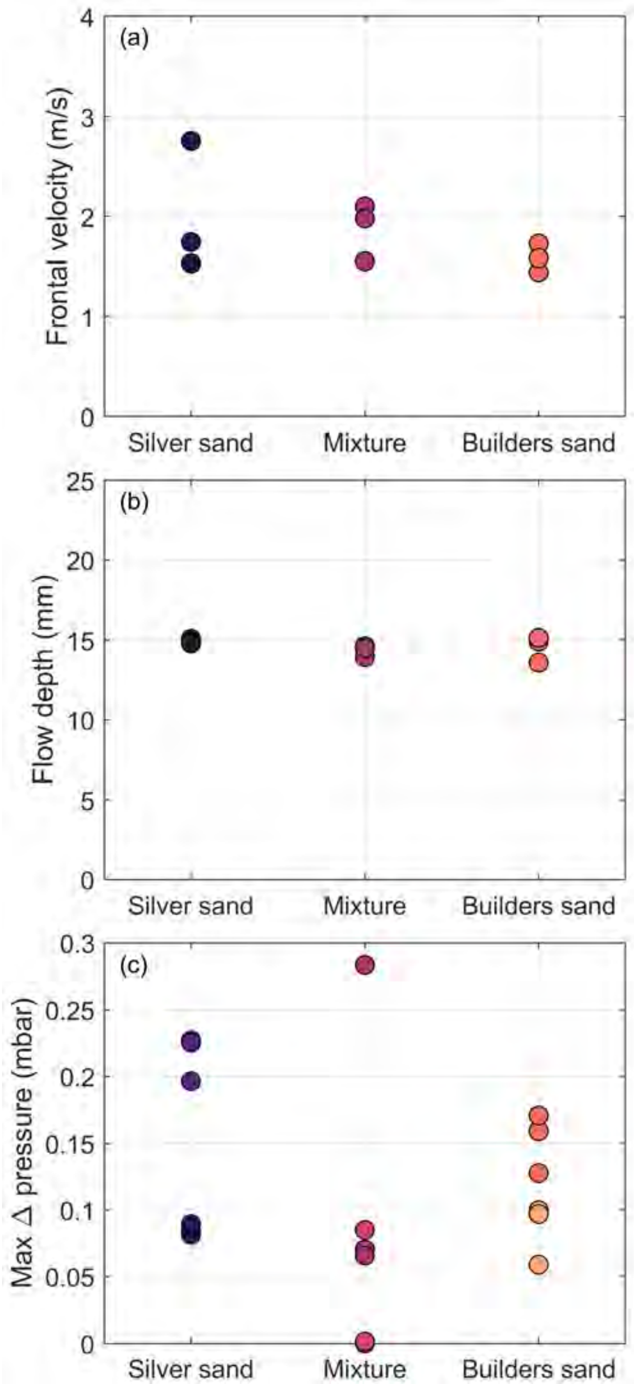

Supplementary Figure 6. Frontal flow velocity (a), maximum flow depth (b), and maximum differential pore pressure of the two different sensors (c) for the small-scale (S) experimental flows with three different sand types; 1) silversand, 2) a mixture of silver sand and builder sand and 3) builders sand. The mixture is used for all other experiments presented in the main text. All experiments presented in this plot are conducted under a chute angle of 30° with a CO_2 mass fraction of 0.15 at the beginning of the experiment, which is derived from data presented in Supplementary Figure 4.

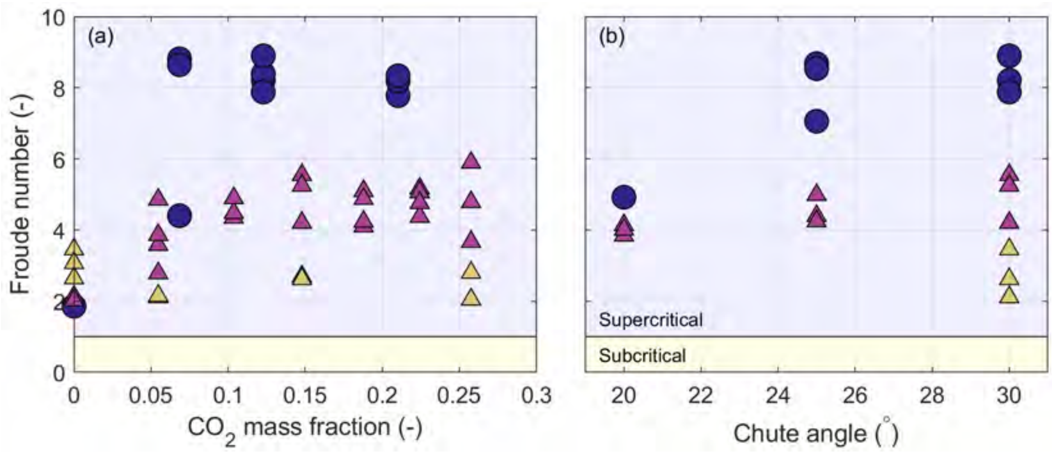

Supplementary Figure 7. Froude numbers for the granular flows in the large-scale and small-scale experiments conducted with different CO_2 mass fractions (left column) and under different chute angles (right column). The horizontal lines indicate the transition from subcritical to supercritical flow.